Final report

1. Project details

Project title	Fast and efficient fatigue test of large wind turbine blades (BLATIGUE)
File no.	64016-0023
Name of the funding scheme	Energiteknologisk Udviklings- og Demonstrationsprogram (EUDP)
Project managing company / institution	DTU Wind Energy
CVR number (central business register)	DK30060946
Project partners	DTU Wind Energy, Siemens Gamesa Renewable Energy A/S, Blade Test Centre A/S, R&D A/S, Olsen Wings A/S, Det Norske Veritas, Danmark A/S, Ørsted A/S, Zebicon A/S
Submission date	26 September 2021

2. Summary

2.1 English version

BLATIGUE is a development and demonstration project that includes the entire process almost up to market introduction for the multi-axis fatigue testing method (track #1) and for the multi-axis fatigue exciter (track #2). The project includes several steps in the development and demonstration of the technologies as the development is stepping from small blades (14 m) over medium size blades (49 m) to large blades (75 m).

The standard certification tests, that blades are tested against today, are not representing the real world very well. In reality blades are exposed to torsion and bending in different directions at the same time. The industry consequently needs fatigue test methods that better match the loads to which the blades are exposed to in real operational conditions. A multi-axis fatigue test methods can do exactly that.

As blades become larger the time needed to perform the necessary certification tests becomes longer. This is converting into a challenge for the industry as 100 m blades are expected to take more than a year to test. There is a need to shorten the test time and multi-axis test methods can do that as flap and edgewise loads can be tested at the same time.

BLATIGUE has developed a fatigue test method and simulation tool that not only is effective, as the test goal can be reached virtually anywhere on the blade at the same time (that is not possible with current standard certification tests), but we have also shown that in some cases we can perform the tests 50% faster than

current standard certification tests. In BLATIGUE, an innovative electric exciter has also been developed that is capable of performing the developed fatigue test method. This exciter is already on the market, as stated on the R&D website and sales material.

2.2 Danish version

BLATIGUE er et udviklings- og demonstrationsprojekt, der omfatter hele processen, næsten op til introduktionen på markedet for fleraksede udmattelsestestmetoder (spor #1) og for fleraksede udmattelses excitere (spor #2). Projektet omfatter flere trin i udviklingen og demonstrationen af teknologier i takt med, at udviklingen går fra små vinger (14 m), over mellemstore vinger (49 m), til meget store vinger (75 m).

De standardtest der anvendes i dag ved certificering af vinger, repræsenterer ikke den virkelige verden. I virkeligheden, er vinger udsat for vrid og bøjninger i forskellige retninger på samme tid. Industrien har derfor brug for udmattelsestestmetoder, der bedre ligner de belastninger, vingerne er udsat for under reelle driftsforhold. En flerakset udmattelses testmetode kan gøre netop dette.

I takt med, at vindmøllevinger bliver større, tager det længere tid, at udføre de nødvendige certificeringstest. Dette er en udfordring for branchen, da det forventes at tage mere end et år, at teste 100 m vinger. Der er derfor et behov for at forkorte testtiden, og fleraksede testmetoder, kan gøre netop dette, da flap- og kantvise belastninger kan testes samtidig.

BLATIGUE har udviklet en udmattelsestestmetode og et simuleringsværktøj, der ikke kun er effektivt, da testmålet kan nås stort set overalt på bladet på samme tid (det er ikke muligt med nuværende standardcertificeringstest), men vi har også vist, at i nogle tilfælde kan vi udføre testene 50% hurtigere end de nuværende standardcertificeringstest. I BLATIGUE er der også blevet udviklet en innovativ elektrisk exciter, der er i stand til at udføre den udviklede udmattelsestestmetode. Denne exciter er allerede på markedet, som det fremgår af R&D hjemmeside og salgsmateriale.

3. Project objectives

The objective of the BLATIGUE project is to develop fast and efficient fatigue test methods for large wind turbine blades and to develop equipment to excite the blades under such tests.

The objective can be summarized in developing and demonstrating two energy technologies: To develop a new fatigue testing method which is faster, better mimics the actual loading, and results in similar damage as observed in wind turbine blades in operation (track #1) and to develop equipment to excite the blades under such tests (track #2). This was done through eight work packages, with the results described in section 5.

4. Project implementation

In BLATIGUE we set off to mainly develop two technologies, namely advanced multi-axis fatigue testing method and multi-axis fatigue exciters - both for very large blades. This has happened. We have developed a fatigue test method and simulation tool that not only is effective, as the test goal can be reached virtually anywhere on the blade at the same time (that is not possible with current standard certification tests), but we have also shown that in some cases we can perform the tests 50% faster than current standard certification

tests. In BLATIGUE, an innovative electric exciter has also been developed that is capable of performing the developed fatigue test method. This exciter has now been demonstrated (June 2021) on a 75m blade at Blaest and the exciter is already on the market, as stated on the R&D website and sales material. The BLATIGUE project has made the project partners the international technology leaders within this area and we look forward to expand this further in the BLATIGUE-2 project.

The project implementation did not develop fully as foreseen. Three times during the project period we needed to get approval for changes and re-budgeting in order to meet the main objectives of the project. The main challenges that the project faced were:

- Development of exciters for both small and large blades needed more work and were more expensive than anticipated
- 1D masses were needed in order to better results with the developed fatigue test method
- Development of fatigue test method took longer time and needed more hours than anticipated

In order to meet these challenges we focusing on the essential parts of the project, reduced work for nonessential parts, transferred funds to the partners that needed more resources and also even developed and demonstrated a 1D mass solution for small blades.

All milestones in the revised project plan were met as summarized in the table below.

Milestones	**Status**
M1: Test simulation tool ready to use (WP2.3)	**Completed**
M2: Multi-axis fatigue test method established (WP6a)	**Completed**
M3: Multi-axis fatigue test method performed on OLW1430 blade (WP5.3)	**Completed**
M4: Multi-axis fatigue test exciter tested on B49 blade (WP7a.2)	**Completed**
M5: Requirement specification for multi-axis exciter (WP5.4) - small blade	**Completed**
M5: Requirement specification for multi-axis exciter (WP6b.1) - large blades	**Completed**
M6: Design description of multi-axis exciter – small blade (WP5.4)	**Completed**
M6: Design description of multi-axis exciter – large blade (WP6b.3)	**Completed**
M7: Final design review of multi-axis exciter – small blade (WP5.4)	**Completed**
M7: Final design review of multi-axis exciter – large blade (WP6b.3)	**Completed**
M8: Factory acceptance test of multi-axis exciter – small blade (WP5.4)	**Completed**
M8: Factory acceptance test of multi-axis exciter – large blade (WP6b.3)	**Completed**
M9: Site acceptance test of multi-axis exciter – small blade (WP5.4)	**Completed**
M9: Site acceptance test of multi-axis exciter – large blade (WP6b.3)	**Completed**
M10: Multi-axis fatigue test method and exciter demonstrated on B75 blade (WP7b.2)	**Completed**
M11: Design evaluation of multi-axis exciter (WP6b.4)	**Completed**
M12: 1D mass demonstrated on OLW1430 blade	**Completed**
Commercial milestones	
CM1: Report on IP in project related areas (WP0.3)	**Completed**
CM2: Market and competition analysis for multi-axis exciters (WP5.4)	**Completed**
CM3: Price structure analysis for multi-axis exciters (WP6b.2)	**Completed**
CM4: Market introduction plan for multi-axis exciters (WP6b.3)	**Completed**
CM5: Market and competition analysis for test simulation tool (WP2.6)	**Completed**
CM6: Market and competition analysis for 3D measurement system (WP4.5)	**Completed**
CM7: Certification scheme proposal on multi-axial fatigue testing (WP8.3)	**Completed**

5. Project results

Introduction

I the following is described the obtained technological and commercial results. As described in the previous section the project met challenges, but these were overcomed and all milestones in the revised project plan were met as described in this section. This was done through eight work packages, with the results described in section 5.1 to 5.8.

5.1 WP1: Aeroelastic simulations of fatigue loads

The work in this WP was completed in September 2018. The loads for the small (14.3m length), medium (49m) and large (75m) size blades have been computed. The load behaviour and the strains around the blade surface were computed. The results have been delivered and discussed in these reports: Aeroelastic Analysis of Olsen Wings 14.3m Blade-DTU Wind Energy Report I-0635, Aeroelastic Analysis of B49 blade-DTU Wind Energy Report I–0638, Analysis of B75 blade-DTU Wind Energy Report I–0816. Additionally two approaches on how to reproduce the IEC lifetime fatigue load targets have been investigated using the medium size blade. The first considered the blade load time series at high wind speeds (near cut-out) only. The second approach considered again the time series at high wind only and on top applies a band pass filter on the time series around the high energy frequencies (1P and the 1st blade edgewise natural frequency). In both approaches the duration of occurrences has been extended accordingly trying to much the reference lifetime blade fatigue damage. The conclusion is that a very good agreement can be achieved with the first approach, while the 2nd is not considered good enough for implementation since the results deviate up to 20% in some parts of the blade surface.

5.2 WP2: Development of blade fatigue test simulation tool

A method for multi-axial fatigue testing of wind turbine blades was established (completion of milestone M2), which can be used to design improved fatigue tests compared to current standard tests in terms of both accuracy and total test time (see more details in Castro et al, 2021[1]). With this method, material-based damage targets along the blade can be reached by applying an optimal combination of different uniaxial test blocks, such as flapwise and edgewise, and multi-axial test blocks, such as chaotic and phase-locked. The material-based damage is accounted for by considering longitudinal strains.

A tool-chain was developed (completion of milestone M1) to implement the developed multi-axial fatigue test method, which consists of a blade fatigue test simulator and an optimization tool, see Figure 5.2.1.

[1] Castro, O., Belloni, F., Stolpe, M., Yeniceli, S. C., Berring, P., & Branner, K. (2021). Optimized method for multi-axial fatigue testing of wind turbine blades. Composite Structures, 257, [113358]. https://doi.org/10.1016/j.compstruct.2020.113358

Figure 5.2.1. Left: Blade fatigue test simulator and Right: optimization tool, developed in BLATIGUE-1 project.

The blade fatigue test simulator is used to obtained a matrix containing the equivalent damage ratio, EDR, (i.e., ratio between the strain-based test damage and the strain-based target damage) along the blade caused for several possible test blocks for a given simulation time, see Figure 5.5.2. For that, information related to the blade properties, target loads, fatigue properties, simulation parameters, and test setups corresponding to the different evaluated test blocks, are needed as input. Then, the optimization tool is used to find the optimal combination of test blocks based on the obtained EDR matrix and defining some optimization constrains related to test time and allowable error.

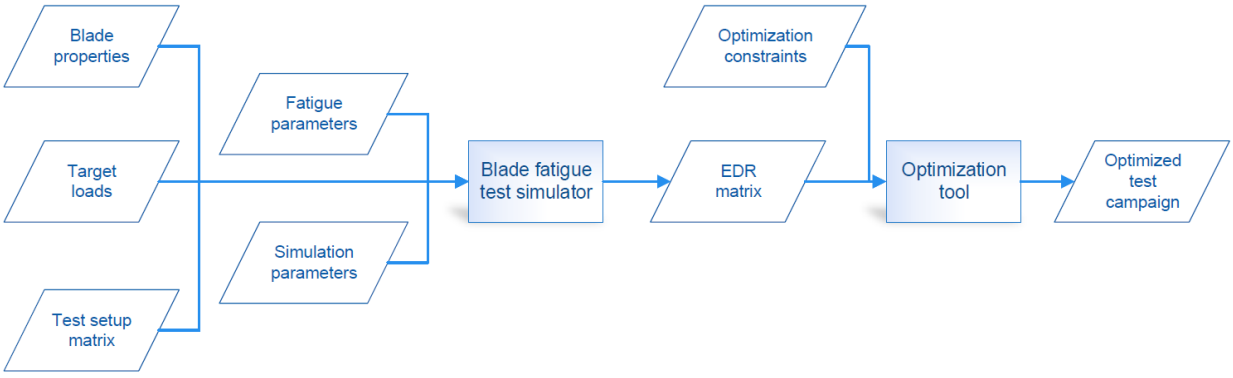

Figure 5.2.2. Flowchart of developed tool-chain for simulation of wind turbine blades fatigue tests.

The developed fatigue test method was applied and demonstrated in small blades (see details in Section 5.5) and large blades (see details in Sections 5.6 and 5.7).

In addition, an alternative approach that uses a modified bending moment variable that is proportional to the longitudinal strains developed in beams, such as blades, when subjected to pure bending moments was also developed (see details in Castro et al., 2021b[2]). This approach was used to estimate a theoretical damage based on the modified bending moment variable, which matches the theoretical damage based on strains. The main advantage of this approach is that it only requires, as inputs, the bending moments applied to the structure and the ratio between the cross-section stiffnesses, which do not compromise the confidentiality of the structure design and, therefore, it can be easier applied in the industry.

[2] Castro, O., Berring, P., Branner, K., Hvejsel, C. F., Yeniceli, S. C., & Belloni, F. (2021). Bending-moment-based approach to match damage-equivalent strains in fatigue testing. Engineering Structures, 226, [111325]. https://doi.org/10.1016/j.engstruct.2020.111325

5.3 WP3: High fidelity simulations and identification of fatigue damage mechanisms

The main objective with this work packaged was to design artificial defects, which should be imbedded into the 14.3 meter blades manufactured by Olsen Wings. The blades with these artificial defects would be subjected to a fatigue test campaign including different load configurations. These configurations should consist of both standard fatigue testing, single axis flapwise and single axis edgewise, and the dual axis fatigue loading developed within this project.

The assumption was that some of the defects would only be triggered when applying dual axis loading, or at least, that a different in propagation rate would be observed. From previous studies, it was known that blades are subjected to very complex loading and some part of the blade is significantly under tested during a standard fatigue test campaign.

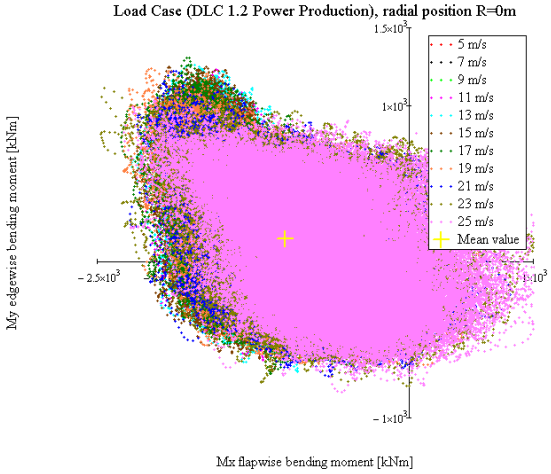

Figure 5.3.1. Example of load cloud from Design Load Case (DLC) 1.2 Power Production.

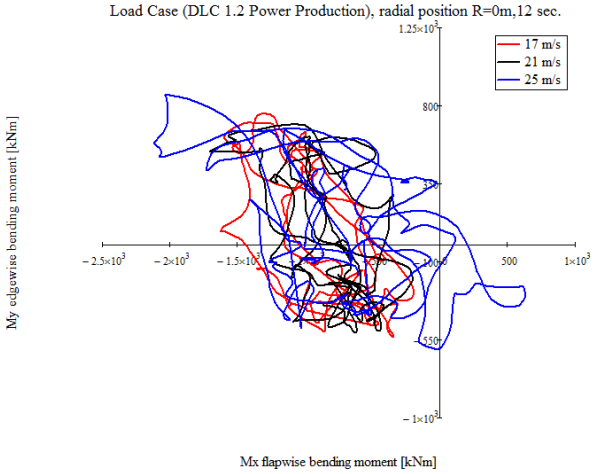

Figure 5.3.2. 12 second sample from the aero-elastic simulations seeds with the following wind speeds 17 m/s, 21m/s and 25m/s showing the complexity of the load a wind turbine blade sees.

In more details, the idea was to perform different fatigue loading (known as block loading) and loop through these different loading types a number of times. The objective was to determine the damage propagation rate of the different artificial damage when applying the different test loading, Including the developed dual axis loading. This idea is schematically depicted below, showing the different damage propagation rate for various defects.

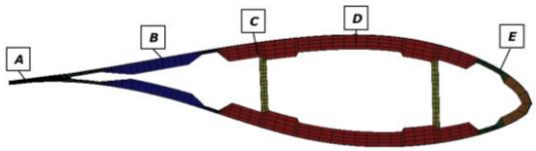

A: Defect/damage trailing region
B: Defect/damage trailing sandwich panel
C: Defect/damage debonding between cap and web
D: Cap wrinkle/delamination
E: Defect/damage leading edge

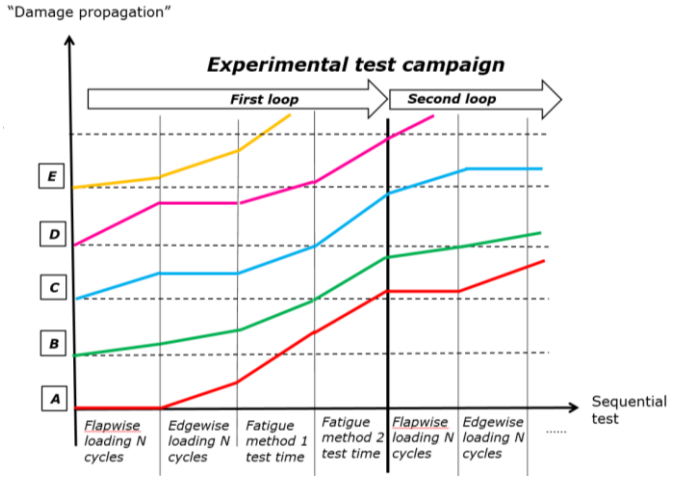

Figure 5.3.3. Illustration of the strategy for quantifying the effects fatigue loading configuration on damage propagation of designed artificial defects.

5.3.1 Model of the 14.3 meter Olsen Wings blade

The 14.3 meter blade from Olsen Wings is modelled using 20-noded layered continuum elements and therefore is a volume representation of the geometry required. 99 cross sections describe the outer geometry of the blade. The curves defining these cross-sections were offset according to the layup definition in order to represent the thickness of the laminates. Finally, the individual cross-sections were connected by spline curves and interpolation surfaces to obtain a volume representation of the blade. This model can be solved via MSC.MARC or Abaqus.

Below are depicting segments from the blade model.

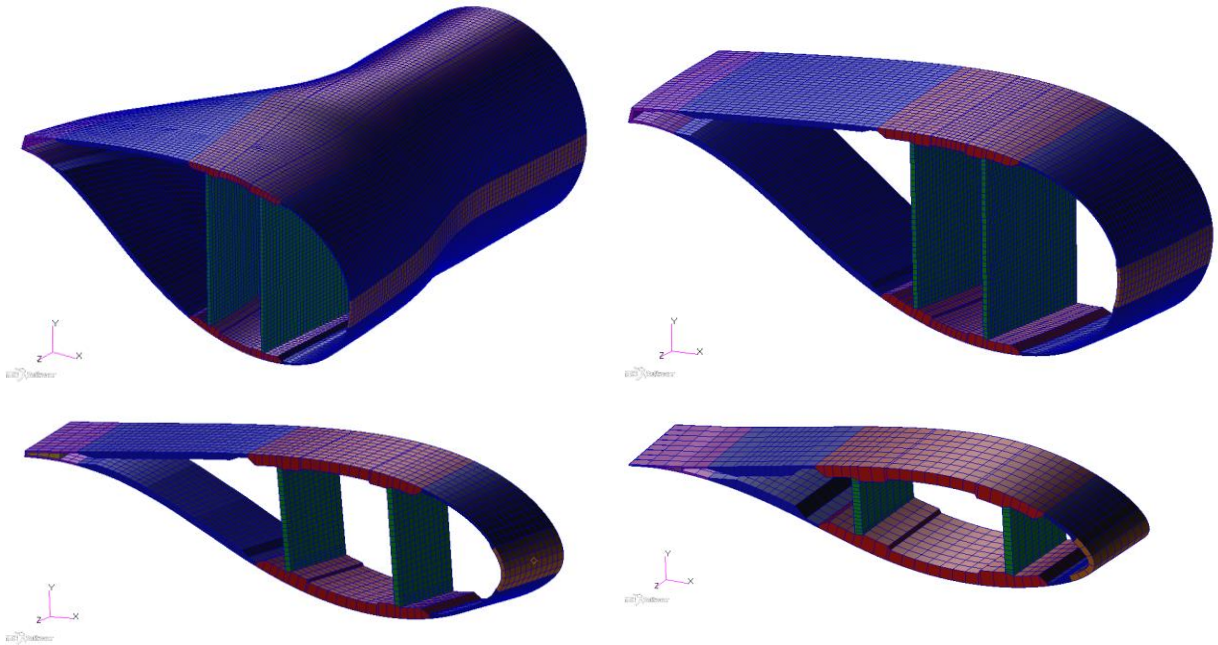

Figure 5.3.4. Segments from the finite element model, top left root segment, top right max chord segment, bottom left mid span segment and bottom right segment of outer part of the blade.

5.3.2 Model validation

To validate the first blade from Olsen Wings a test campaign was performed to determine the structural properties. These properties are applied for simulating the different test method using the DTU fatigue testing tool described in section 5.2. To determine the structural properties a Beam Property Extraction (BPE) method utilizing a least squares algorithm was developed. This method determines flap- and edgewise stiffness, location of elastic center and orientation of the principle bending axis. The experimental results were also used to validate the 3D finite element model.

Figure 5.3.5. Digital Image Correlation (DIC) setup used to measure the displacement field during the BPE test campaign

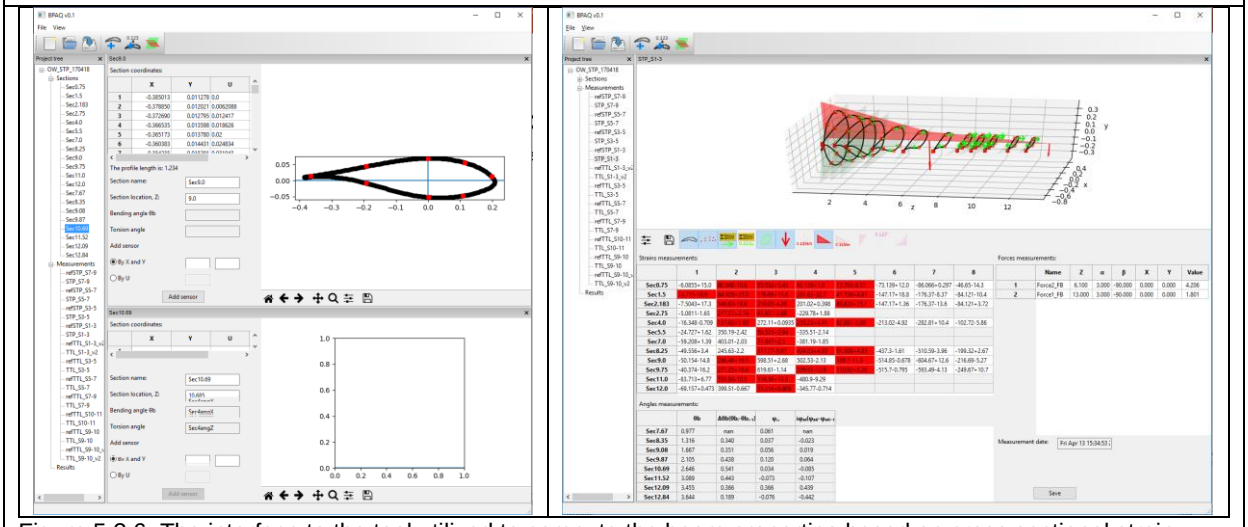

Figure 5.3.6. The interface to the tool utilized to compute the beam properties based on cross sectional strain measurements from a combinations of load cases.

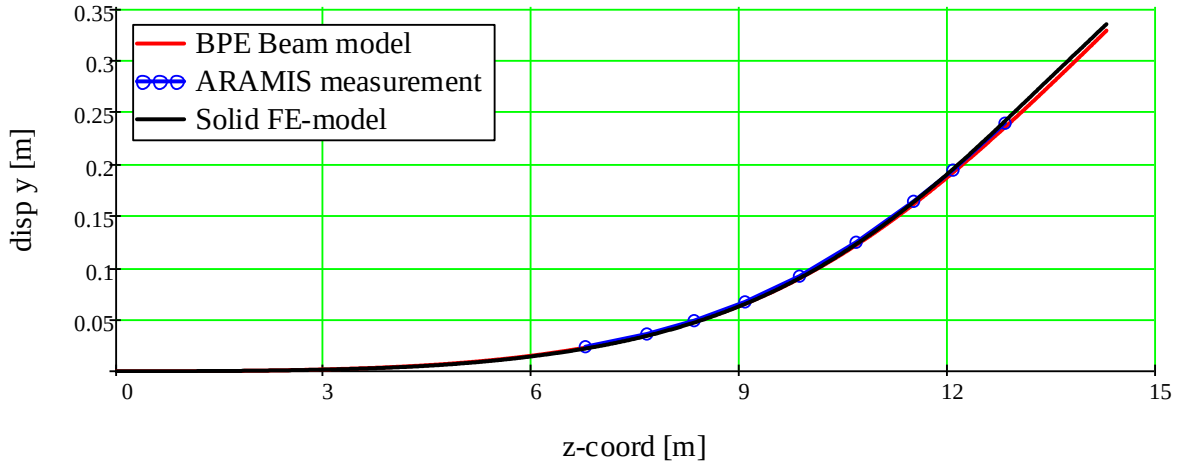

Figure 5.3.7. A comparison between measured deflections (via DIC ARAMIS), computed deflection via the BPE beam model and the 3D finite element model. The defection response depicted in this plot is the flapwise load case used to determine the blade structural properties.

To demonstrate the effect of the different fatigue methods developed within this project, it was important to numerically determine the surface strains at different cross sectional locations. Presented below are a comparison between measured strain values and computed via 3D finite element simulations and finally the strain values computed via the beam model generated based on the BPE-method.

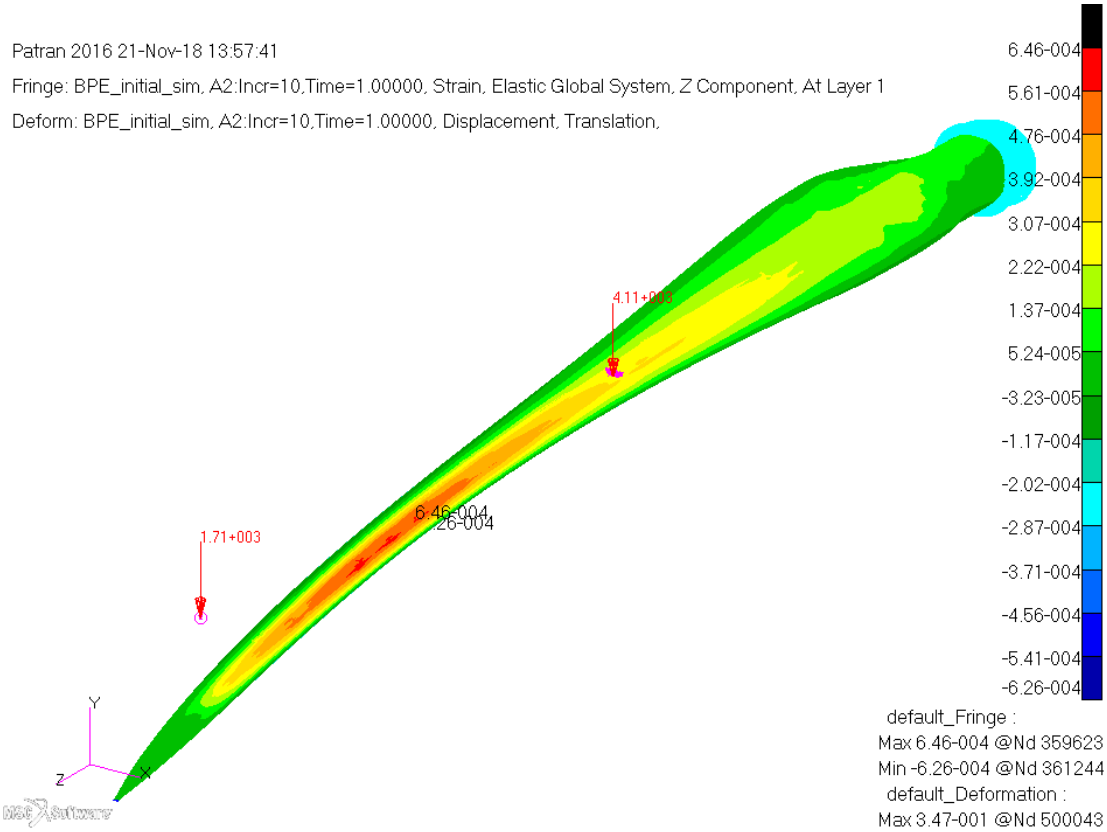

Figure 5.3.8. Longitudinal strain response from the flapwise loading applied in the BPE test campaign.

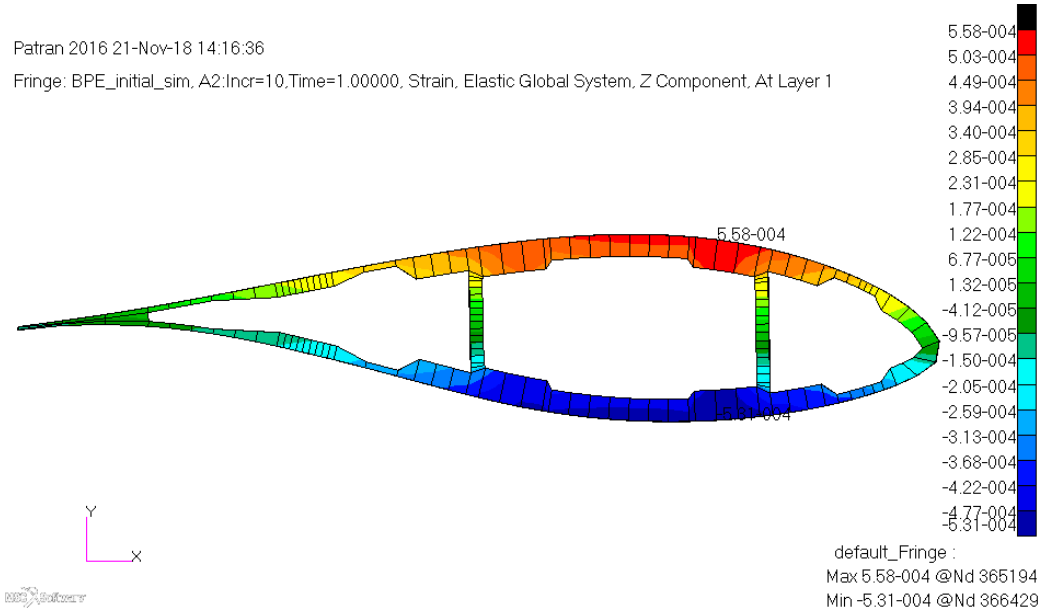

Figure 5.3.9. Longitudinal strain response from the flapwise loading applied in the BPE test campaign depicted on a cross section from the finite element model at radial position 9 meter.

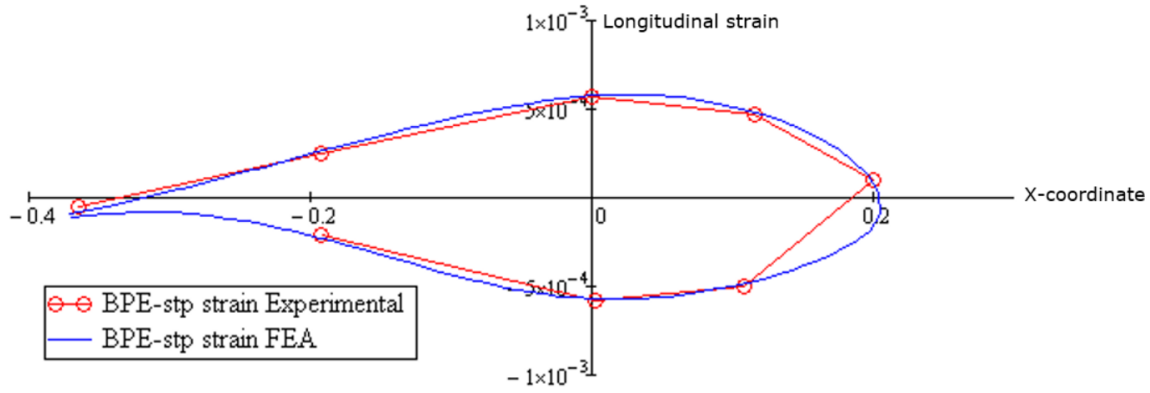

Figure 5.3.10. Comparison between measured longitudinal strain measured, at a cross section located at radial position 9 meter, and the computed strain via the 3D finite element model.

Further validation activities of the models were performed. This includes modal test, which shows an excellent agreement between experimental and numerical results. The first 10 modes are within 3% variations in eigenvalues.

5.3.3 The designed artificial defects

The design of the individual defects are aided by numerical simulations. Do to the lack of fracture mechanical properties the results of these simulations are subjected to large uncertainties.

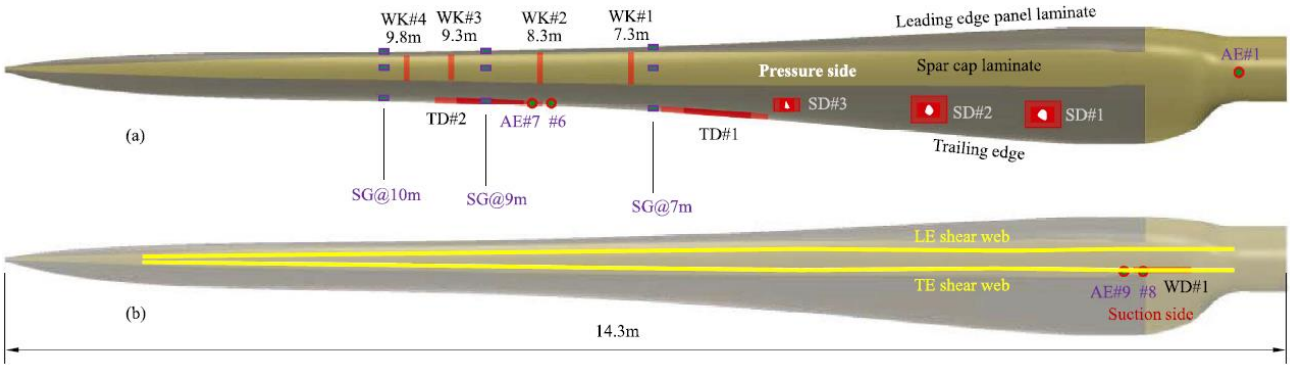

Figure 5.3.11. Distribution of artificial defects over the blade. Defect types: wrinkle insert – WK; sandwich skin/core debonding – SD; trailing edge adhesive joint debond – TD; shear web/spar cap debond – WD. (a) The distribution of defects and sensors over the pressure side shell and trailing edge of the blade. (b) The adhesive joint debonds between the rear shear web and the spar cap at the suction side of the blade.

Wrinkles in pressure cap laminate

A simplified 2D plan strain modelling subjected to strain levels seen during the fatigue testing campaign was utilized to estimate the crack propagation. These predictions are performed based on computing the strain energy release rate, as illustrated below.

Assumptions:

- Linear elastic materials
- G_{IC}= 200 J/m^2; G_{IIC}= G_{IIIC}= 1000 J/m^2
- 2D plane strain
- Delamination initiated by ply waviness

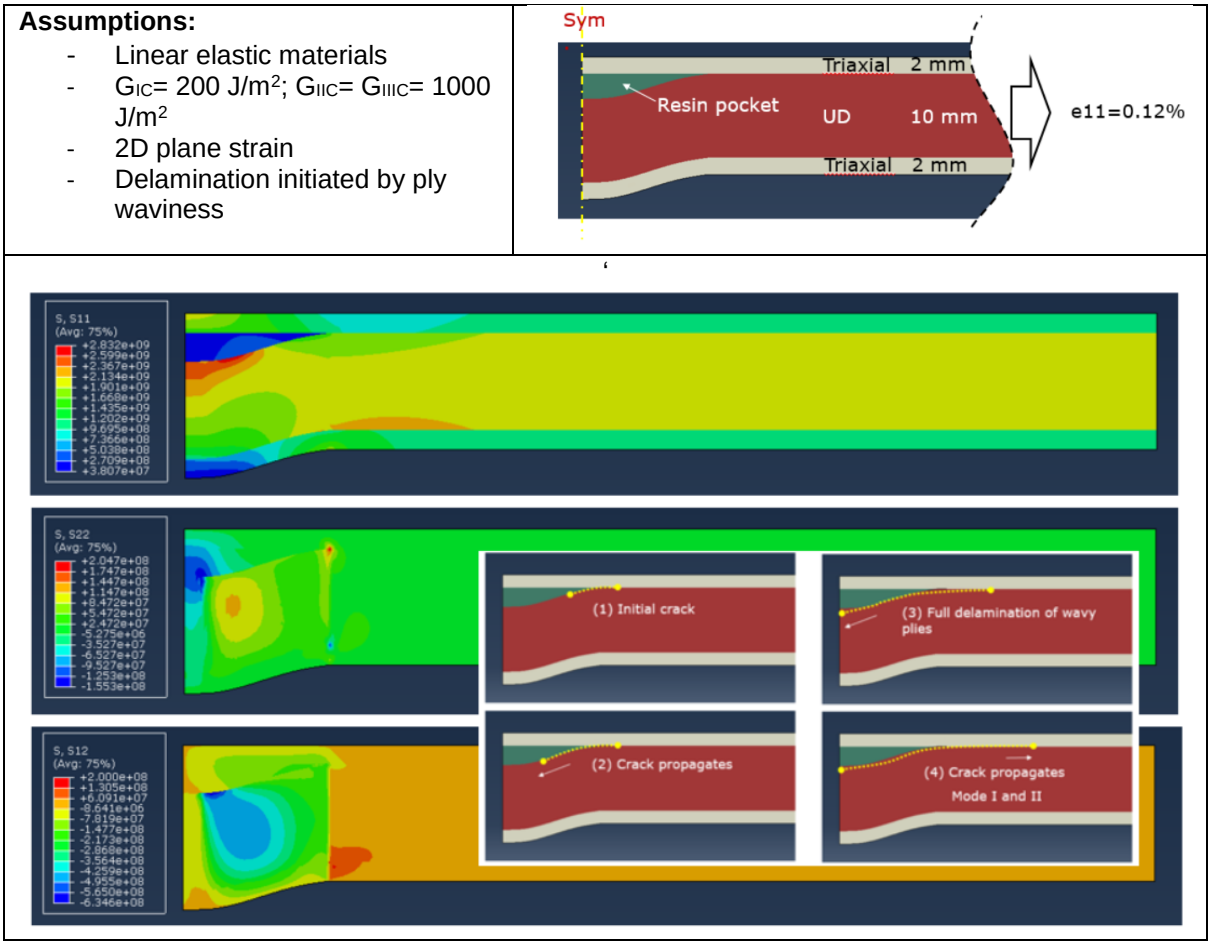

Figure 5.3.12. Numerical simulations performed to design the resin inserts which generates the wrinkles in the blade.

Four resin inserts are embedded in the spar cap laminate to create out-of-plane wrinkles. The resin inserts are cast in a mold that is milled, see Figure. 5.3.13. The resin inserts have a wave height of 4 mm and a width of 40 mm and fit the curvature of the spar cap. The polyester resin used to cast the inserts is the same as the one used to build the blade. Once the resin inserts are manufactured, they are placed in the spar cap between UD fiber fabrics, as seen in Figure 5.3.14 left.

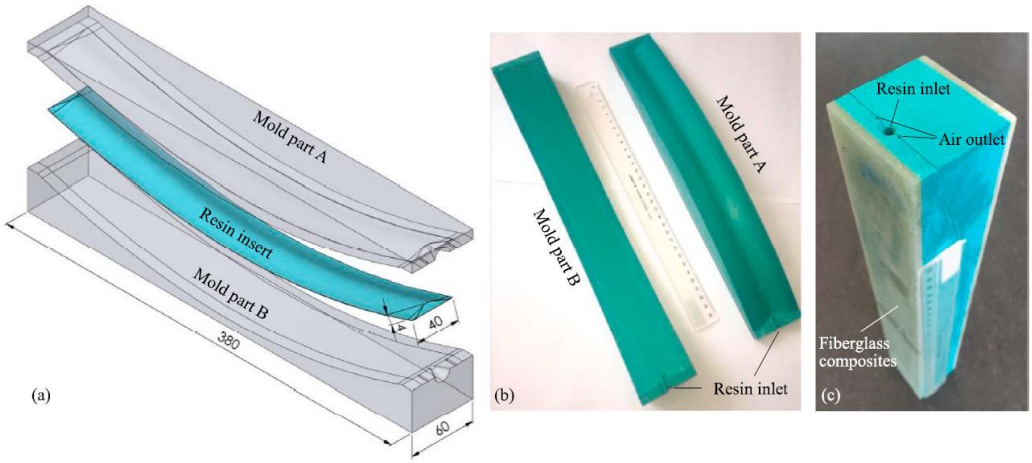

Figure 5.3.13. The mold tool for casting the polyester resin inserts

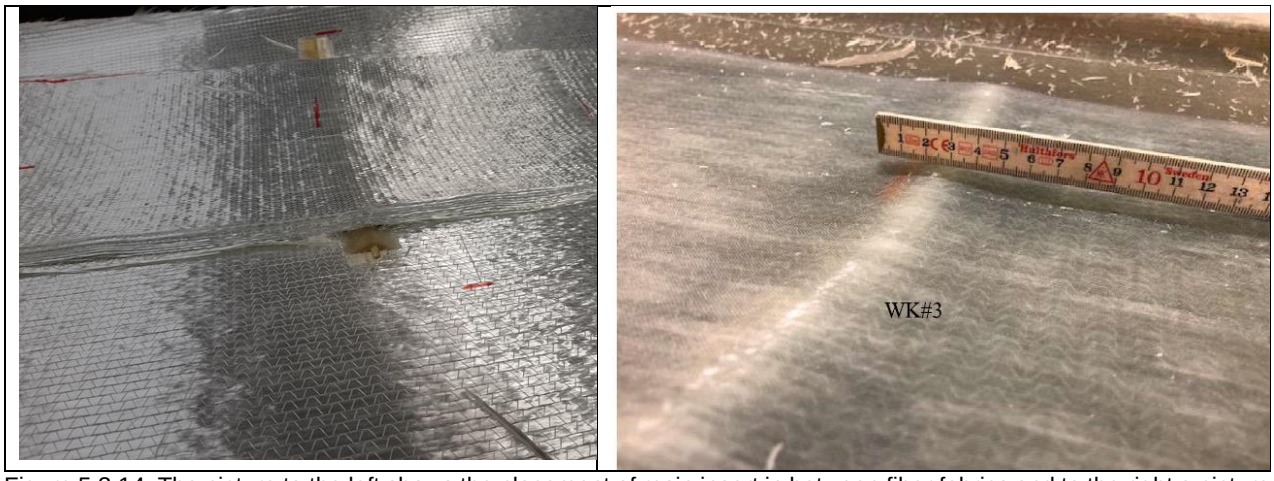

Figure 5.3.14. The picture to the left shows the placement of resin insert in between fiber fabrics and to the right a picture showing the wrinkle created by introducing the resin insert into the layup of pressure shell.

Debonding between skin and core

A number of simulations of the debonding between skin and core were performed, which included different placements both in radial position and on both suction and pressure side of the blade.

Below are an example of one of these simulations. The debonding has a size of 30x40cm and is located at radial position 2.4 meter. The detailed sub-model is linked to the blade via Glued Contact (cinematic couplings). Contact conditions is added between the interface between skin and sandwich core.

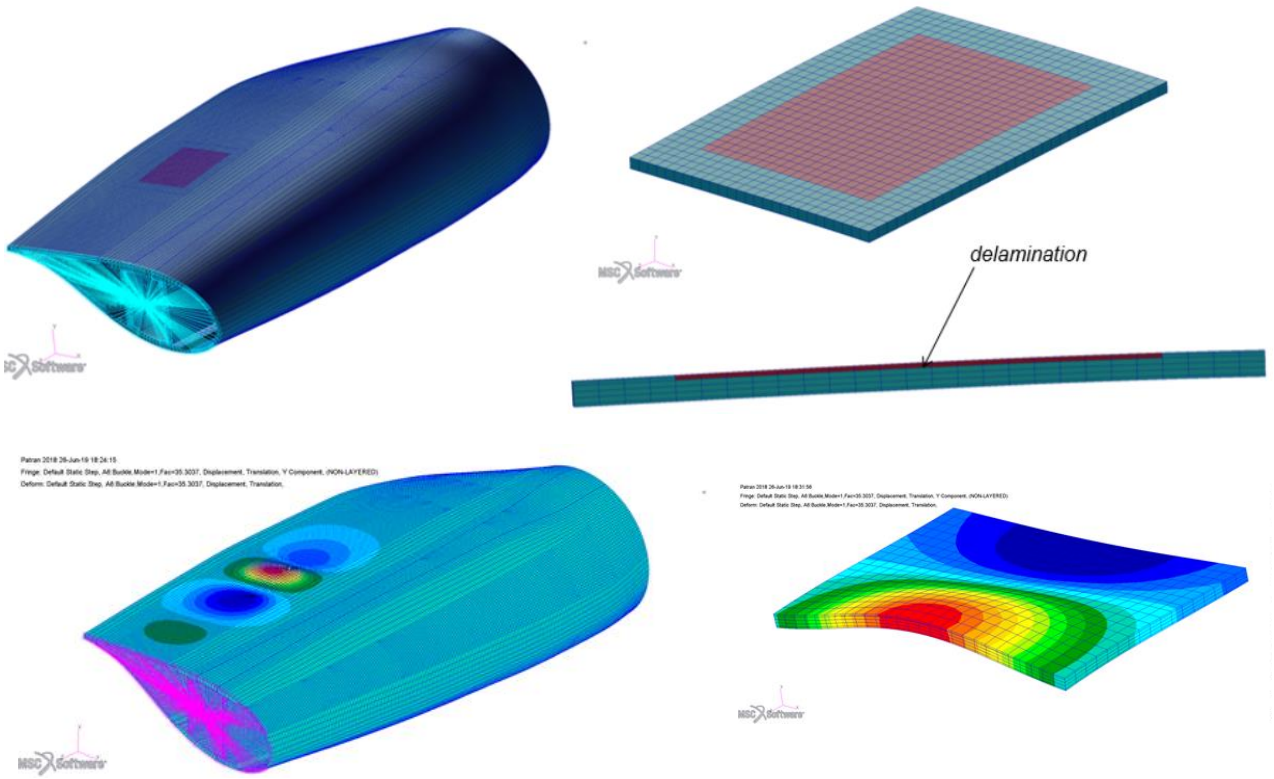

Figure 5.3.15. Showing the modelling technique utilized to model the debonding between skin and core material in the trailing edge sandwich panels.

The assumptions was that if an opening mode was triggered the chance of damage propagation was large. However simulations showed that to trigger this opening mode the blade had to be unrealistically overloaded during the fatigue test campaign for most of the simulated debondings.

The most promising debonding based on simulations was SD#2 located at radial position 4 meter on the trailing pressure panel. This debonding is 15x15cm an in the simulations triggered at load levels, which was realistic during the fatigue test campaign. Depicted below are the results of combined loading (dual axis).

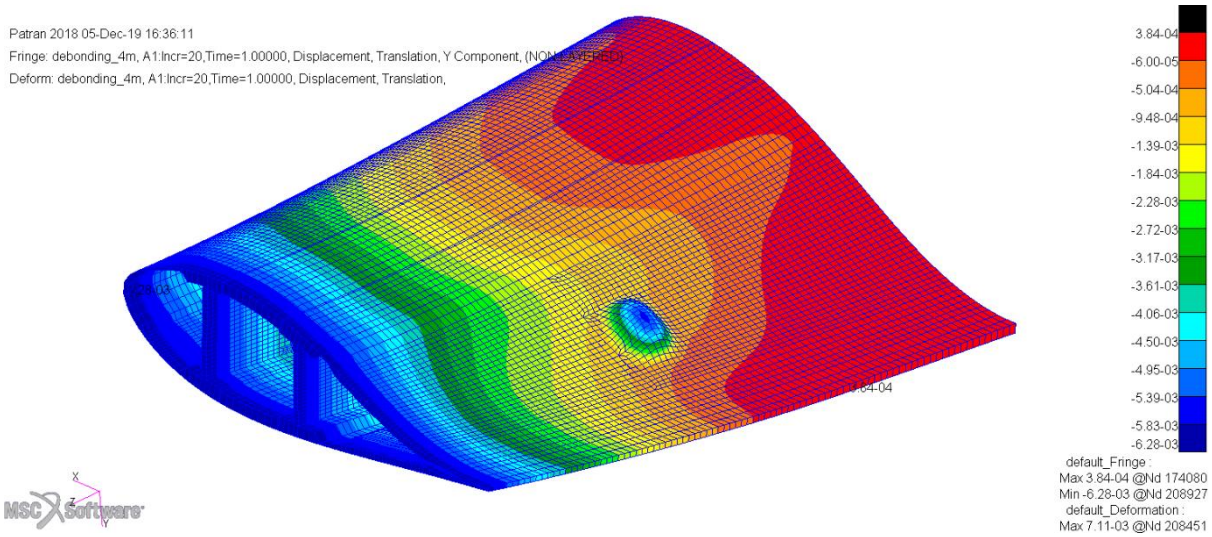

Figure 5.3.16. Segment from the full finite element model showing the the debonding SD#2 located on the pressure trailing edge panel at radial position 4 meter.

To create debonded regions between core materials and skin laminates in the sandwich panels, slip foils, or perforated release films R120-P3, with a thickness of 28 µm are inserted at the interface of interest. The slip foils are divided into two parts: the center part is made by the original slip foils to create a fully debonded region while the outskirt part is made by perforating the slip foils with holes with a diameter of 10 mm to create a partially bonded region. The purpose of including this partially bonded region is to facilitate the progress of debonding during the fatigue test.

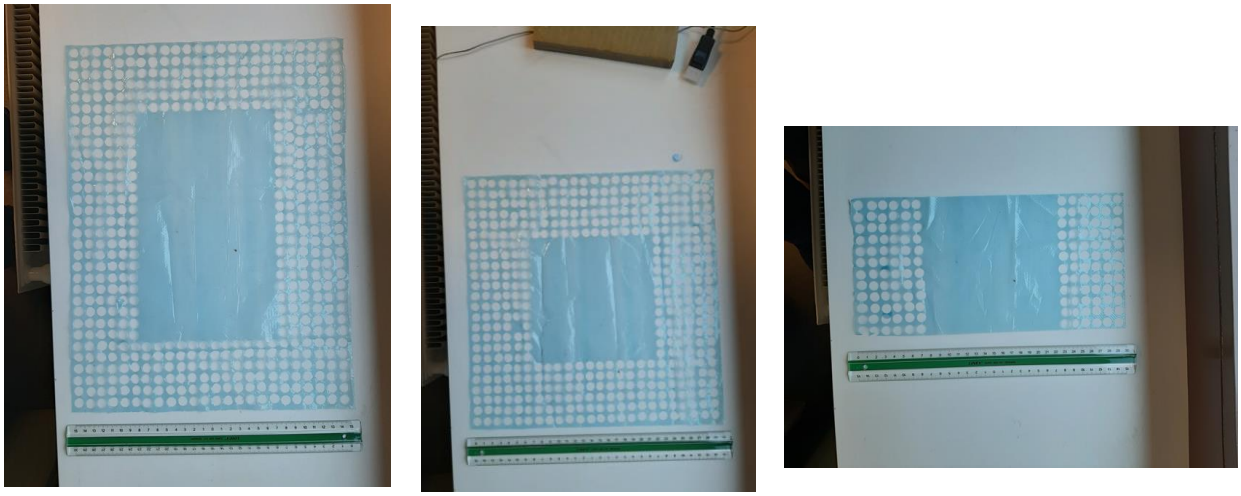

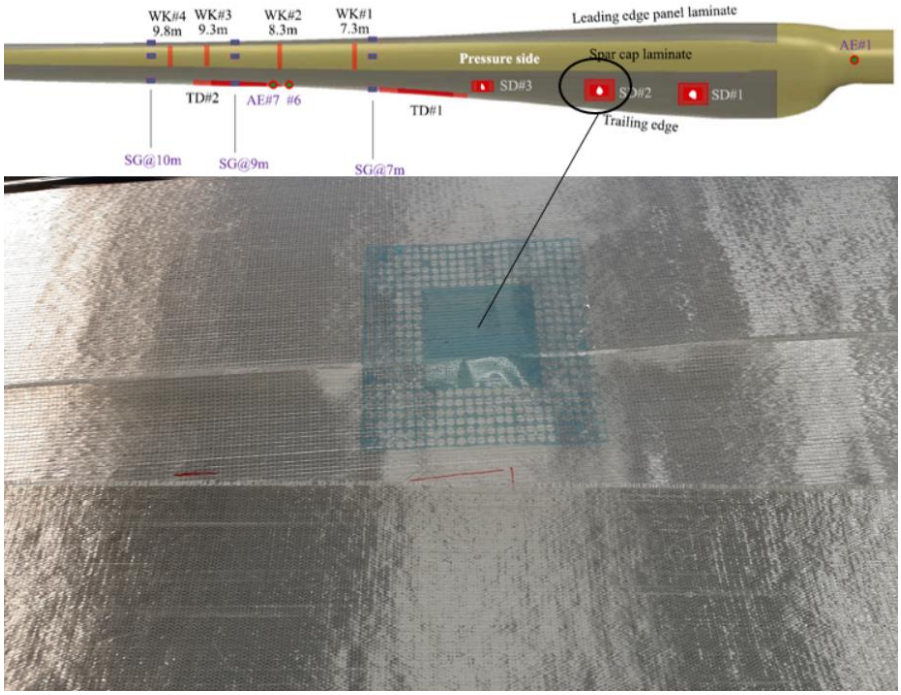

Figure 5.3.17. This figure shows the three sizes of slip foils which were imbedded into the blade. Top left corresponds to SD#1, mid top SD#2 and finally top right *corresponds* to SD#1. The picture in the bottom shows the placement of the SD#2 slip foil in the manufacturing at Olsen Wings.

Debonding in trailing edge

The OLW 14.3m blade is modeled to simulate trialing edge crack response under fatigue loads. The blade is modelled within the commercial FE software package Abaqus. Fig. 5.3.18 shows the global model of the blade with an adjacent detailed depiction of the section of interest. A through crack as shown in the red hatched region is introduced in the adhesive trailing edge joint whose crack plane is situated in the bulk adhesive centre. The crack front is perpendicular to the blade axis denoted as zb-direction aligned with the crack propagation directions.

The bondline thickness measured 2 mm on average. Hard, frictionless surface-to-surface contact conditions were assigned to the two matching surfaces of the crack plane in order to avoid crack overclosure. The readily implemented VCCT tool in Abaqus was used to compute the SERRs in the four nodes on both sides. The total crack propagation increment was computed as the average propagation increment of the four separate nodes.

Two load levels, i.e., the maximum and the minimum loads, during the fatigue loading are simulated in such a way that the resulting bending moment distribution matched the equivalent target bending moment distribution along the blade. The energy release rate at the crack fronts is then calculated for fatigue crack growth calculation.

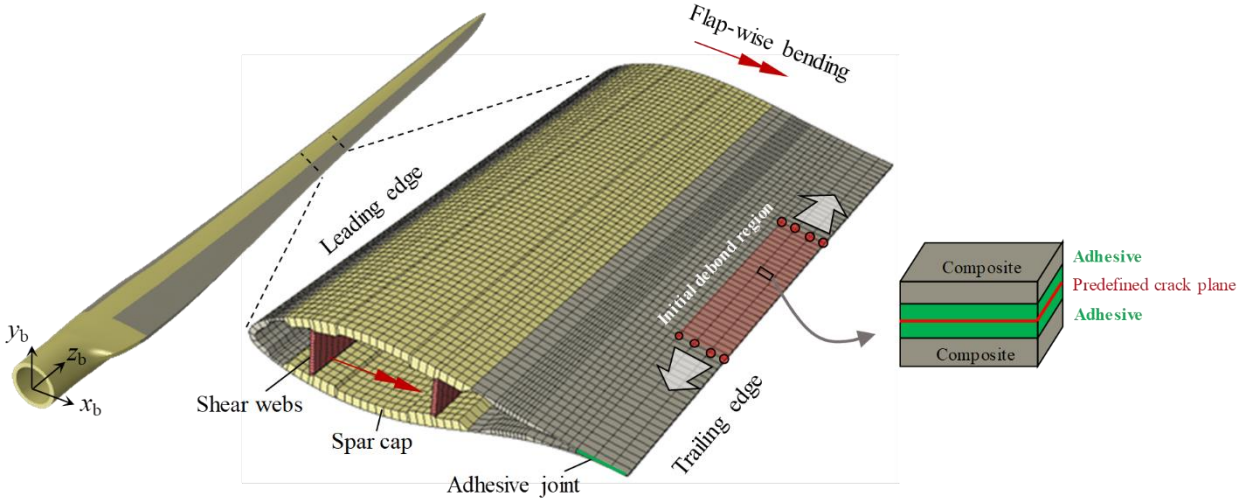

Figure 5.3.18. Showing the modelling technique used to design the trailing edge debonding.

In Figure 5.3.19 is depicted the local buckling response of the cracked trailing edge under the maximium bending. The crack growth may be driven by the local buckling, however, it is found that the growth rate is very much dependent on the loading pattern as well as loading amplitude. In this particular simulation, the crack growth is less likely to occur if the blade is loaded in edgewise loading. The fatigue loading schedule that combines edgewise fatigue loading and flapwise fatigue loading appears to be the most susceptible test setup that triggers crack growth in the trailing edge bondline.

A very similar buckling response of the trailing edge was observed during the dual axis fatigue loading, see Section 5.5.

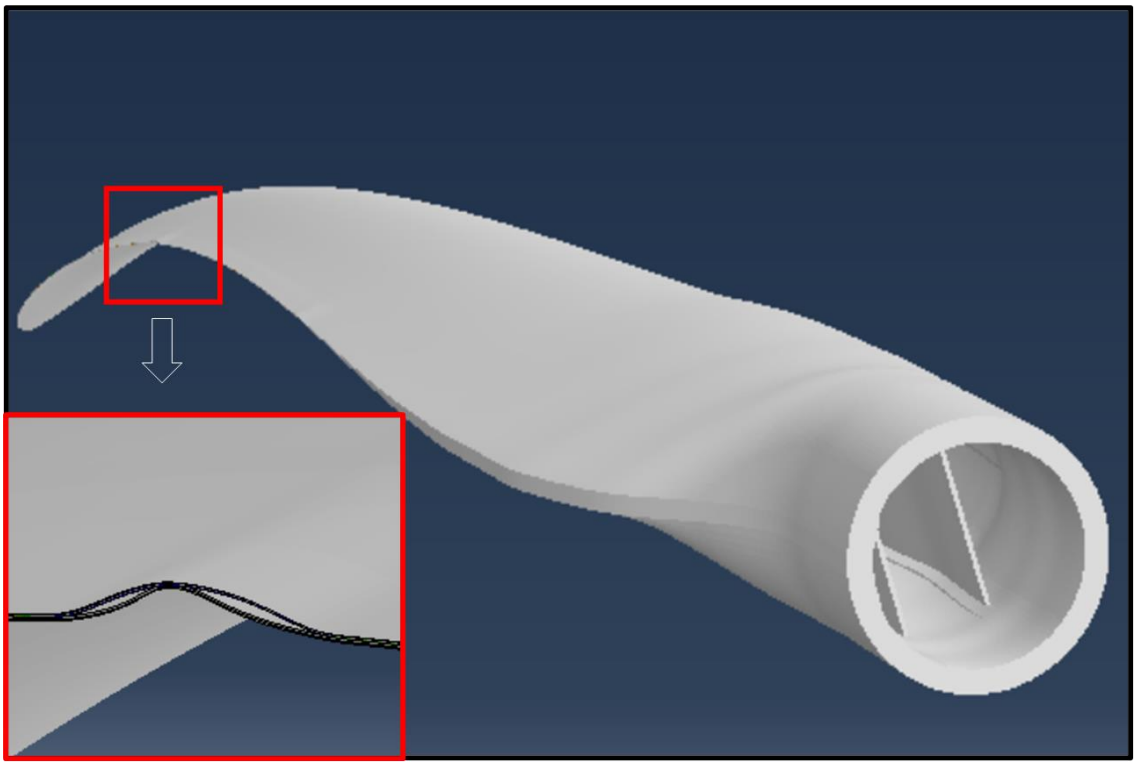

Figure 5.3.19. Shows the local trailing edge buckling response when subjected to combined loading (dual axis).

The two artificial debonded zones are created by two pieces of slip foil with a length of 1.2 m and a width of 20 cm are placed on top of the adhesive bond line along the trailing edge before the two blade shells are glued to form an entire blade. The slip foil is of the same type used to create the debonded regions in trailing edge panels.

5.4 WP4: Development of full-span 3D measurement system

The main goal of the work package was to develop and demonstrate digital image correlation (DIC) measurement system combined out of multiple stereo systems with not overlapping field of views (FOV) and bring measured values to one common coordinate system for further analysis and comparison with finite element simulations. There are some commercial systems available on the market with FOVs around 4x4x4 meters, some of these systems available in multi camera configurations, but FOVs stiching is usually done through fitting of common areas. In the project another strategy was used. First one was to use photogrammetry to build a virtual calibrated volume of markers and use this volume to obtain outer calibration of stereo systems, another one was to use laser tracker with some markers presented to the stereo systems.

Two stereo systems were made out of Teledyne Flir ORX-10GS-123S6M-C 12 megapixel (MP) cameras capable to deliver 68 frames per second (FPS) and Keyence CA-LHE16 16 mm low distortion lenses (see Figure 5.4.1). These cameras were installed on carbon booms to provide thermal stability and mounted on the wall.

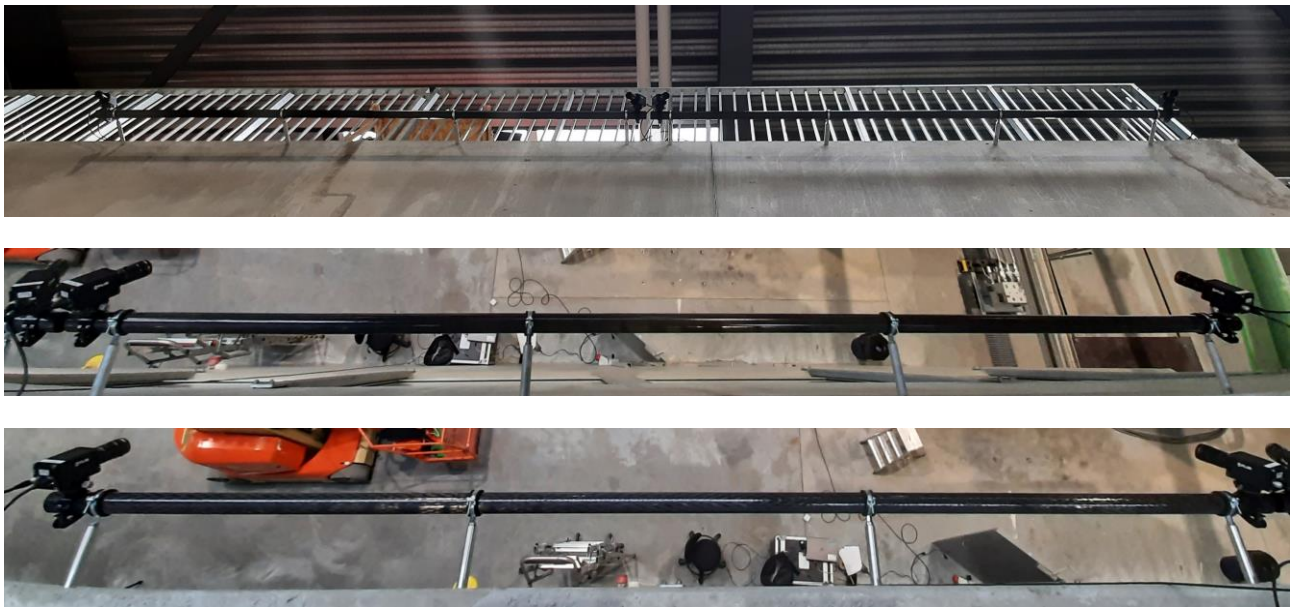

Figure 5.4.1. Stereo systems for DIC measurements

These cameras have a 10GigE interfaces generating quite intense data stream, therefore they were connected to high performance Ethernet switch Dell S4048-ON with 40GigE uplink to a server. Such configuration allows to stream the data with full speed to a server but for high frame rates there is only an option to buffer it in RAM. The data flowchart is presented in Figure 5.4.2. The server has a connection to a trigger box made on basis of FRDM64 development board. The trigger box has a web interface which controls simultaneous camera triggering with microsecond accuracy.

The calibration procedure follows GOM's "Large Area Calibration" recipe. It consists of 2 stages: inner calibration (all cameras installed at one spot and set of snapped images of calibration object is used to determine parameters of individual optical system distortion model) and outer calibration (all cameras installed at their predefined positions and these positions and cameras orientations are determined with support of photogrammetry). Some screen dumps of calibration process are presented in Figure 5.4.3.

After calibration process all measurements can be brought in one coordinate system the accuracy of such transformation is demonstrated in Figure 5.4.4 where coordinates of markers on carbon calibration bars were measured by two different stereo systems and brought in common coordinate system to calculate the distance.

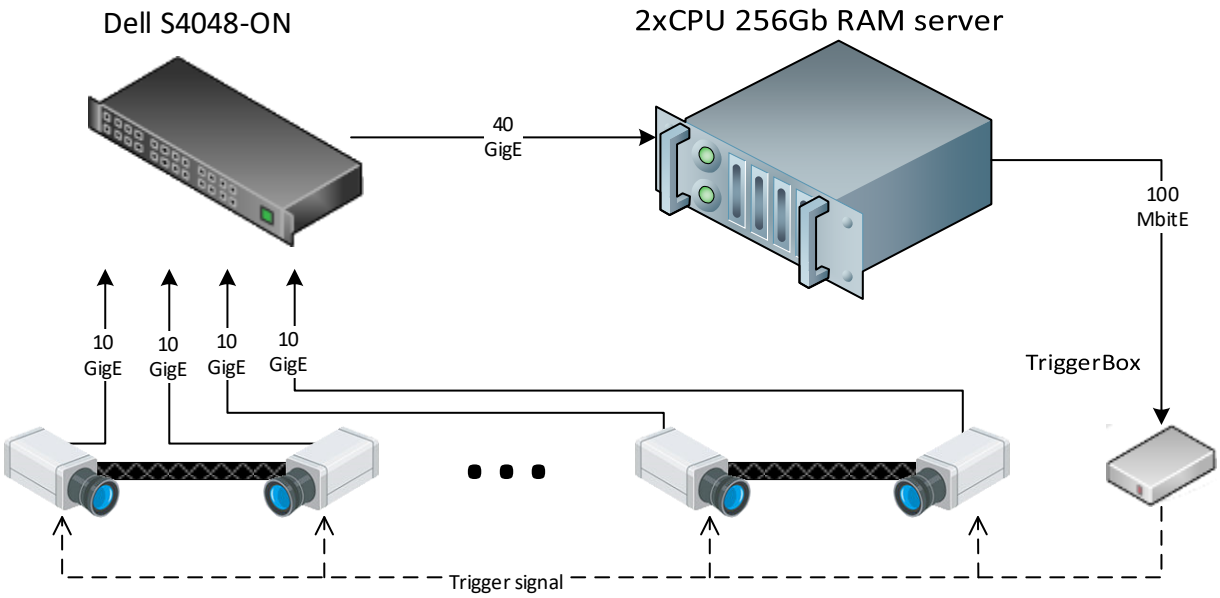

Figure 5.4.2. Data flowchart for DIC measurement system.

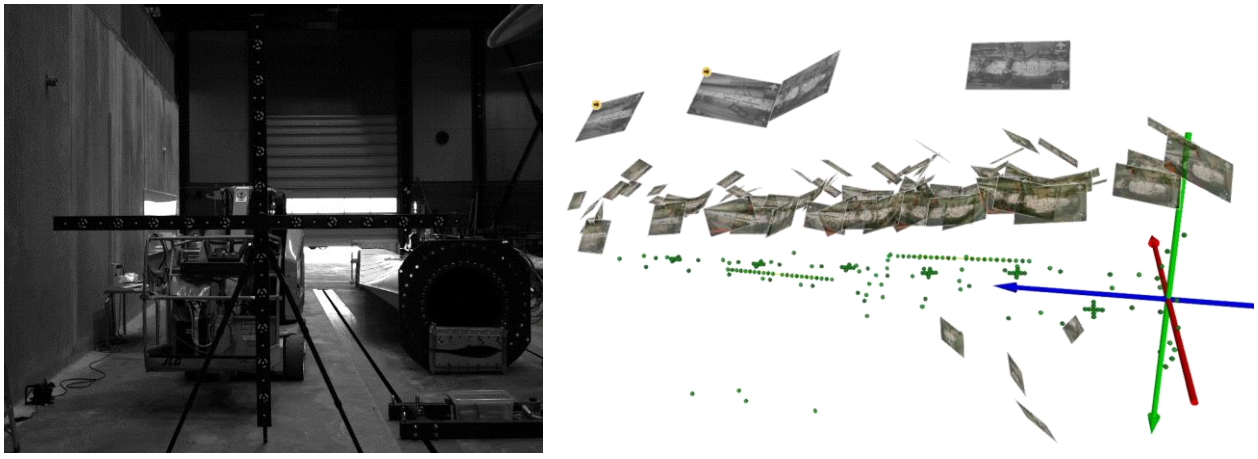

(a) (b)

Figure 5.4.3. (a) Inner calibration of individual cameras with carbon calibration cross, (b) Outer calibration of two stereo systems (black and white images) with assistance of photogrammetry (color images) system.

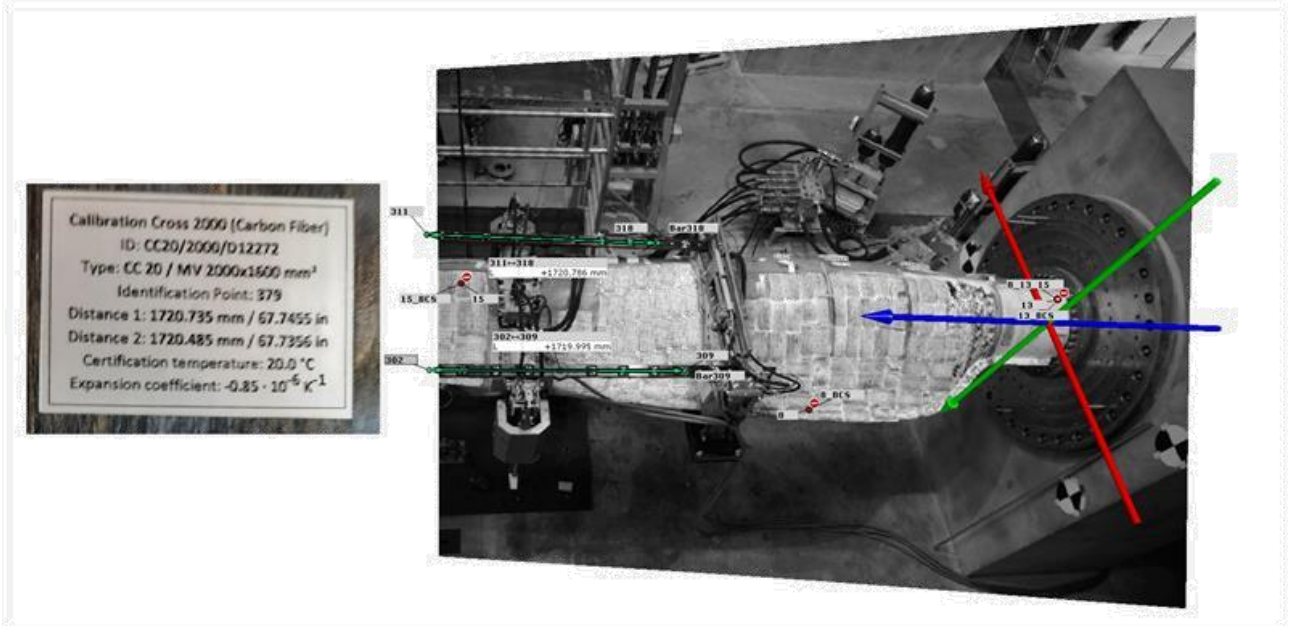

Figure 5.4.4. Accuracy check of coordinate transformation.

After calibration procedure accomplishment some typical loading patterns (see Table 5.4.1) were applied to the blade and images from 4 cameras were simultaneously captured.

Table 5.4.1. DIC load cases

Load case name	Description	Amount of images	Frame rate, FPS
Flap1000us	Standard flapwise fatigue test with max strain range 1000με at cross section 8.25m, station 7 (pressure side cap) at 2.255Hz	100x4 half frame	90.20
Flap2000us	Standard flapwise fatigue test with max strain range 2000με at cross section 8.25m, station 7 (pressure side cap) at 2.255Hz	100x4 half frame	90.20
Flap3000us	Standard flapwise fatigue test with max strain range 3000με at cross section 8.25m, station 7 (pressure side cap) at 2.255Hz	100x4 half frame	90.20

Edge1000us	Standard edgewise fatigue test with max strain range 1000με at cross section 8.25m, station 7 (pressure side cap) at 4.429Hz	100x4 half frame	88.58
Edge1500us	Standard edgewise fatigue test with max strain range 1000με at cross section 8.25m, station 7 (pressure side cap) at 4.429Hz	100x4 half frame	88.58
Phase-Lock2000us/ 1000us/0deg	One of the Lissajous patterns loaded both in flapwise 2.2145Hz and edgewise 4.429Hz (1/2) with max strain range 2000με at cross section 8.25m, station 7 (pressure side cap) at, max strain range 1000με at cross section 5.5m, station 1 (trailing edge) with no phase shift.	100x4 half frame	88.58
Phase-Lock2000us/ 1000us/90deg	One of the Lissajous patterns loaded both in flapwise 2.2145Hz and edgewise 4.429Hz (1/2) with max strain range 2000με at cross section 8.25m, station 7 (pressure side cap) at, max strain range 1000με at cross section 5.5m, station 1 (trailing edge) with 90deg phase shift.	100x4 half frame	88.58

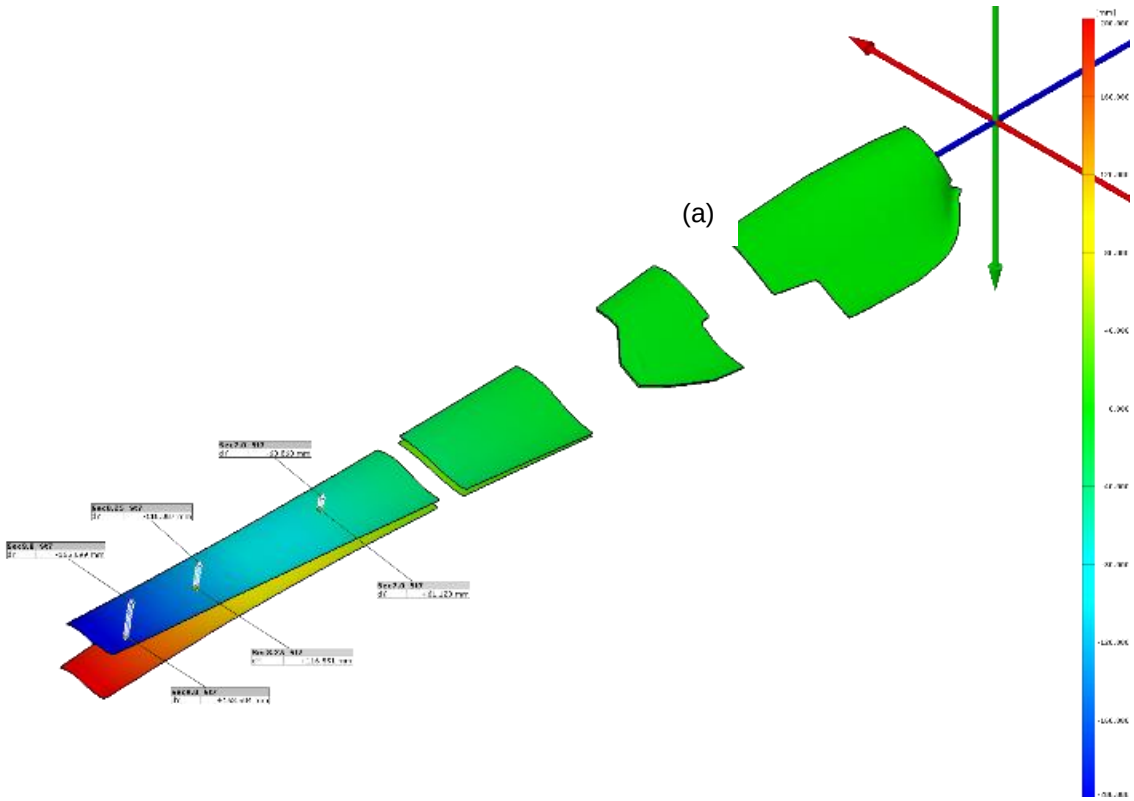

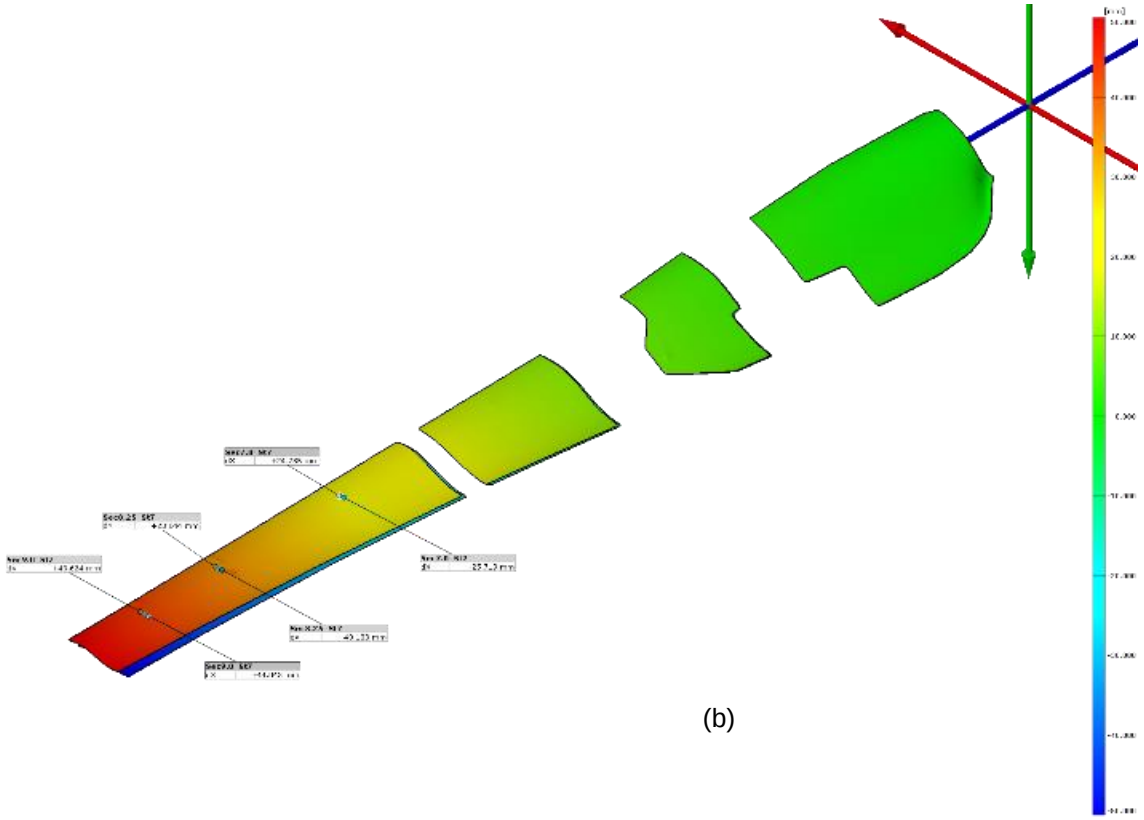

(b)

Figure 5.4.5. Global displacements of the blade surface at ultimate positions for Flap3000us (a) UY and for Edge1500us (b) UX tests.

In Figure 5.4.5 displacement fields (patched because of the mounted equipment) of the blade pressure side surface captured with two stereo systems as well as trajectories of some points (strain gauges on the cap) for standard certification tests.

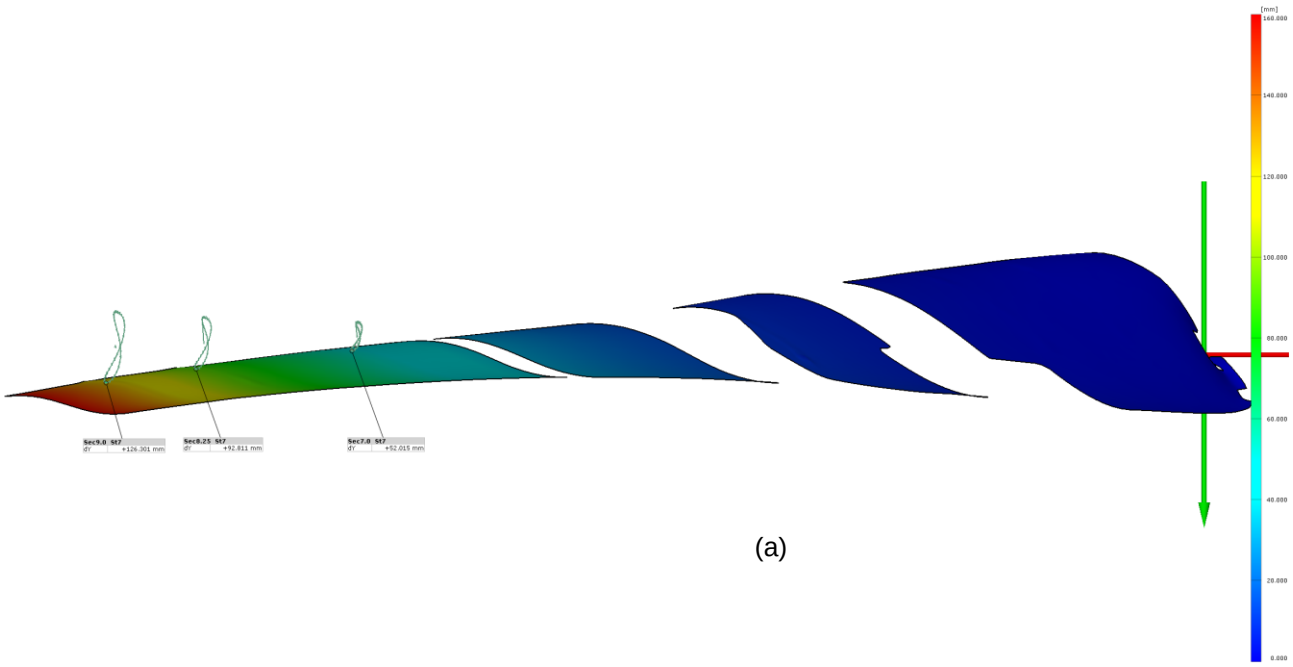

(a)

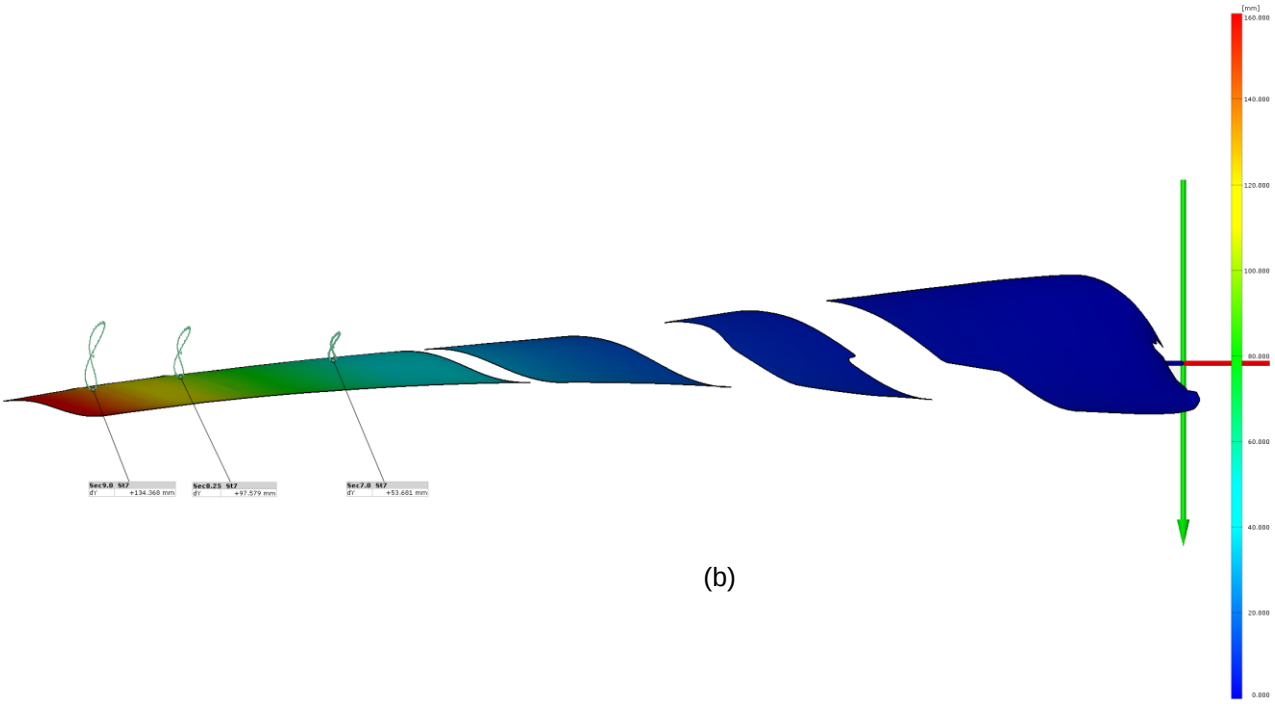

(b)

Figure 5.4.6. Global displacement field (UY) and some trajectories for phase lock loading with (a) no phase shift and (b) 90 deg flap edge shift.

In Figure 5.4.6 vertical (UY) displacement fields and trajectories of some pointes are presented for phase lock load cases.

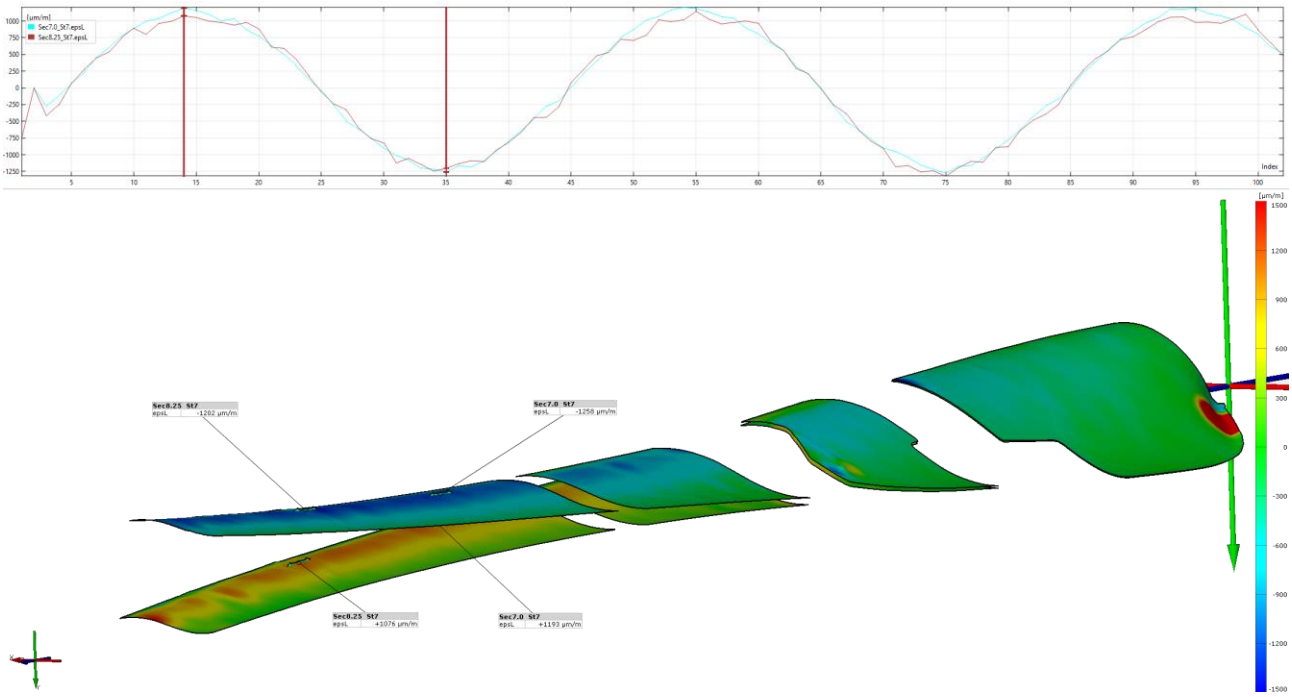

Figure 5.4.7. The longitudinal strain distribution for Flap3000us load case.

In Figure 5.4.7, averaged longitudinal strain distribution and some virtual extensometer values are presented for the flapwise load case.

With obtained results it can be concluded that stiching procedure works and can be used for displacement measurements with high accuracy, strain fields are quite noisy and additional efforts like increasing resolution (amount of stereo systems along a blade) and/or introducing multicamera DIC algorithms should be made to reach accuracy comparable with strain gauges.

5.5 WP5: Development on small blades

5.5.1 Exciter requirement specification

Based on aeroelastic load simulation in WP1 and the test program developed in WP2, a requirement specification was developed for the multi-axis exciter. The simulations provided top-level requirements in terms of necessary excitation position, force, stroke and frequencies as provided in “BLATIGUE-WP2-Design data for 15 m blade test excitation-Rev02” also shown below in Table . The requirements include extra margin to ensure capacity for testing beyond the test plan for the 15m blade (The additional capacity was utilized to test a 49m blade towards the end of the project). Furthermore, interface requirements between exciter and adjacent systems were identified (blade, foundation, power supply, DAQ).

Table 5.5.1 Design parameters 15m blade exciter.

Direction	Force [kN]	Stroke [m]	Frequency [Hz]
Flap	± 10.0	± 0.125	2.5
Edge	± 3.0	± 0.050	5.0

The parameters provided in Table are meant to define the load and displacement envelopes shown in Figure 5.5.1. The depicted force envelope is possible within the entire position envelope (milestone M5).

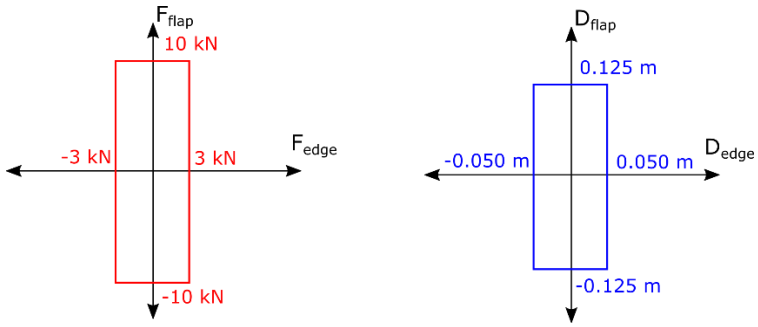

Figure 5.5.1 - Possible force and position envelope.

5.5.2 Exciter concept development

Based on the requirement specification and an investigation of existing IP rights (milestone CM1), a number of exciter concepts were drafted and assessed. An electro-mechanical exciter concept for single-axis flap excitation is used as the basis for a novel dual-axis excitation concept. The dual-axis excitation concept is shown as Configuration C in Figure 5.5.2. This arrangement allows for independent control of flap and edge excitation through control of the two exciter units.

Configuration A Flap tests on two individual blades.	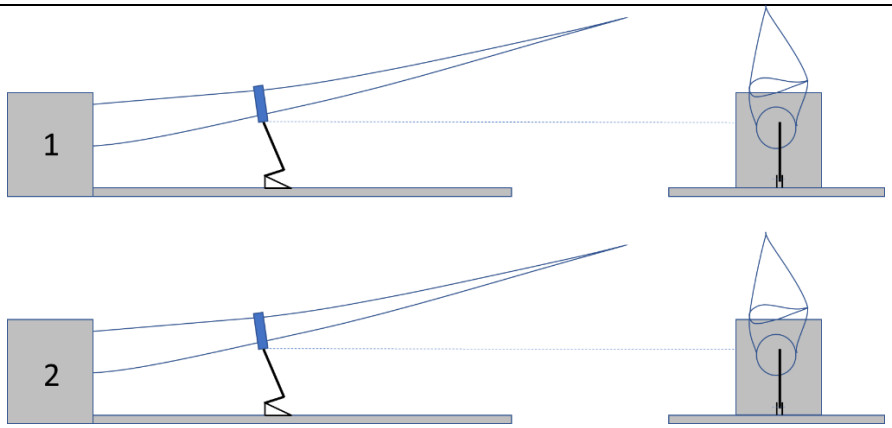
Configuration B Parallel test with two flap exciters on two yokes (gaining extra force).	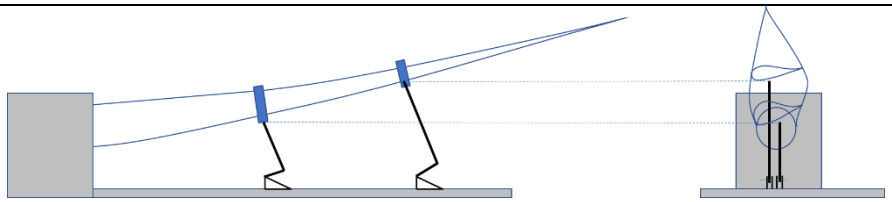
Configuration C Dual-axis test where both exciters connect to the same yoke.	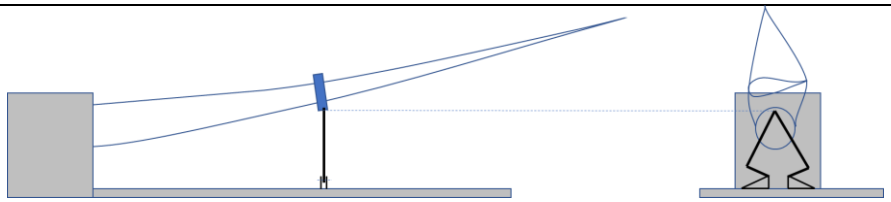

Figure 5.5.2 – Possible excitation configurations with modular ground-based exciter concept using two exciter units.

Based on the requirement specification and the concept choice described above an exciter design was completed.

The exciter design is generally divided into the following main systems:

- Drive line and bottom frame
- Rocker arms and push rods
- Blade yoke

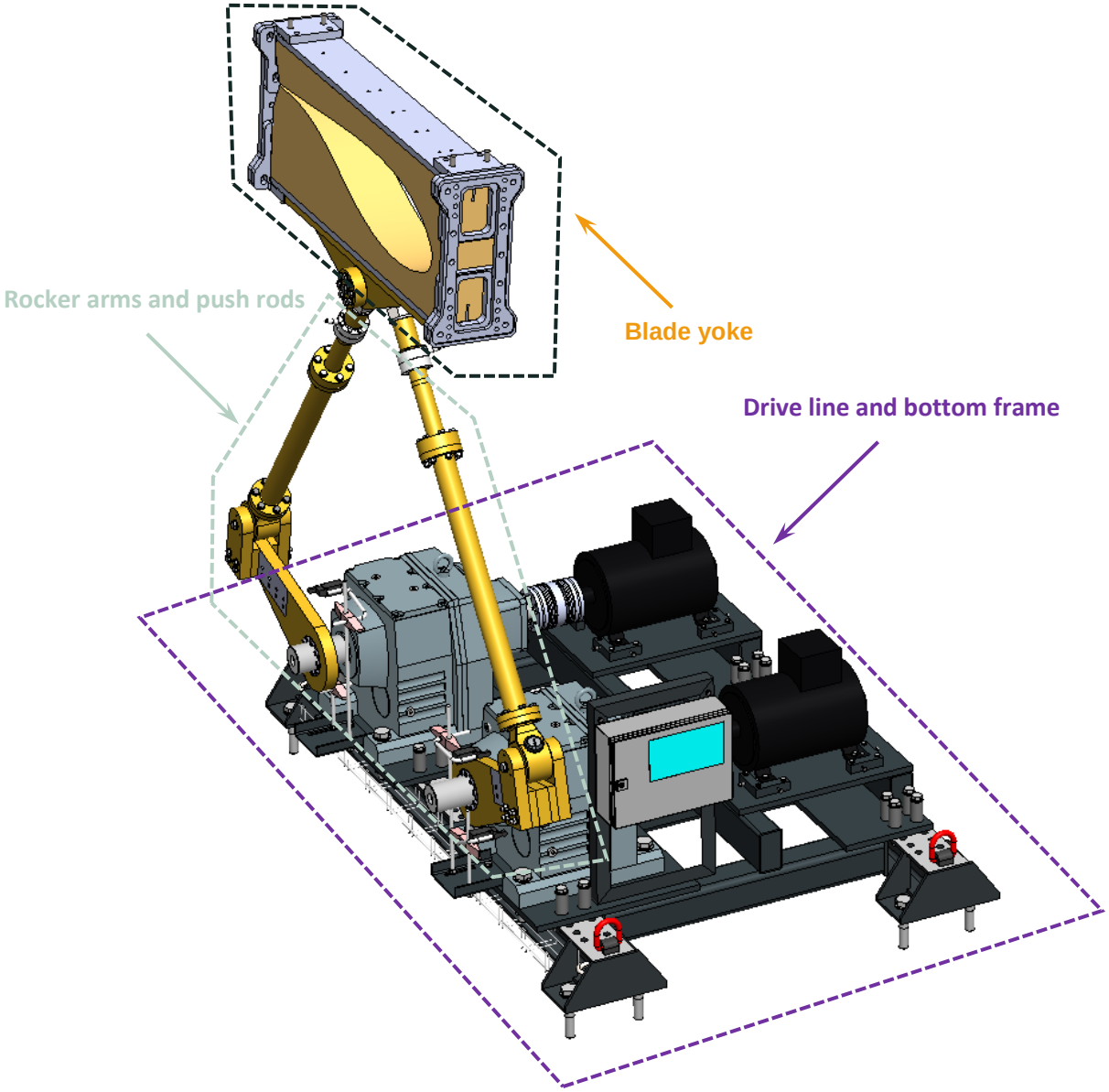

Figure 5.5.3 Small blade exciter design (version 1)

The finished design of the first version of the exciter is shown in Figure 5.5.4. Each exciter unit applies force to the blade through a linkage mechanism (push rod and exciter arm) connected to a single gearbox driven by a permanent motor controlled by a variable frequency drive. The two exciter units are controlled together to apply the requested resultant force input to the blade.

Figure 5.5.4 – Version 1 of the Small Dual Axis Exciter mounted with 14m blade at the DTU test facility

Version 1 of the exciter was commissioned in 2018 at DTU Large-Scale Facility and tested with a 14m Olsen Wing. During commissioning of the first version of the ground-based dual-axis exciter it was observed the machine was not able to track the force reference as closely as desired. Different excitation trajectories were tested; edge, flap and various dual-axis combinations. In each excitation mode during force reversal it was observed that the force applied to the blade had significant overshoot as shown in Figure 5.5.5. Furthermore, the exciter produced significant noise and non-smooth operation. The issue was investigated and found to be due to backlash in the gearbox causing a torque spike during torque reversal when the gear mesh changes engagement from one tooth flank to the other. A control solution which previously had been applied successfully in single-axis configuration (i.e. Configuration A in

Figure 5.5.2) was tested on the dual-axis configuration. However, this solution was not found to mitigate the spike issue sufficiently and hence another solution was sought.

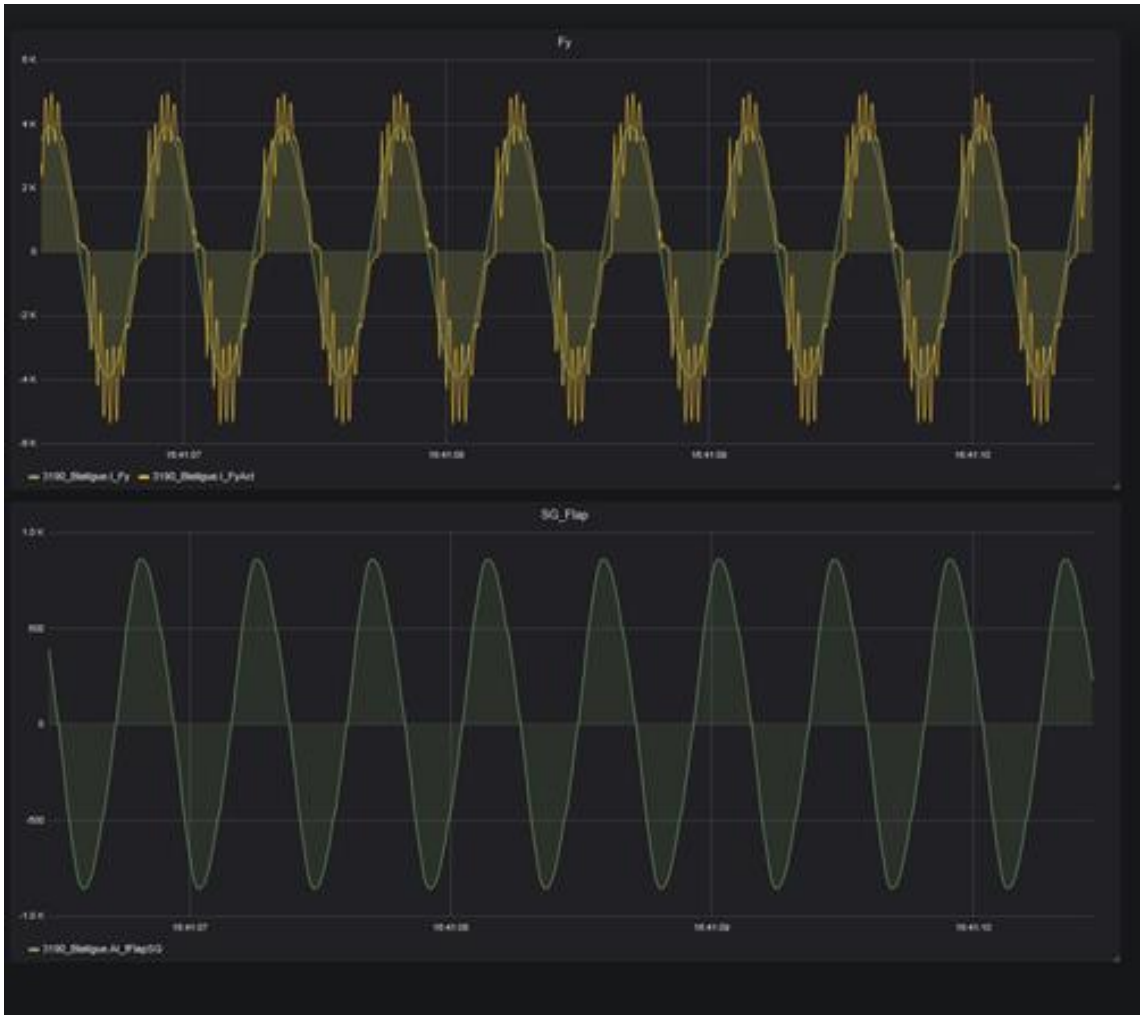

Figure 5.5.5 – Flap force for exciter version 1. F_ref = 3900 N

5.5.3 Exciter concept development – Version 2

The design for version 2 of the exciter was updated with a novel driveline concept to reduce the backlash induced force ripples in the force application. The R&D patented backlash free drive line concept relies on two gearboxes attached to a single hollow axle permanent motor. The bottom frame, rocker arms and push rods from the first iteration of the exciter were reused for version 2 as shown in Figure 5.5.6.

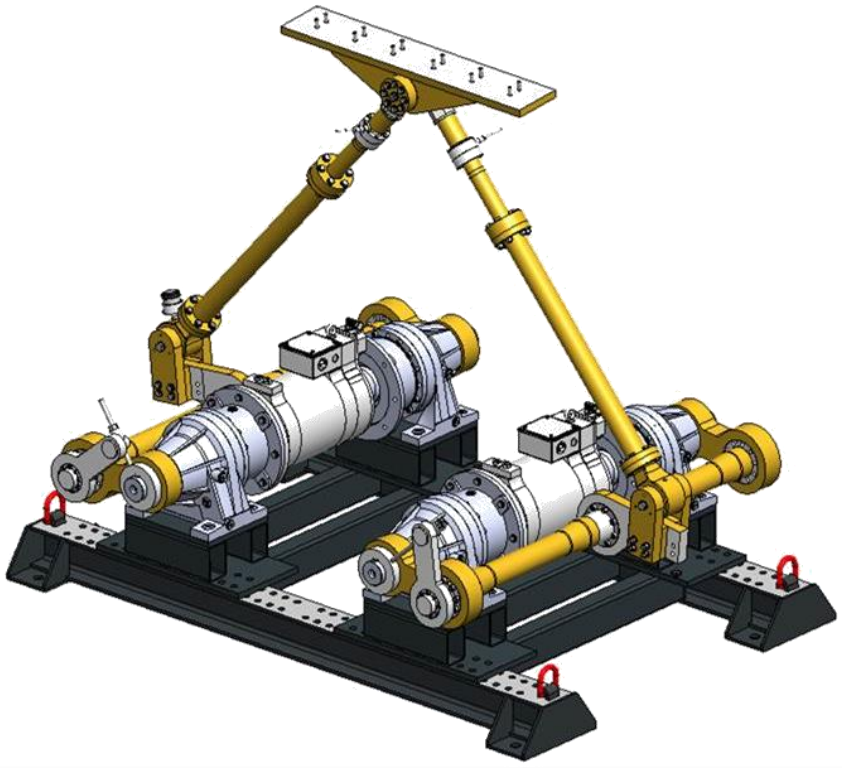

Figure 5.5.6 – Small blade exciter design (version 2)

During commisioning of the eciter the force application was compared to that of the version 1 of the exciter to monitor the effect of the updated driveline design. As seen in Figure 5.5.7 the force spikes during testing were greatly reduced with the updated design.

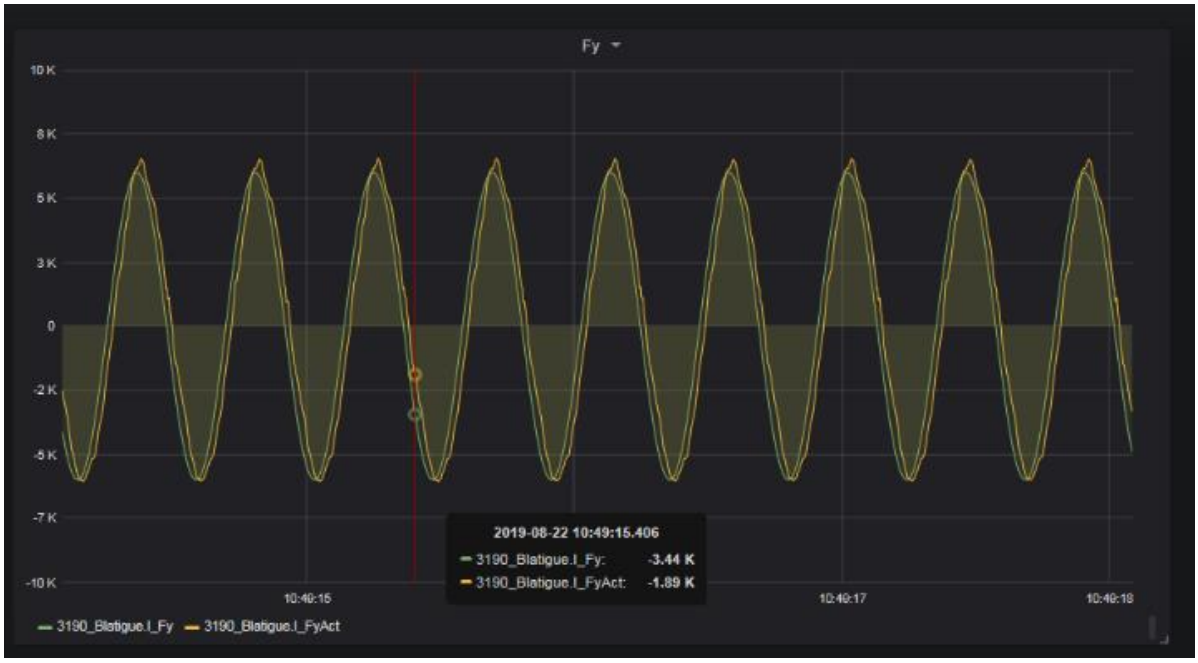

Figure 5.5.7 – Flap force for exciter version 2. F_ref = 6000 N

5.5.4 Summary

The output of the small exciter development in WP5 was a successful demonstration of a viable dual axis exciter concept. During the work package the design underwent to iterations, with the second iteration being based on a novel backlash-free driveline concept. The exciter concept and driveline design were used as basis and input for the large exciter designed for testing full-scale commercial blades.

Figure 5.5.8 – Dual axis exciter version 2 with backlash-constrained drivetrain installed at DTU Large-Scale facility during test.

Reports/deliverables

[1] BLATIGUE-WP2-Design data for 15 m blade test excitation-Rev02, rev. 02, 2017-07-03 (milestone M5)

[2] Design Description – Small Exciter, rev. 02, 2017-10-30 (milestone M6)

[3] Market and competition analysis, 2019-06-25 (milestone CM2)

[4] Factory Acceptance Test Protocol, rev. 02, 2018-07-08 (milestone M8)

[5] Site Acceptance Test Protocol, rev. 03, 2018-07-12 (milestone M9)

5.5.5 1D mass development and demonstration

5.5.5.1 1D-mass description

The 1D-mass is a tool that be used for reducing the resonance frequency of the blade in flap-wise direction without affecting the edge-wise resonance frequency.

The 1D-mass tool consists of a saddle with a rail, on which a mass can move freely edge-wise but will follow the motion of the blade in the flap-wise direction. The mass is fixed (in this case to the wall of the test facility) in edge-wise direction so it does not fall of the blade. Since the blade motion is only affected in the flap-wise direction, we call it a 1D-mass.

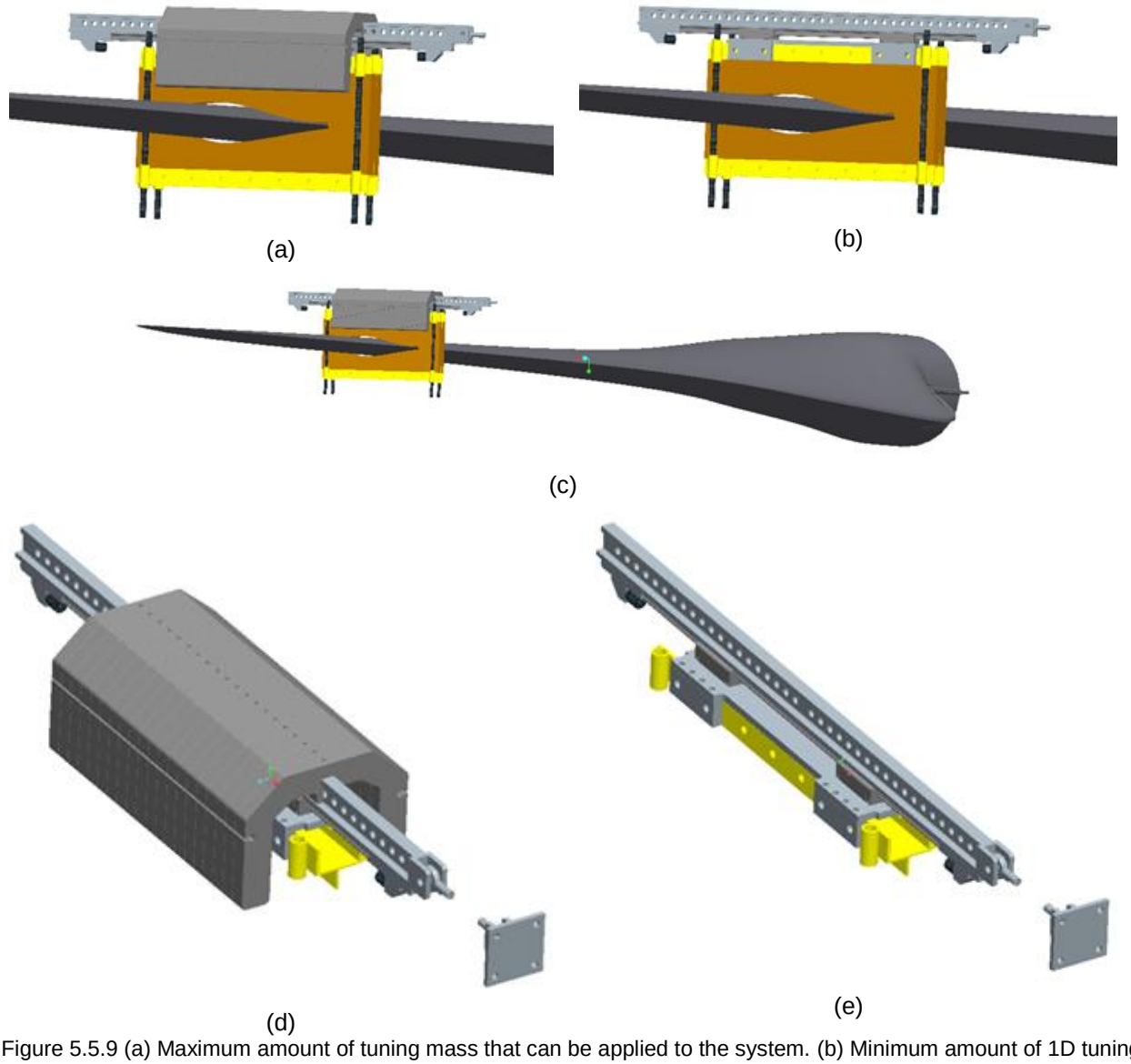

Figure 5.5.9 (a) Maximum amount of tuning mass that can be applied to the system. (b) Minimum amount of 1D tuning mass the system can apply. (c) Depicts the 1D tuning mass placed at radial position 10m (center picture)). (d) and (e) 1D mass system mounted onto a standard load saddle used at DTU.

A series of test was performed with the RD-exciter on an OW1430 blade to demonstrate the 1D-mass (milestone M12). The test set-up is shown in Figure 5.5.9.

Figure 5.5.10. Test set-up, 0W1430 blade, R&D exciter and 1D-mass (rail only, no added mass). Load saddle is located at 5,2m, the 1D-mass saddle at 10m.

First part of the test was to run a biaxial fatigue-test with varying mass on the saddle rail. The mass was varied from no additional mass (except the weight of saddle and rail) and up to 305 kg of mass mounted on the rail. In Table 5.5.2 the frequencies and their ratio are listed for different added masses. It can be seen that the 1D-mass can be used to reduce the flap-wise frequency by a third, and thereby increase the edge/flap-ratio from 2 to 3.

Table 5.5.2. Tests with increasing 1D-mass and corresponding resonance frequencies.

Mass [kg]	Flap frequency [Hz]	Edge frequency [Hz]	Ratio [m]
0	1.97	4.02	2.04
60	1.77	4.01	2.27
90	1.72	4.01	2.33
120	1.63	4.01	2.46
130	1.60	4.01	2.50
200	1.48	4.01	2.71
305	1.34	4.01	3.00

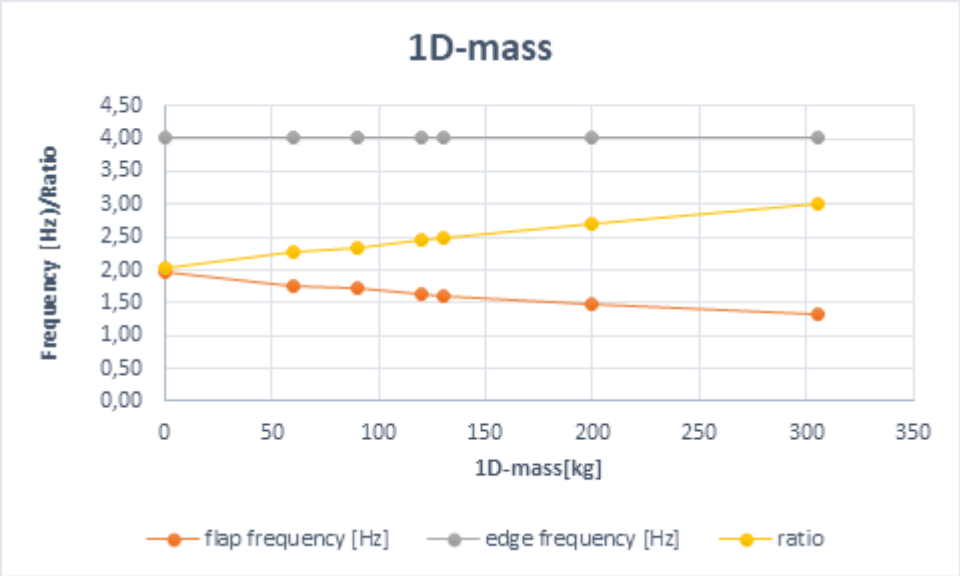

Figure 5.5.11. Resonance frequencies as 1D mass is increased (data from Table 5.5.2).

By use of the 1D-mass it is thus possible to obtain integer ratios between flap- and edgewise resonance frequencies, in this case we get a 2:5 ratio and a 1:3 ratio using 130 kg and 305 kg 1D-masses respectively.

5.5.5.2 Phase-locked biaxial testing by use of 1D-mass

With an integer ratio between flap- and edgewise resonance frequencies it possible to control (within limits) how the blade is loaded. To demonstrate this we have run a number of test with a 1:3 ratio between the flap- and edgewise resonance frequencies and varying the phase between the flap-wise and edge-wise force of the R&D exciter.

The figures 5.5.12 below show how the strains vary with the phase at the 7m cross-section of the blade. On the x-axis is the strain on the LE, and the curves show the strain at the center of the two spar caps. In figure (a) the flap-wise force is in phase with the edge-wise force, in following figures (b) to (m) phase-shift is added. A biaxial test where there is no integer ratio between the flap- and edgewise force would correspond to an overlay of all figures. In figure (a) (no phase the strains are at maximum simultaneously, while in figure (k) (180° phase shift) strains on the spar caps are at maximum when the strains on the LE are at minimum and vice-versa.

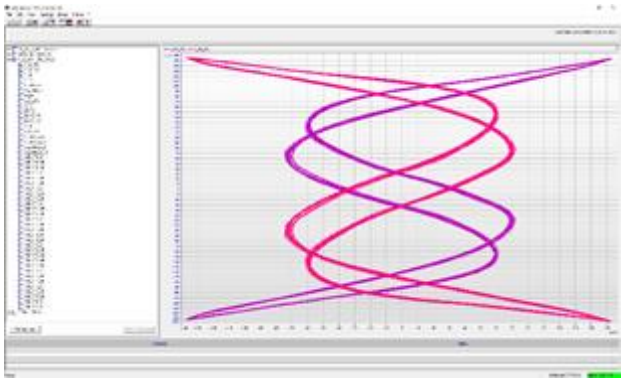

(a) 0° phase shift

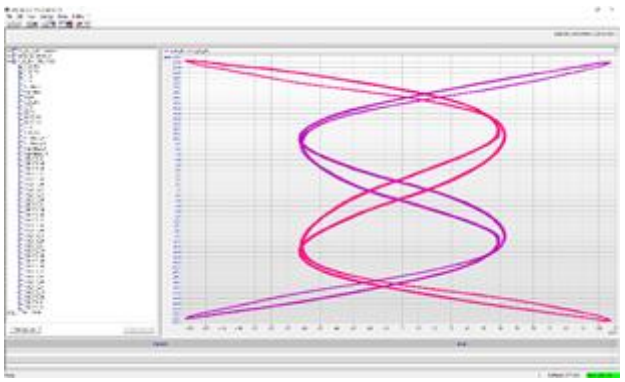

(b) 30° phase shift

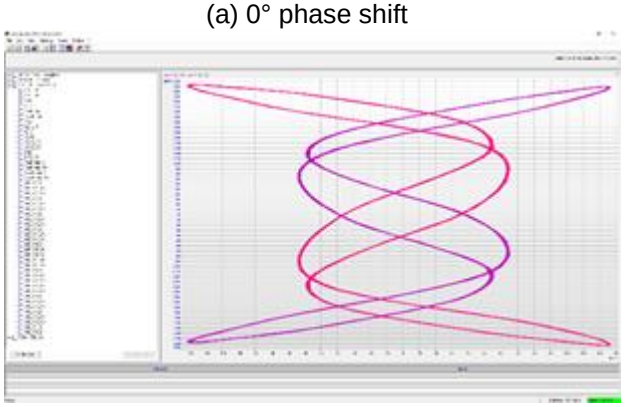

(c) 45° phase shift

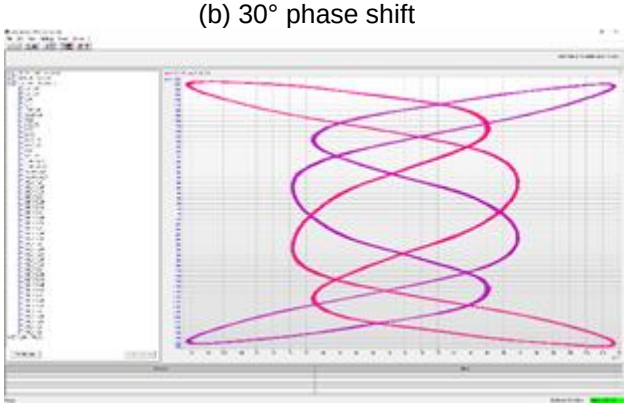

(d) 60° phase shift

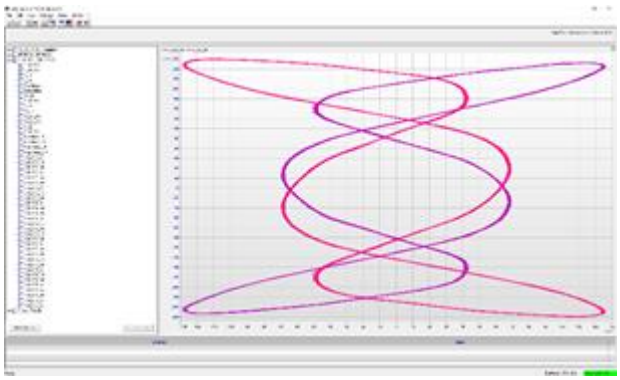

(e) 67.5° phase shift

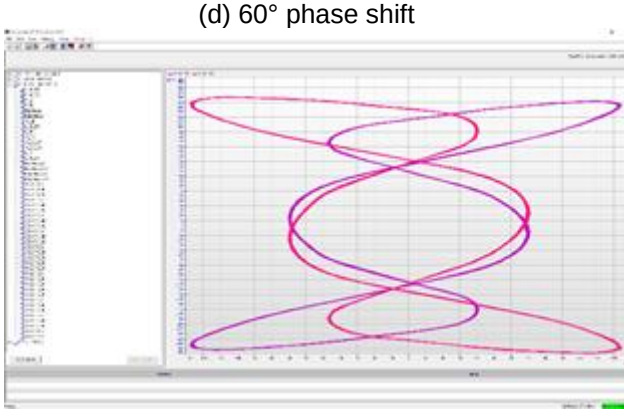

(f) 75° phase shift

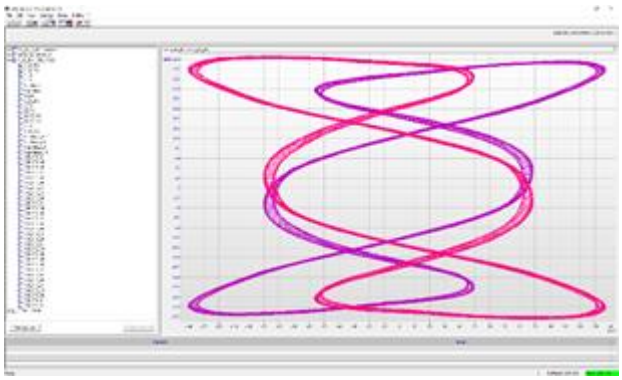

(g) 90° phase shift

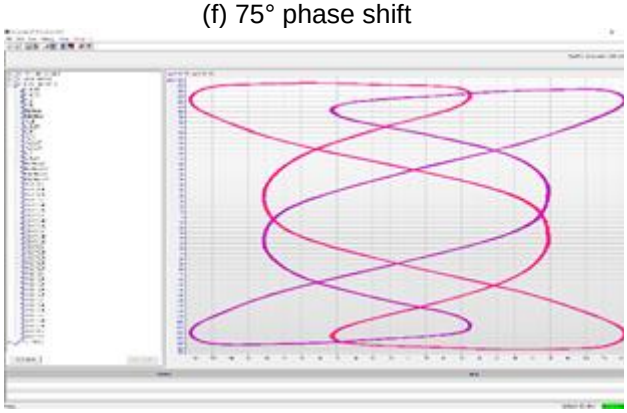

(h) 120° phase shift

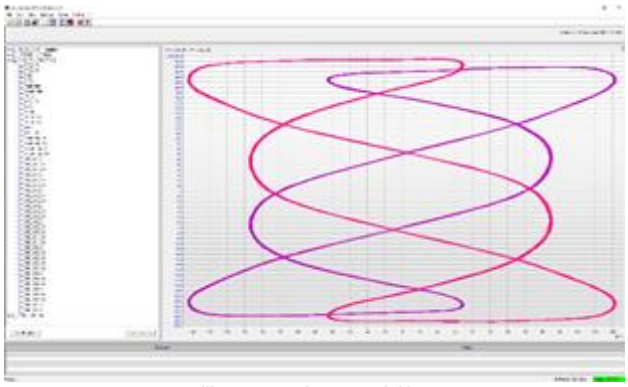

(i) 135° phase shift

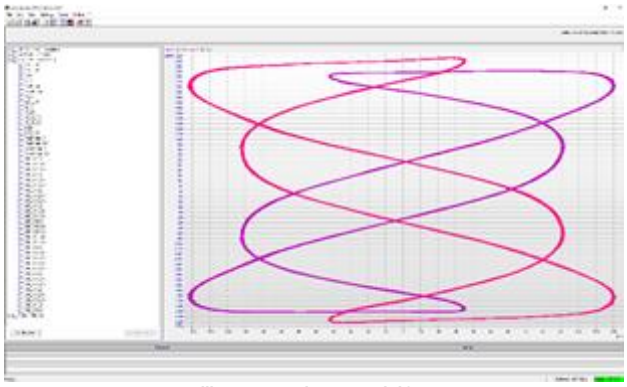

(j) 150° phase shift

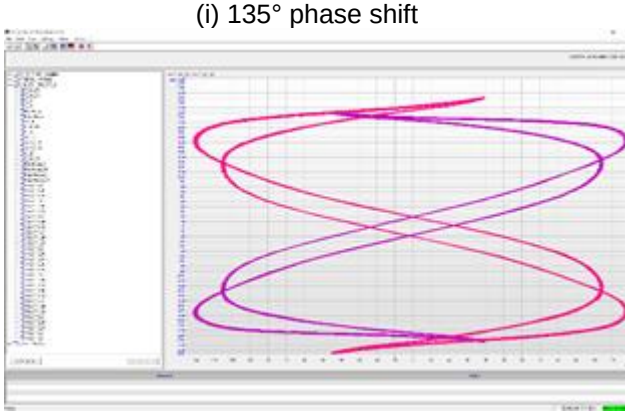

(k) 180° phase shift

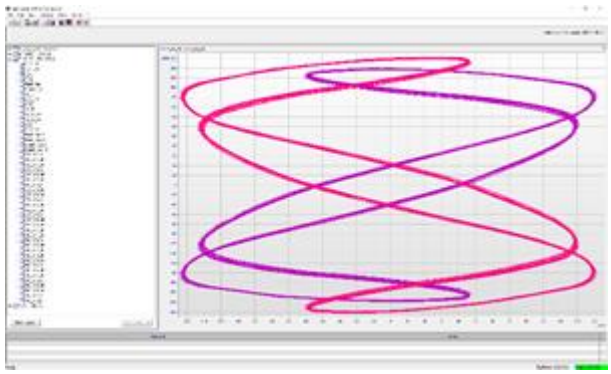

(l) 225° phase shift

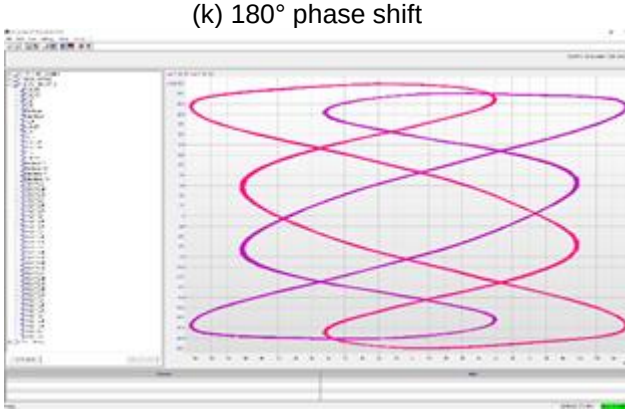

(m) 270° phase shift

Figure 5.5.12. Strain envelopes at different phase shift angles

5.5.6 Blade with defects

5.5.6.1 Damage propagation results for the different artificial defects

The overall objective with designing the different artificial defects were to show that the damage propagation depends on the fatigue load configurations and that some damages are not triggered by standard single axis fatigue testing, as indicated via finite element simulations.

The overall conclusion is that it was not possible to experimentally showcase that the damage propagation rate of the different artificial defects was significantly different when applying dual axis fatigue loading. Presented below are the experimental results for the different artificial defects and a description of the effort

performed to during the test campaign to generate a level of damage propagation which could be determined and reported.

The wrinkles was trigger mainly by flapwise fatigue loading as expected. The damage propagation of the wrinkles grew into delaminations and grew significantly faster than the other defects. Via visual inspection it was possible to quantify the crack front of the delamination resulting from the wrinkles, as the wrinkles were located close to the outer surface. Other means of monitoring the damage propagation was also applied, such as DIC and thermal imaging.

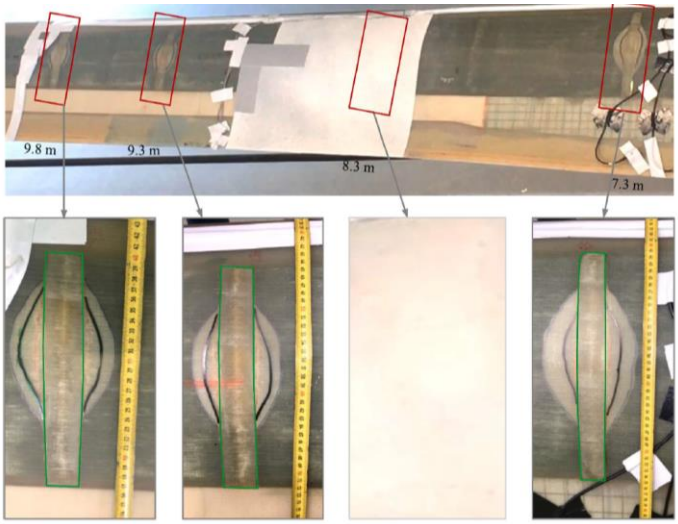

Figure 5.5.13. Shows damage propagation of the wrinkles/delaminations. The one covered with white paint was measured via DIC and thermal imaging.

For both the debonding between skin and core (type SD#) and the debonded zones in trailing edge (type TD#) only very limited damage propagation were observed during the first part of the fatigue testing campaign.

The deviation between numerical- and experimental results can partly be explained by:

- The foil used for both the debondings between skin and core and debonding in the trailing edge zones did not create regions, which were fully debonded as, expected. Both glue and resin had still some level of bonding to the foil.
- The debonded regions in the sandwich panels were also affected by a difference between the layup used in the manufacturing at Olsen Wings and what was used in the models. In the manufacturing an overlap of triax fabric through all debonded regions in the sandwhich panels are used. The models applied for designing this type artificial defect doesn't have this overlap. This will significant effect the local response of the debonded skin layers.
- Olsen Wings has very thin trailing edges and a very thin adhesive layer. This creates a stronger adhesion than seen in simulations as the crack will not propagate in the glue but kink into the laminate and this will result in fiber bridging and a higher fracture toughness.
- Vacuum effects in the void between skin and core was not included in the simulations but in the real blade it prevented or minimized the out-of-plan response of the debonded regions in the sandwich panels.
- The wrinkles to some extent prevented applying higher flapwise loads as it would result in complete failure of the blade.

To speed up the damaged propagation rate, for the two types of debonding, the following was performed:

- A small hole was drilled in the center of the fully debonded regions for the three debondings (type SD#). This was performed to remove the vacuum effects, see Figure 5.5.14. After drilling the holes larger out-of-plan displacements were observed.
- With a heat gun a small out-of-plan imperfection was added to the debonded region SD#2. This also increased the out-of-plan response and the response became more similar to the numerical predictions.
- In the trailing edge regions the monolithic laminates in the trailing edge were mechanically pulled apart to ensure a fully debonded region.

The described measures above increased the damage propagation but it was still not possible to quantify the propagation rate coming from different fatigue load configurations. Most likely, the damage propagation for the different artificial defects was not stable as jumps in the size of the damaged zones were observed.

Furthermore, it was very difficult to quantify the damaged zones based on visual inspections. This was the case both for the debonding between core and skin but also for the debonding in the trailing edge, where it was difficult with high certainty to determine the crack front.

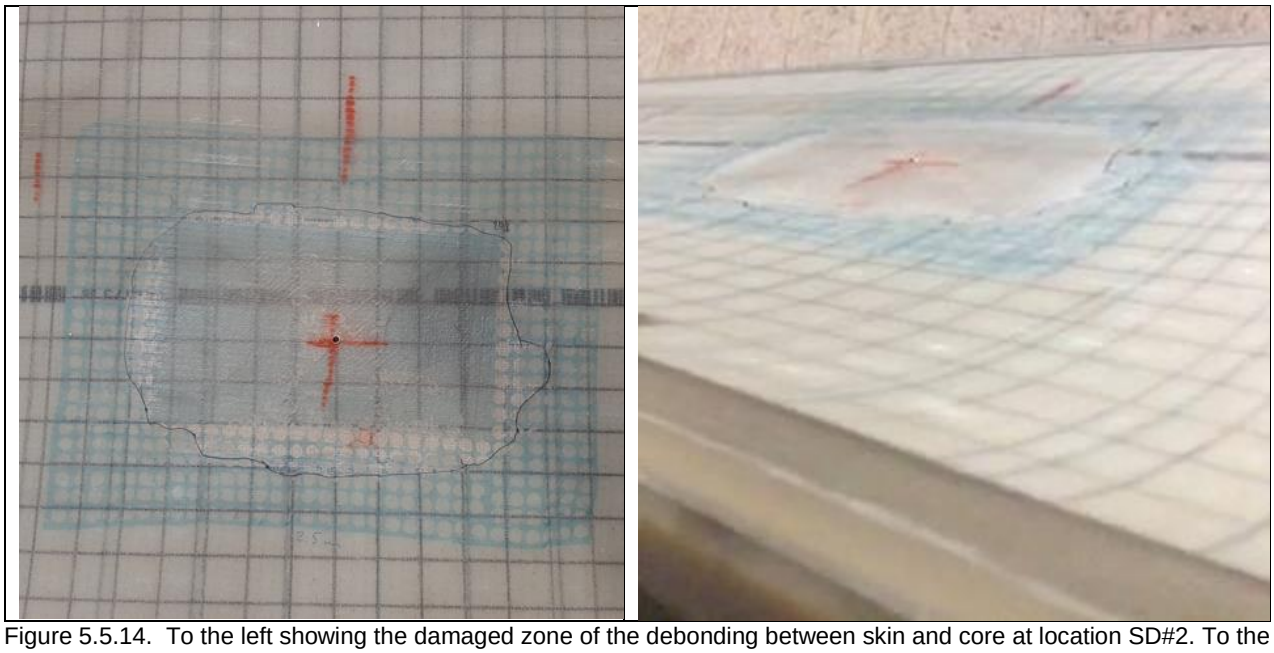

Figure 5.5.14. To the left showing the damaged zone of the debonding between skin and core at location SD#2. To the right a picture extracted from a video showing how the debonded region buckles out during fatigue loading.

Attached along with the final Blatigue report is also a video (debonding_SD#2_fatigue_loading) showing the out-of-plan response for debonding SD#2 subjected to dual axis fatigue testing. On this video, a whistling sound can be heard. This sound comes from air moving in and out of the void between skin and core.

In the late stages of the fatigue test campaign the two debonded zones in the trailing edge was mechanically increased into one large debonding. Still this did not result in the speeded up damaged propagation as expected. Presented below are pictures extracted from a video of the dual axis fatigue testing moving in a c-shape pattern. The three pictures shows the outer positions during one load cycle. This response is similar to the numerically computed bucling response of the trailing edge. Attached along with the final Blatigue report is also a video (*TE_debonding_fatigue_loading*).

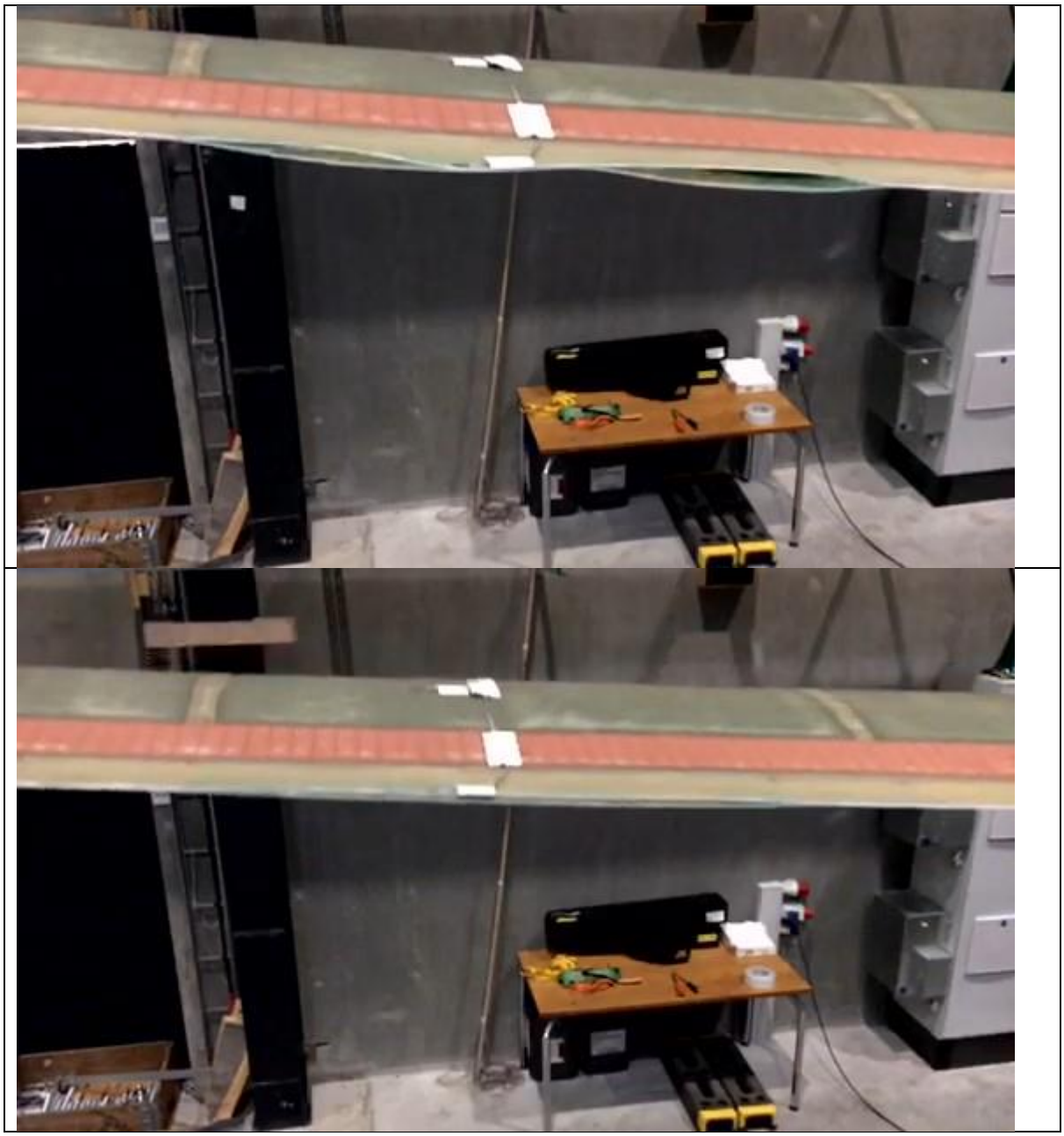

Figure 5.5.15. Showing the three outer position during “one load cycle”. The blade moves in a C-shaped pattern.

5.5.7 1D damping using blade mounted liquid container

Phase locked biaxial testing can be obtained by applying relevant 1D masses at selected sections of the blade length, hence obtaining relevant desired frequency ratios. The technique yields several advantages, but as the application of masses reduces frequency while increasing the obtained moment, over-testing of areas can be an undesired effect of tuning phase locked biaxial testing by masses only.

The demonstrated 1D mass methodology shows beneficial properties in the selected test setup, while other test setups could challenge the mechanical system. As large-scale blade testing to some extend is performed outside at test centres, the anchor points for the system can be tedious to realize. As the mechanical system is highly dependent on blade test edge- ad flap-frequency, changes in the frequency caused by e.g. structural fatigue in the blade or stiffness changes resulting from temperature changes, external effects can limit the system performance.

In order to reduce effects from over testing and limit external constraints, a blade based 1D damping system was examined in the project. The concept consists of container with a selected amount of liquid attached to the blade. By dimensioning the volume, amount of water and the total mass of the system, it is possible to tune the system eigenfrequency in e.g the edgewise direction, hereby damping the blade in one direction only, see figureFigure 5.5.16. Principle of 1D damping.

The principle has been protected through patent application, while testing of the system in reality has been limited.

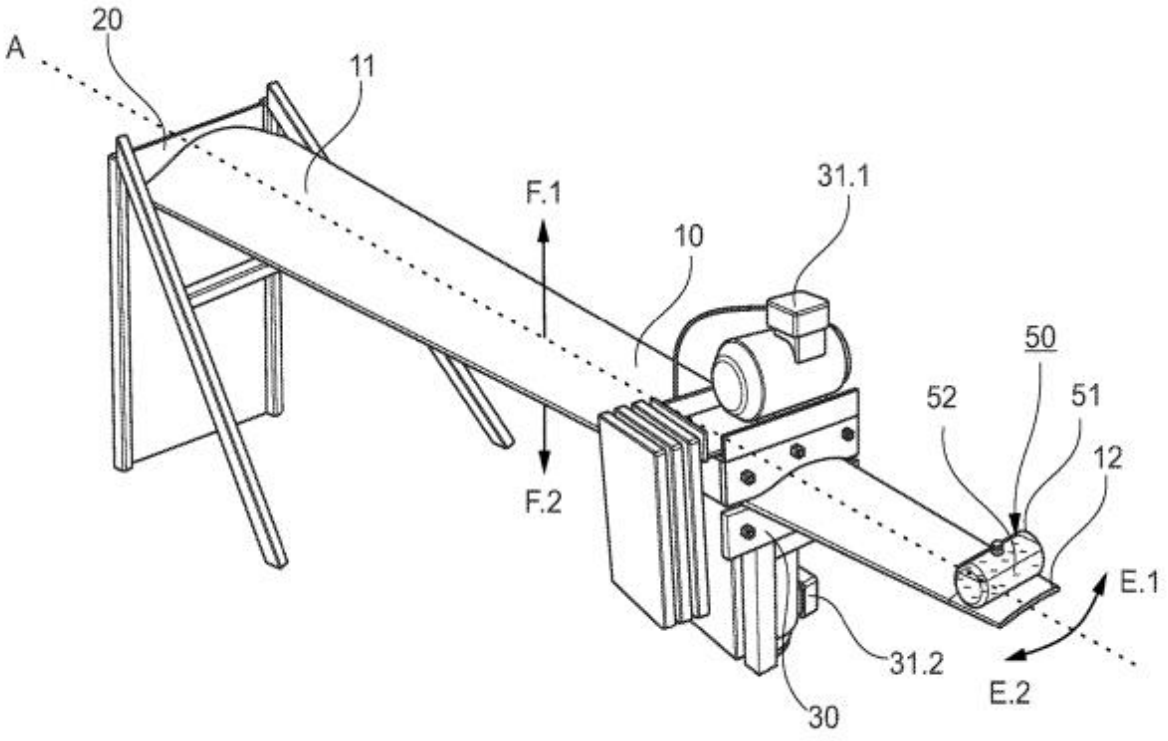

Figure 5.5.16. Principle of 1D damping

5.5.8 Small scale bi-axial phased locked trials

As the BLATIGUE project has targeted to demonstrate biaxial testing on a large offshore blade, it has been important not only to develop theory, but in parallel collect experience from small scale trials. SGRE has been home for the first trials where theory was showcased on small scale.

First small test setup was setup using a wooden stick, in order to have a test specimen with uniform stiffness and different edge- and flap frequencies. The stick was fixed in one end and small electrical “exciters” and dead masses could be added to the specimen. Strain gauges were installed at relevant positions, enabling the control of the exciters using real-time measured strains, similar to large scale testing

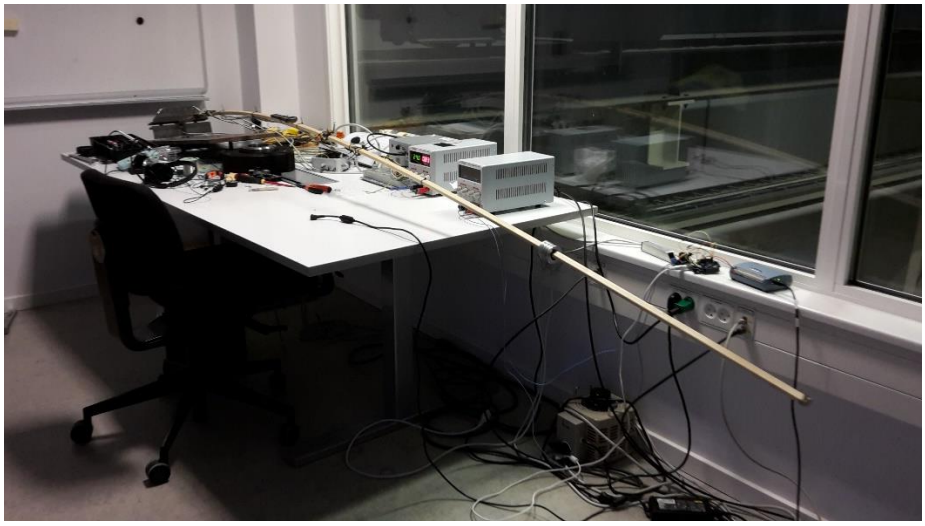

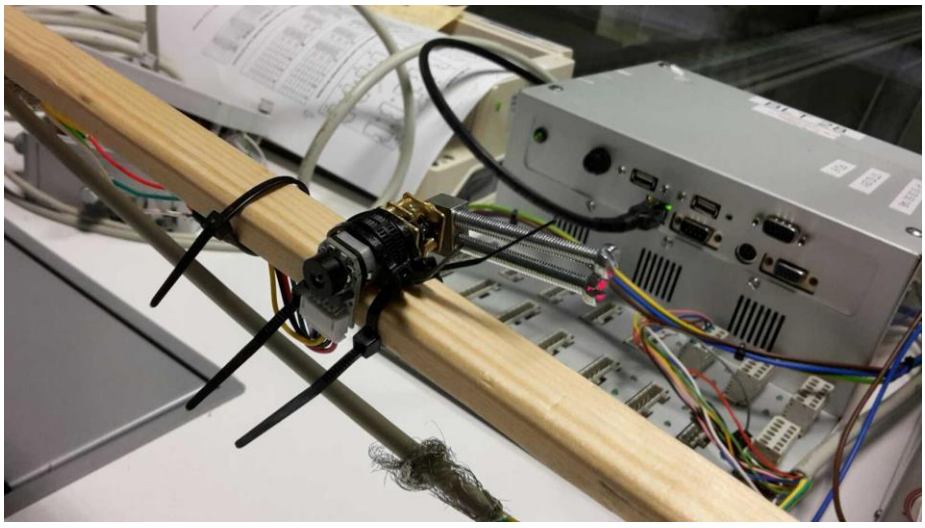

The eigenfrequency of the wooden stick was measured with the following results:

- 1st flap: 0.833 Hz
- 1st edge: 1.144 Hz

- Flap/edge ratio: 72.8%

By tuning the setup using small masses, SGRE was able to obtain a ratio of ¾ between flap and edge. The test frequencies were then:

- 1st flap: 0.82 Hz
- 1st edge: 1.09 Hz = 0.82 /3*4 Hz

Theoretically the phase locked biaxial test should, based on the frequency ratios and phase lock, provide a pattern in the displacement of the wooden stick with the following pattern:

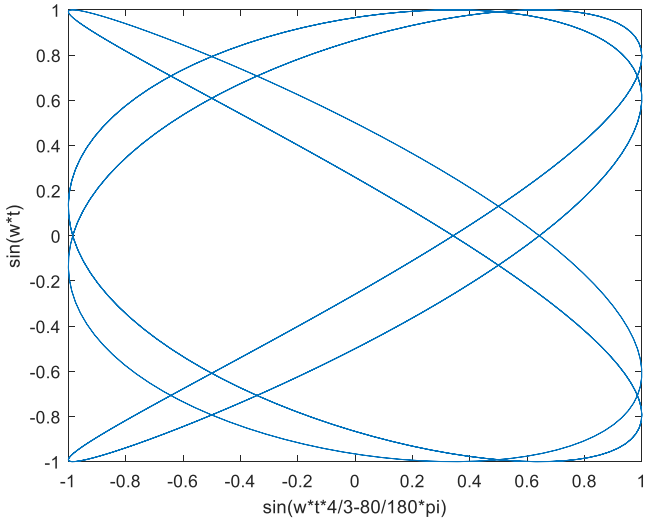

As displacement was not measured, the ranges in strain values measured in the edgewise and flapwise direction was collected and the results shows that SGRE was able to obtain strain range time series in the same pattern as expected:

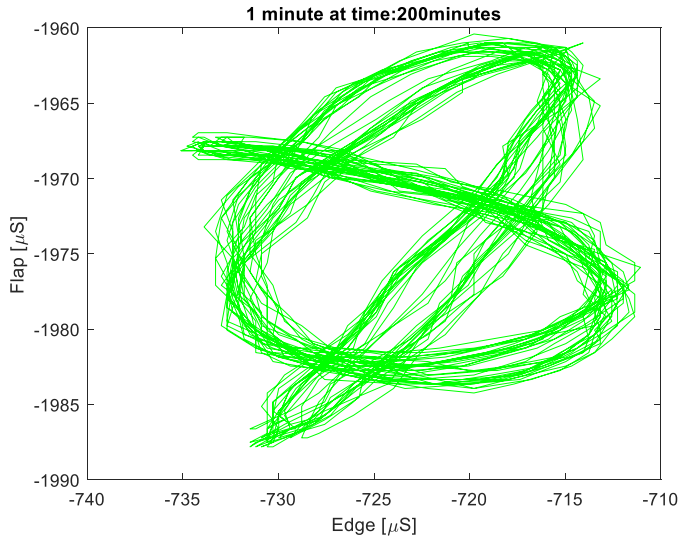

The following step was to exchange the wooden stick with a larger test specimen. As Olsen Wings were part of the consortium, it was agreed to use a OLW 510 blade (5.1 m blade for 15-20 kW generators) for the small scale trials

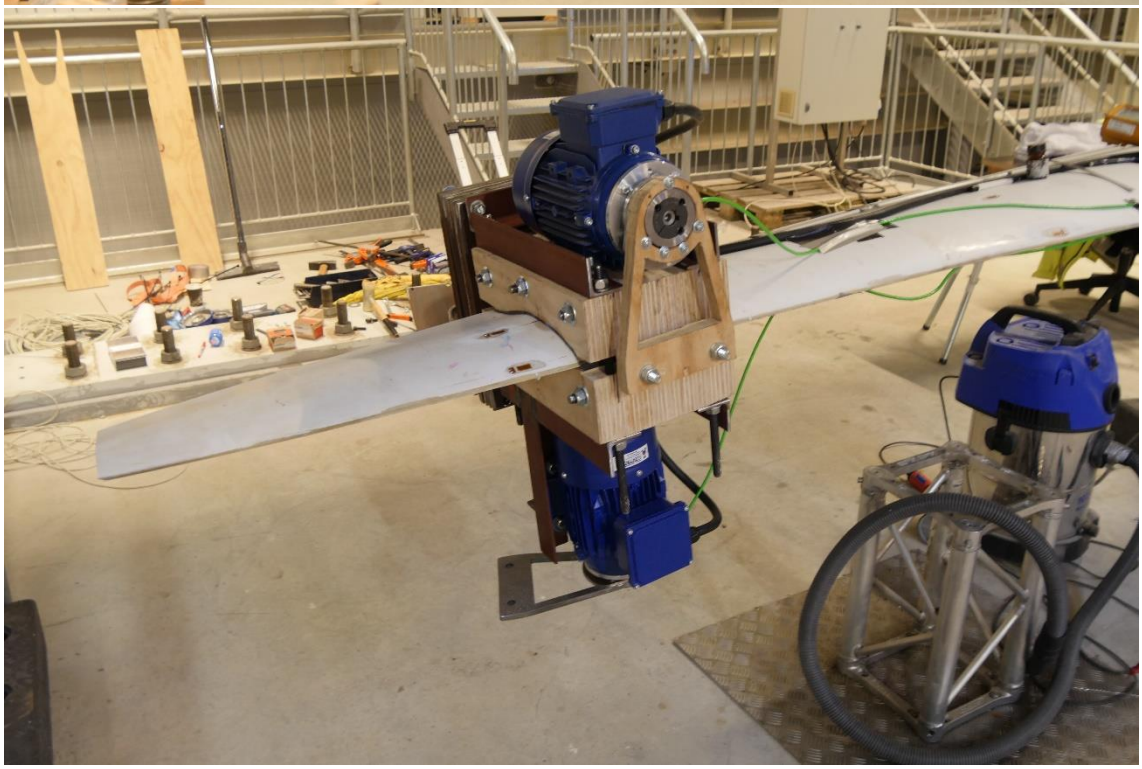

Exciters using rotating masses were installed on the blade, and the control was designed using strain in edge- and flap-wise direction as input.

The eigenfrequency of the OWL 510 blade was measured with the following results:

- 1st flap: 1.390 Hz
- 1st edge: 2.300 Hz

- Flap/edge ratio: 60 %

By tuning the setup using small masses mainly on the exciters, SGRE was able to obtain a ratio of 2/3 between flap and edge. The test frequencies were then:

- 1st flap: 1.380 Hz
- 1st edge: 2.070 Hz = 1.38 /2*3 Hz

The expected result based on the frequency ratio and the angle of the phased locked testing was similar to what was obtained by mapping the strain range for edge and flap:

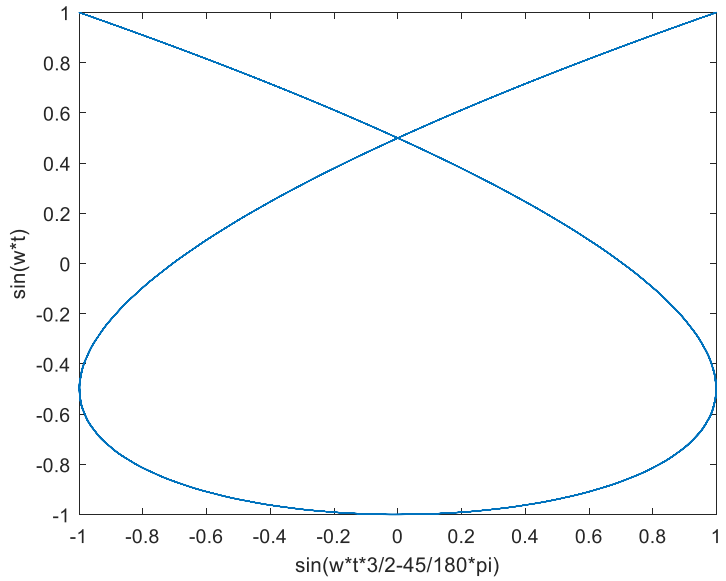

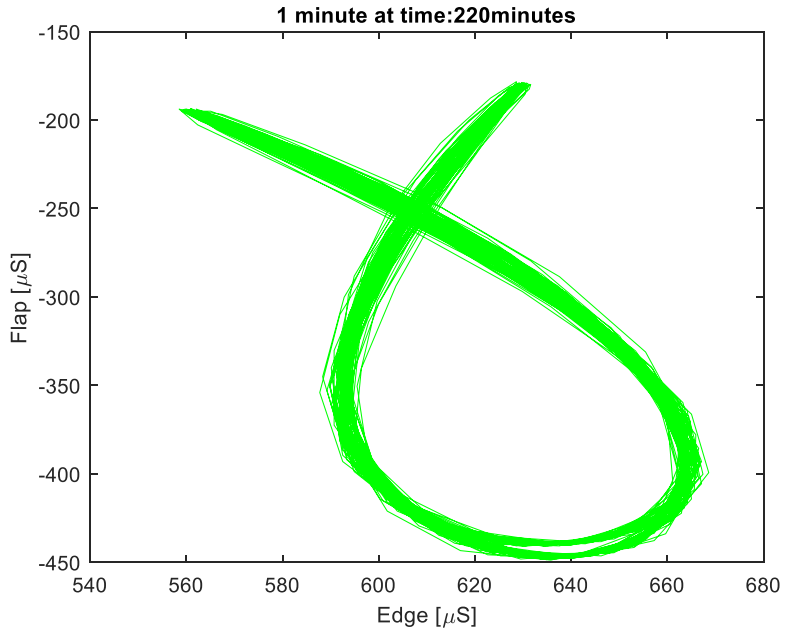

It was concluded that phased locked bi-axial testing using rotating mass excitation was possible on small test specimen with both uniform and irregular stiffness along the length of the specimen.

5.5.9 Demonstration of the developed fatigue test method on the OLW1430 blade

The demonstration of the developed multi-axial fatigue testing method on the OLW1430 blade was achieved (milestone M3), see Figure 5.5.17. The method was used to design a fatigue test campaign, in which an optimal combination of two edgewise tests and four chaotic test blocks was shown to save approximately half of the test time in comparison with the standard tests while reaching the strain-based target damage in all blade regions. While the standard test requires 15.8 days to complete the test for this blade, the obtained optimal test campaign requires 8.0 days. The suggested test blocks were experimentally demonstrated with success.

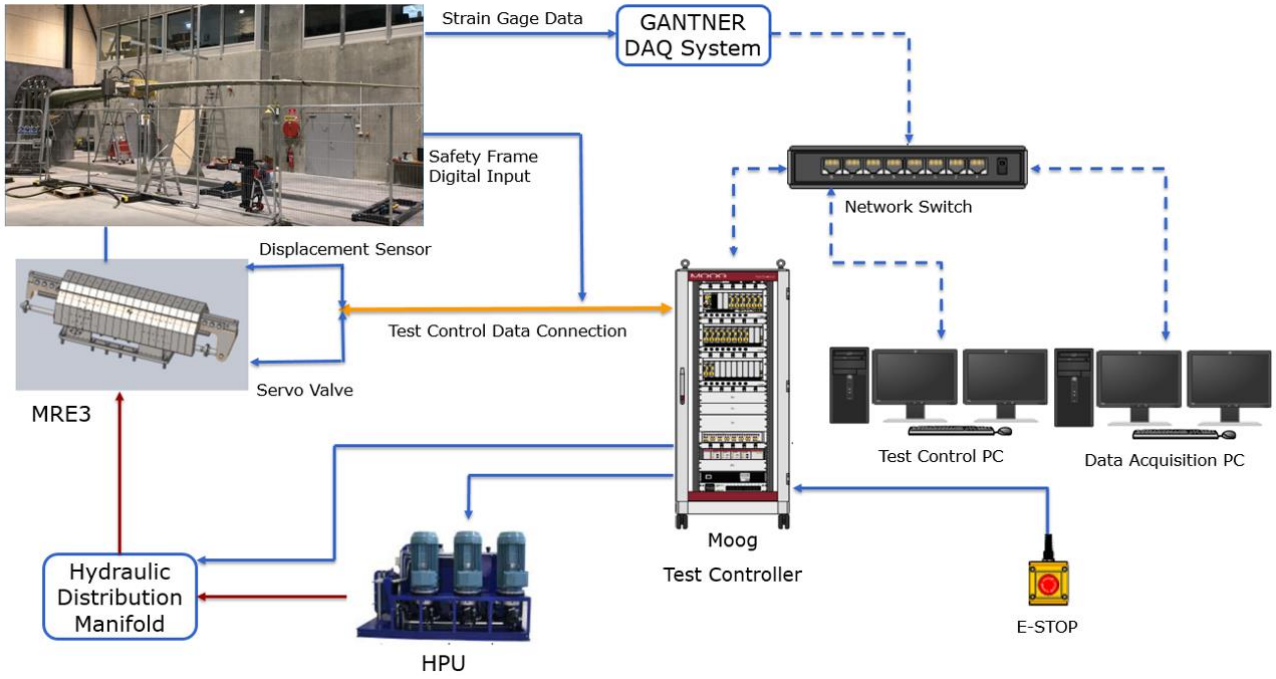

Figure 5.5.17. Test set-up for demonstration of developed fatigue test method on OLW1430 blade.

A comparison between the simulated and experimental EDR for different cross-section regions and different cross-sections along the blade is shown in Figure 5.5.18. As seen in this figure, in general a good agreement was obtained between the simulated and experimental results. Moreover, the strain-based target damage was reached during the test in most of the blade regions (i.e., when EDR≥1), except for a few cross-section regions in the inner part of the blade (i.e., between the root ant 4.0m span). These differences between the simulated and experimental results might be due to different factors, including possible errors obtained during the measurement of the cross-section properties in the inner part of the blade, and possible inertia effects of the edgewise-exciter that were probably not well captured by the blade fatigue test simulator. In BLATIGUE-2, these possible causes of error will be studied in more detail to improve the prediction accuracy.

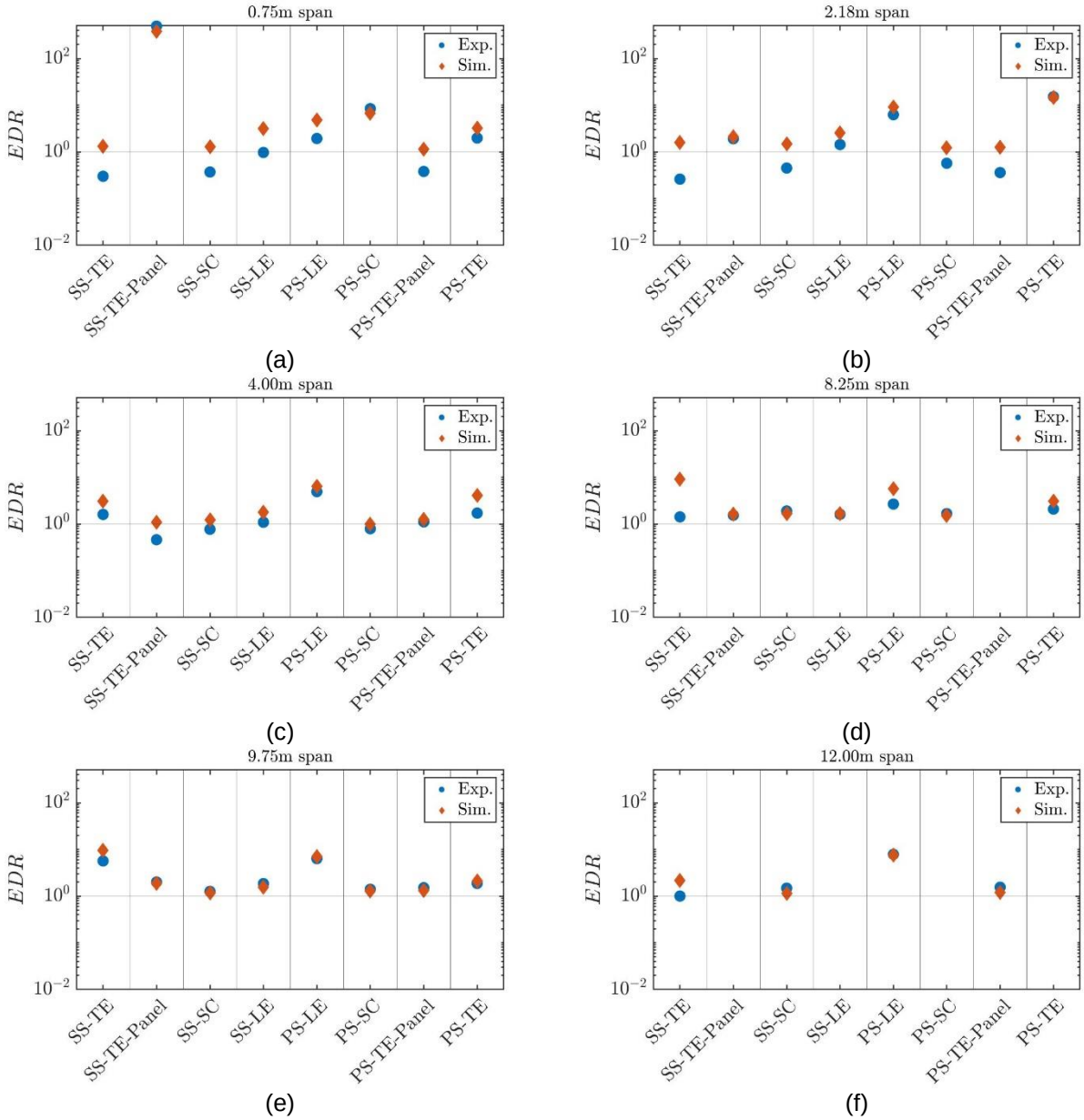

Figure 5.5.18. Comparison between the simulated and experimental equivalent damage ratio, EDR (i.e., ratio between the strain-based test damage and the strain-based target damage), at different cross-section regions (i.e., trailing-edge, TE, trailing-edge panel, TE-Panel, spar-cap, SC, and leading-edge, LE, all at both the suction-side, SS, and pressure-side, PS) and at different blade spans: (a) 0.75m; (b) 2.18m; (c) 4.00m; (d) 8.25m; (e) 9.25m; and (f) 12.00m; of the Olsen-Wings-14.3m blade.

5.5.10 Implementation of the developed fatigue test method on the B75 blade

The implementation of the developed multi-axial fatigue testing method on the B75 blade was achieved. In this process, the requirements and constraints regarding exciter load limits, tuning mass values, and exciter and tuning mass locations were agreed upon between DTU, SGRE, Blaest and R&D. Whereas, the requirements and constraints regarding bending moment distributions were agreed upon between DTU, SGRE, and Blaest.

An optimal combination of one flapwise test block and three chaotic test blocks was found with the method, see Table 5.5.3.

Table 5.5.3. Simulated test blocks. Exciter position at 33.5m using yokes located at 33m and 34m from the root.

Solution name	Test 1	Test 2	Test 3	Test 4
Tuning mass location (m)	Tuning mass (Kg)			
20	4675	4675	2350	7000
26	2160	2160	4580	7000
33.5	8330	8330	11000	11000
42.3	6210	6210	0	2420
56.5	0	0	0	0
70	40	40	40	0
73	190	190	0	20
FlapForce (N)	78182	14394	59375	59375
EdgeForce (N)	0	9697	7200	7200
FlapFrequency (Hz)	0.406964	0.406964	0.473400	0.458884
EdgeFrequency (Hz)	0.656964	0.656964	0.762277	0.721190
Ideal Time (hours)	422.16	270.56	277.69	1048.58
Ideal Time (days)	17.59	11.27	11.57	43.69
Ideal Total Test Time (days)	84.12			

The comparison between the EDR simulated in each cross-section (see Figure 5.5.19) and along the blade for the standard test campaign and optimized test campaign is shown in Figure 5.5.20. In this figure, the regions where the target EDR is reached or exceeded (i.e., when EDR≥1) are shown in yellow, while the regions under-target are shown in other different colors. As shown in this figure, the target EDR ratio is reached almost everywhere on the blade when the optimal solution is considered, see Figure 5.5.20-b; whereas, for the standard fatigue test (see Figure 5.5.20-a), many areas within the cross-section regions are not well tested, especially those at the root and where the sandwich panels are normally located.

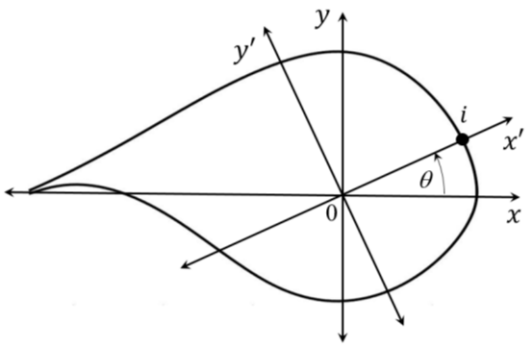

Figure 5.5.19. Location θ of point i within cross-section.

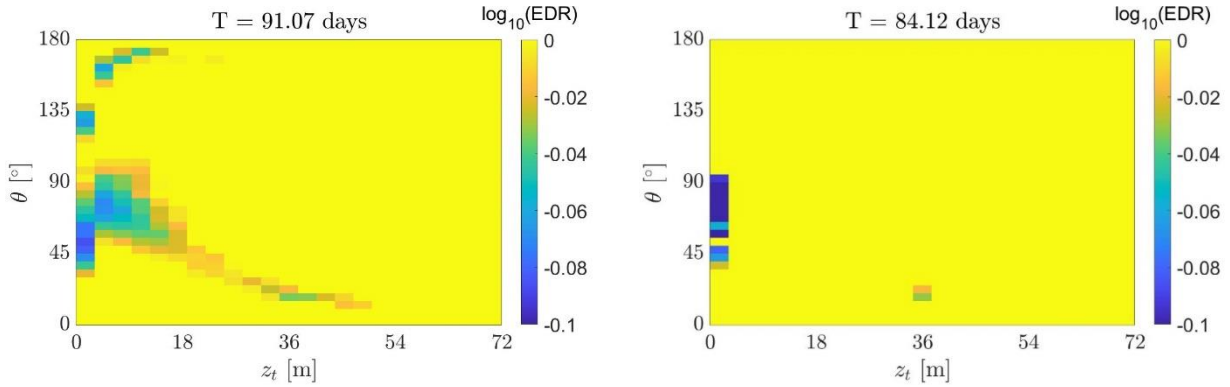

(a) Standard test campaign (b) Optimized test campaign

Figure 5.5.20. Comparison between the simulated EDR along the B75 blade for (a) the standard test campaign; and (b) the optimized test campaign.

In addition, a reduction in testing time was also found for this blade. While the standard test requires 91.07 days to complete the test, the obtained optimal test campaign requires 84.12 days. Although the test time reduction is not as high as that obtained in OLW1430 small blade, it was shown that by applying the method developed both in small and large blades, faster and more accurate tests can be found. In BLATIGUE-2 we will work to reduce testing time even more by using, for example, blade segmentation.

5.6 WP6: Development on large blades

Based on the successful demonstration of the small exciter with the upgraded drive train to reduce backlash-induced spikes in the excitation it was decided to scale up the exciter to perform the final demonstration on the 75m SGRE blade.

5.6.1 Exciter requirement specification

The large Backlash Constrained Dual Axis (BCDA) was designed from the requirement specification outlined by the project group. The input for the requirements were a series of simulations and inputs regarding capacity for future blade testing, to ensure an exciter which is capable of testing future turbine blades (milestone M5). The concluding table is shown in Figure .

• Summary of the test configurations – Maximum values are highlighted

Direction	Force [kN]	Stroke [m]	Frequency [Hz]	Peak Power (From Sim) [kW]
FLAP_@30m_SA	**± 95.0**	0.94	0.427	120
FLAP_@45m_SA	**± 32.0**	**3.23**	0.439	138
FLAP_@30m_CH	± 95.0	**1.06**	**0.432**	145
FLAP_@45m_CH	± 32.5	3.10	**0.451**	150
EDGE_@30m_SA	± 7.2	0.65	**0.689**	10
EDGE_@45m_SA	± 3.1	1.51	0.703	10
EDGE_@30m_CH	**± 12.0**	**0.85**	0.688	19
EDGE_@45m_CH	**± 5.55**	**2.08**	**0.716**	22

* Stroke is the range of displacement * SA: Single Axis CH:Chaotic

Figure 5.6.1 – BLATIGUE exciter requirements.

The performance of the exciter designed for the 75m blade test is described in the following sections.

5.6.1.1 Single axis excitation capabilities

Single axis excitation is obtainable by splitting the BCDA exciter into two individual exciter units.

The exciter unit push rod push/pull peak force capabilities and peak power are:

- Blade applied push/pull force (peak): 95 kN
- Blade applied power (peak) 142 kW

The obtainable force amplitude of the exciter is a function of vertical blade displacement and displacement frequency.

5.6.1.2 Dual axis excitation capabilities

In dual-axis configuration the forces that can be applied by the BCDA exciter in flap-wise and edge-wise direction are dependent on the geometric setup of the exciter. When configured with the shortest possible exciter arm length (for maximum push rod force) and the push rods position each at an angle of 30° from vertical, the following edge- and flap-wise peak forces can be achieved:

- Blade applied flap force (peak): 165 kN
- Blade applied edge force (peak): 95 kN
- Blade applied power (peak) 2 x 142 kW

Many different geometric configurations can be arranged and thus the force capabilities change depending on the angle of attack of the push rod.

5.6.2 Exciter concept development

The concept of the BCDA exciter is based on the concept of the small exciter described previously. To add further functionality, scalability and mobility the concept consists of two separate exciter units, which combined make up one BCDA. A single exciter unit with annotations is shown in Figure . The exciter unit consists of a concrete foundation with a large footprint raft and two concrete plinths in the middle that support the drive train. The drivetrain consists of a permanent magnet synchronous machine (PMSM) that is connected to two planetary gearboxes. The motor produced torques are converted to forces via the exciter arm and hinged push rod.

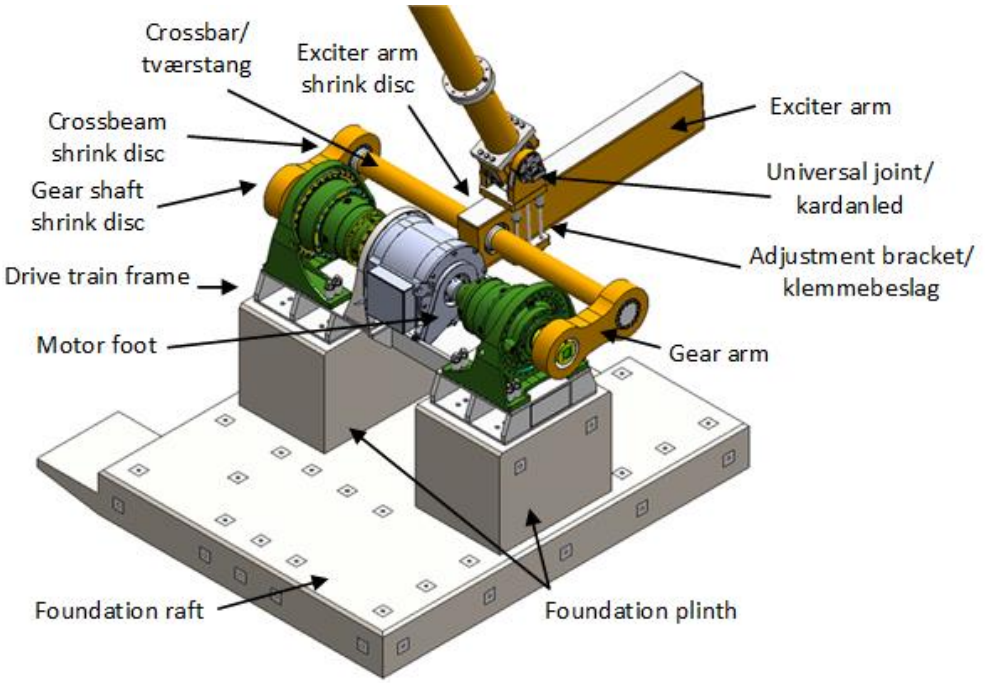

Figure 5.6.2 – BCDA exciter unit.

The BCDA exciter can be configured in different geometric configurations by varying the position of the universal joint on the exciter arm and by varying the length of the push rod. Furthermore, in dual axis configuration, the BCDA exciter geometry can be varied further by positioning the two exciter foundations closer or further apart (milestone M5 & M6). The geometry of the exciter is described using variables as shown in Figure .

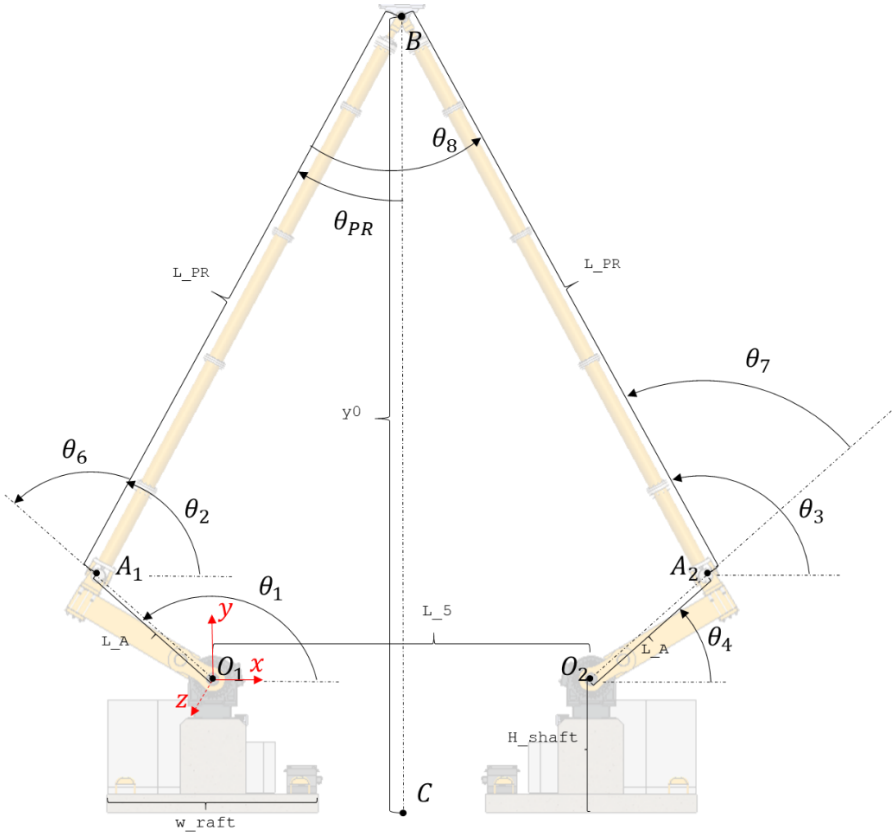

Figure 5.6.3 – Geometric definitions of the BCDA exciter.

The large dual axis exciter was commissioned at BLAEST's test facility, were a series of tests were executed to validate the exciter functionality and design. The commissioning process validated not only the design and concept of the large BCDA but also provided valuable input for further development of the exciter software functionality.

Figure 5.6.4 Large exciter demonstration test SGRE B75 blade at BLAEST.

5.6.3 Summary

The output of the large exciter development in WP6 was development, design and subsequent successful demonstration of a full-scale dual axis exciter capable of testing a 75m blade in different test modes. The design relies on the concept developed for the small exciter, while adding additional functionality and value by relying on separate exciter units which can be used separately for single-axis excitation, or for dual-axis excitation as in this project.

The commissioning of the system was overall successful and provided input for additional developments in commercial projects. The finished design is assessed to be fully scalable for wind turbine blades of the future, capable of handling multiple test modes as required by dual-axis test programs and to have a large commercial potential. (milestone M11)

Reports/deliverables

[1] Design Data for 75m Blade Test Excitation, rev. 04, 2019-04-24 (milestone M5)

[2] Design Description, 3190 BLATIGUE BCDA75, Rev 02, 2020.05.12 (milestone M6)

[3] SAT protocol, BLATIGUE – Backlash Constrained Dual Axis Exciter, rev. 00, 2021-04-25 (milestone M9)

5.7 WP7: Demonstration on full-scale blades

5.7.1 - Demonstration of R&D Exciter on a Siemens B49 blade

DTU upgraded the electrical installation of the Large Scale Facility and modified the R&D exciter developed for the 15m test stand so that the exciter can be used all over the facility.

A test set-up was made for the B49 on the 45m test stand (see Figure 5.7.1) to demonstrate the versatility of the R&D exciter (milestone M4).

(a)

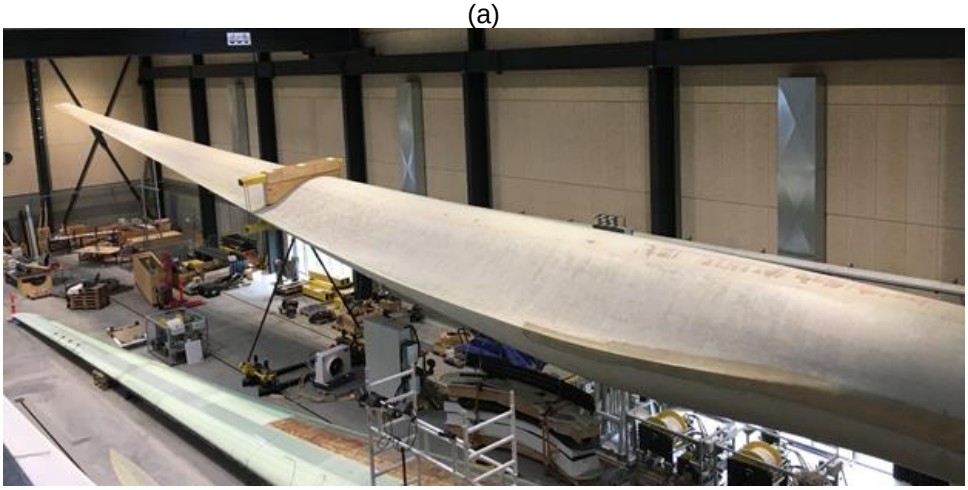

(b)

Figure 5.7.1. (a) The modified R&D exciter on the 45m test stand. (b) Test set-up, B49 blade, R&D exciter. Load saddle is located at 20m. View from 2nd floor of the facility.

Three fatigue test runs were conducted, pure flap-wise, pure edge-wise and chaotic biaxial loading. Figure 5.7.2 shows the displacement of the load saddle during test (10s of testing). No strains were recorded during testing.

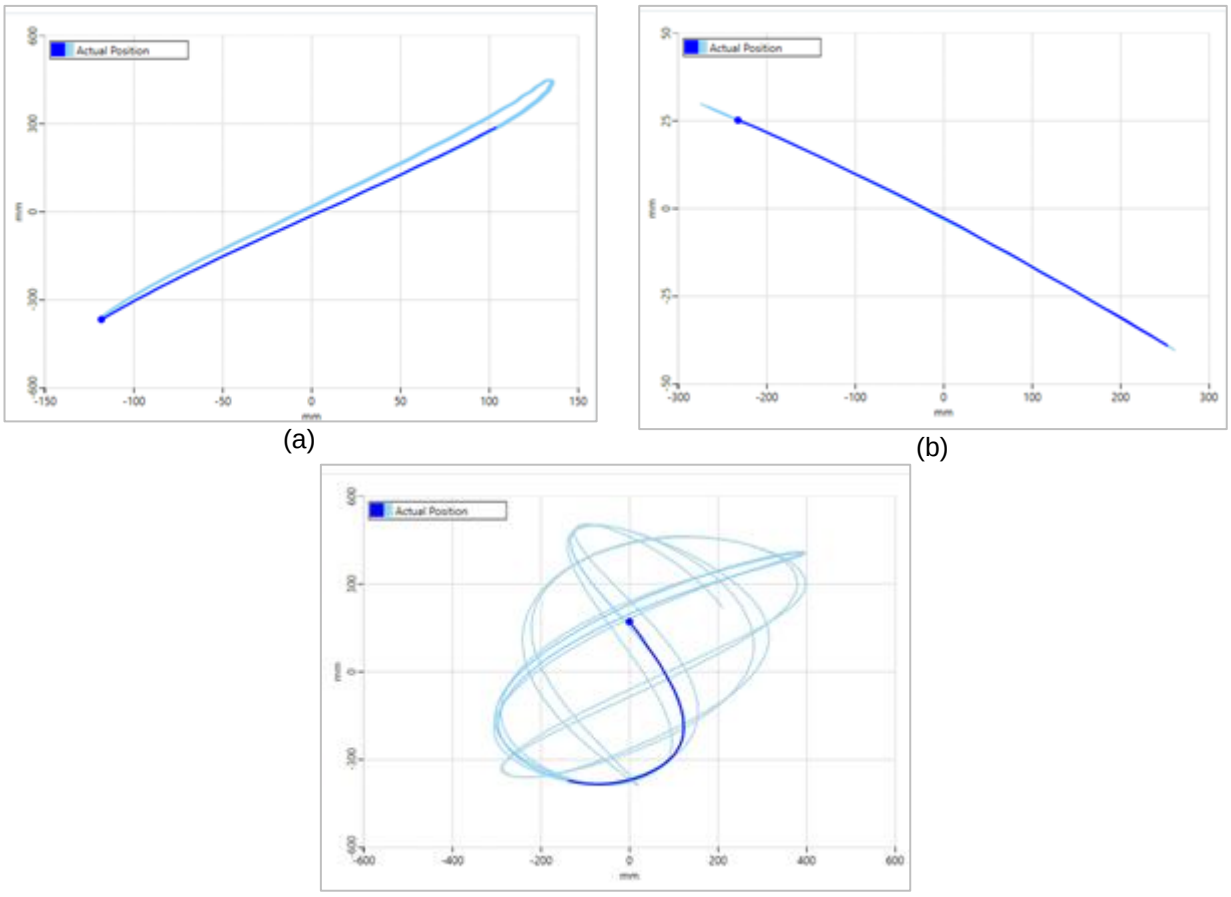

Figure 5.7.2. Position of the load saddle during (a) pure flap-wise sinusoidal force excitation; (b) pure edgewise sinusoidal force excitation; and (c) combined flap- and edgewise sinusoidal force excitation.

5.7.2 Fatigue method demonstration with exciter

The developed multi-axis fatigue test method and dual-axis exciter were successfully demonstrated on the B75 blade (milestone M10). Below is a description of the tests performed for the demonstration and the results.

5.7.2.1 Description of test setup

The demonstration was carried out at the BLAEST's test facility located in Aalborg, Denmark. The test campaign was performed on the B75 blade provided by SGRE, which was mounted on the test rig B3 with an inclination angle of 5°.

The test campaign consisted of a static calibration test and a group of fatigue test blocks. The static calibration test was carried out to estimate the calibration constants that correlate the applied bending moments and the induced strains along the blade, so that the applied bending moments can be quantified during testing. The fatigue test blocks consisted of uniaxial and dual-axis fatigue tests and were performed to demonstrate the developed fatigue test method. A more detailed description of these test blocks and corresponding results are given in sections 5.7.2.2 and 5.7.2.3.

The loads on the blade were applied using the dual-axis exciter developed in the BLATIGUE project, see section 5.6. The developed dual-axis exciter is a full-scale multi-axis fatigue blade test system that can apply flapwise and edgewise loads simultaneously. The exciter is powered by two independently controlled electric

motors that simultaneously can apply combined flapwise and edgewise forces to the blade. The BLATIGUE exciter apply up to 165-190 kN to the blade in the flap direction and 95 kN in the edge direction while being able to supply around 275 kW of excitation power to the blade. A feature that provides more precise test data is the new development of the “dual gearbox solution”, as the drivetrain relies on an R&D patented backlash-free design. The development of the dual gearbox solution ensures a precise and smooth force application to the blade which in turn results in better strain measurements and low noise operation.

The exciter control was based on an open loop controller with sinusoidal flap and edge forces as input reference. In the dual axial tests, the setpoint for the test was determined by four input parameters, which were amplitude and frequency for the flap force reference and the same for the edge force reference.

5.7.2.2 Description of evaluated test blocks

The test blocks obtained by applying the developed optimization method (see Table 5.7.1) were carried out experimentally at BLAEST test facility. Each test block was performed for no more than 15 minutes, and only 5 minutes were considered when making the EDR calculations.

The comparison between the experimental test setups for the different test blocks with respect to the simulated ones is shown in Table 5.7.1. As seen in this table, the values of the tuning masses used during the actual test coincided very well with those suggested by the simulation, with the highest difference being 10% for the tuning mass located at the blade tip for Test 4. The experimental frequencies applied in the flapwise and edgewise directions also matched well with the ones obtained from the simulations, with the highest difference being 2.5%. This shows the capabilities of the developed blade test simulator to predict the dynamic response of blades under different test setups.

Table 5.7.1. Comparison between the test setups for the different test blocks with respect to those obtained by means of the simulations (see Table 5.5.2). Exciter position at 33.5m using yokes located at 33m and 34m from the root.

Solution name	Test 1	Test 2	Test 3	Test 4
Tuning mass location (m)	Error tuning mass (%)			
20	4.1	4.1	4.1	2.8
26	-1.3	-1.3	-1.1	0.2
33.5	0.5	0.5	0.6	0.6
42.3	-0.6	-0.6	NaN	2.1
56.5	NaN	NaN	NaN	NaN
70	-1.3	-1.3	-1.3	NaN
73	1.8	1.8	0.0	10.0
Error FlapFrequency (%)	0.5	0.5	0.6	0.6
Error EdgeFrequency (%)	NaN	1.3	2.5	2.1
Ideal Time (hours)	422.16	270.56	277.69	1048.58
Ideal Time (days)	17.59	11.27	11.57	43.69
Ideal Total Test Time (days)	97.12			
Test time (min)	5	5	5	5
Total Test Time (min)	20			

Furthermore, to avoid possible failures, it was decided not to apply 100% of the target loads on all test blocks during the test campaign. This considering that the blade used for the test was old, not painted or wrapped, and was exposed to sunlight for several years while stored outdoors. Figure 5.7.3 shows an example of the experimental test setup for one of the test blocks.

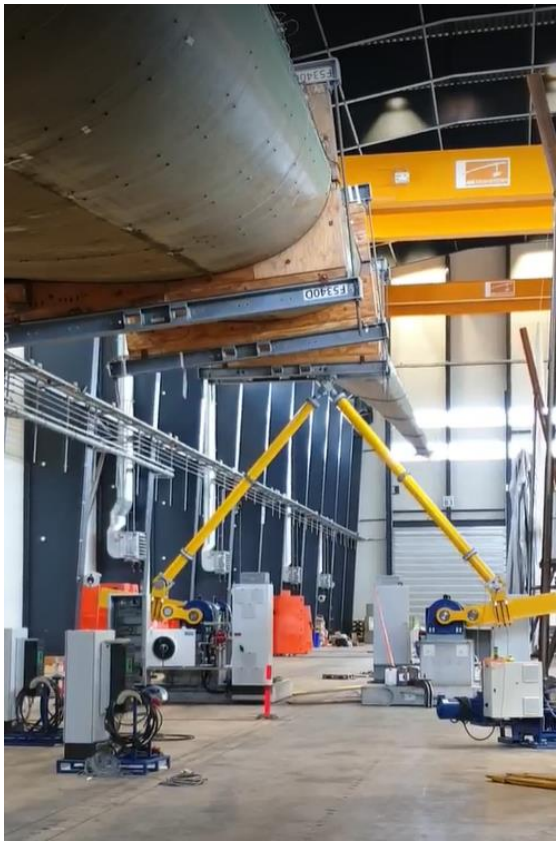

Figure 5.7.3. Example of test set-up for B75 blade demonstration.

During tests, the blade was excited in the natural frequencies for flap and edge for the specific test setup, consisting of blade and lumped masses. The approach for determining these natural frequencies was to run initial single axis tests in flap and edge. In both cases the test frequency was adjusted to the setpoint having an estimated phase lag of -90° between actual exciter force and blade position. The load level during the initial test was close to the relevant target load.

The reference forces in flap and edge were found afterwards by increasing the two parameters until the required level in both directions were achieved. In the single axial tests, the two relevant parameters were found as for dual axis testing, and the two excessive parameters where set to zero.

5.7.2.3 Results and brief discussion

The comparison between the experimental bending moments, M_{test}, along the blade and the simulated ones, M_{sim}, for the different test blocks in the flapwise and edgewise directions are shown in Figure 5.7.4.

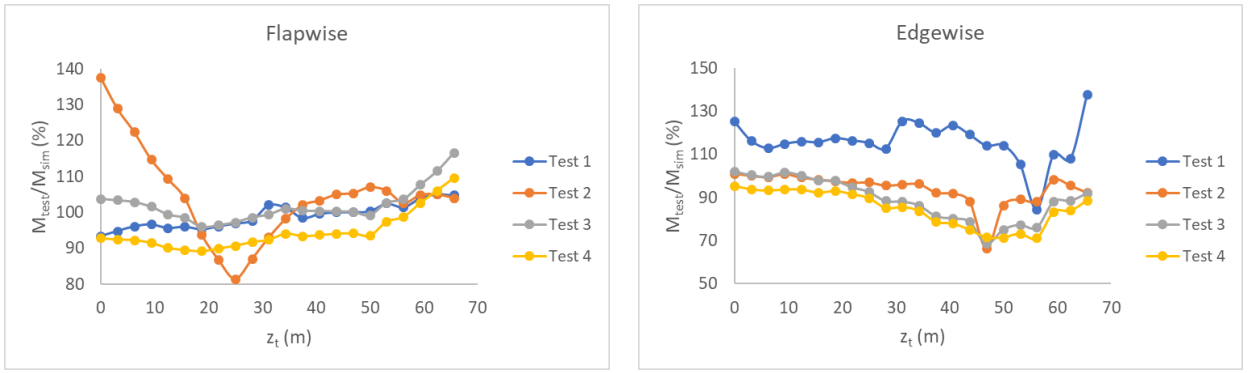

(a) (b)

Figure 5.7.4. Comparison between the experimental bending moments, M_{test}, and the simulated bending moments, M_{sim}, for the different test blocks in the (a) flapwise and (b) edgewise directions.

The total projected EDR along the blade obtained by scaling the 5-min-EDR of each test block during the experiment to the corresponding ideal test block time (see Table 5.7.1) is shown in Figure 5.7.5. As seen in this figure, most of the blade would be properly tested (i.e., yellow area where EDR≥1) after the test, while some regions at the root and at the leading-edge panels between $30m \leq z_t \leq 60m$ would not be well tested (i.e., areas with colors other than yellow). The differences between these experimental results and the simulated ones (see Figure 5.5.6-b) are due to the differences in the magnitude of the forces applied in most of the test blocks with respect to what was suggested in the simulations. The applied loads were in general lower than the simulated ones, especially in the root and in the edge direction (see Figure 5.7.4).

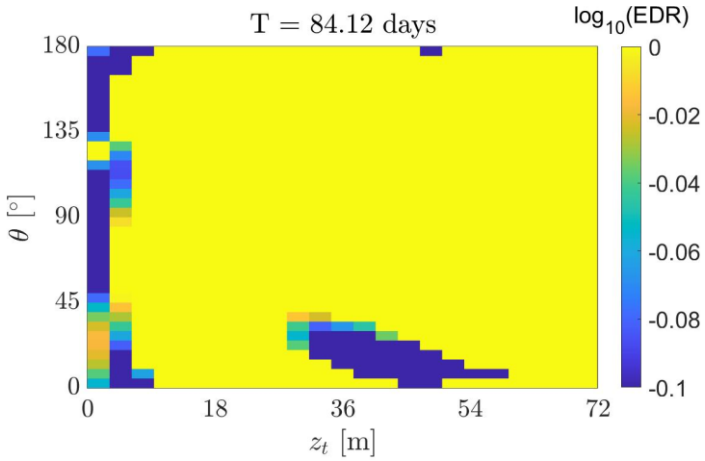

Figure 5.7.5. Total projected EDR after total test time calculated based on experimental 5-min EDR from the different test blocks.

Furthermore, the comparison between the EDR distribution along the blade for the different test blocks obtained from the experiments and simulations is shown in Figure 5.7.6. According to this figure, it can be concluded that the developed blade test simulator tool has the ability to predict with high reliability the theoretical damage in the the blade under different types of load. This can be seen as the experimental and simulated EDR distributions match well each other under flapwise loading (see Figure 5.7.6-a and -b), edgesiwe-dominated chaotic loading (see Figure 5.7.6-c and -d), and flapwise-dominated chaotic loading (see Figure 5.7.6-e and -f). This is in agreement with what was shown with the OLW1430 blade, see section 5.5.

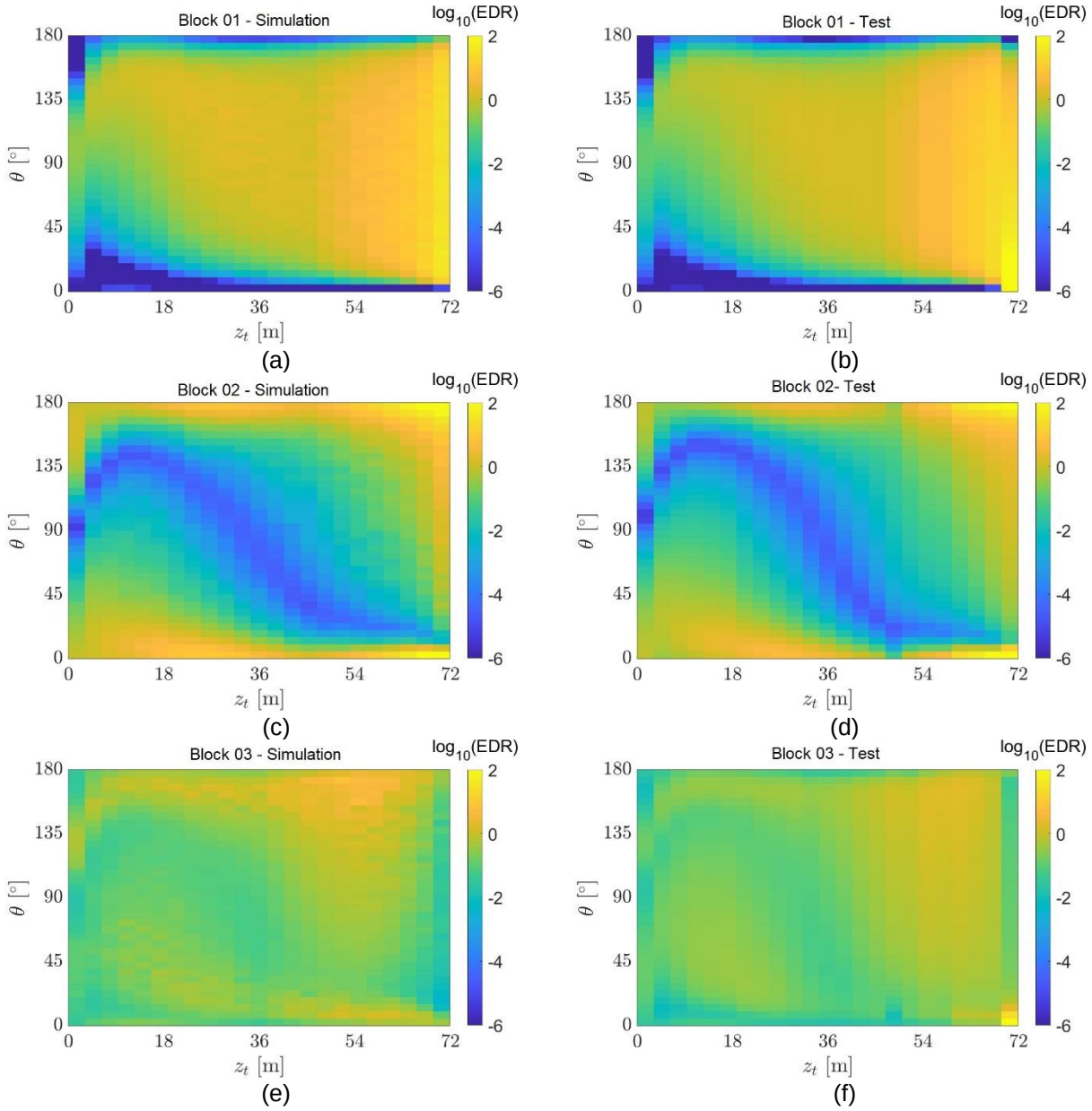

Figure 5.7.6. Comparison between simulated and experimental EDR from different test blocks. (a) Simulated and (b) experimental EDR for test block 01; (c) Simulated and (d) experimental EDR for test block 02.

5.8 WP8: Improved certification scheme

When carrying out blade fatigue tests, we want to apply a test load which is sufficiently high to ensure that design assumptions are met and the blade has fatigue resistance at least as high as what is assumed in the design. Due to the spatial variation in the blade properties, and due to potential measurement, material, and model uncertainties (Figure 5.8.1), it is not guaranteed that the actual test loads exceed the design load targets over the entire blade – hence, it is not guaranteed that a blade test will verify the validity of the design assumptions over the entire blade. BLATIGUE Work Package 8 suggests a scheme where the knowledge on the variation and uncertainty in blade properties can be combined with the uncertainty in the applied test loads, to provide a probabilistic estimate of how likely it is that the test loads are sufficient to verify the design assumptions over the entire region of interest in a blade.

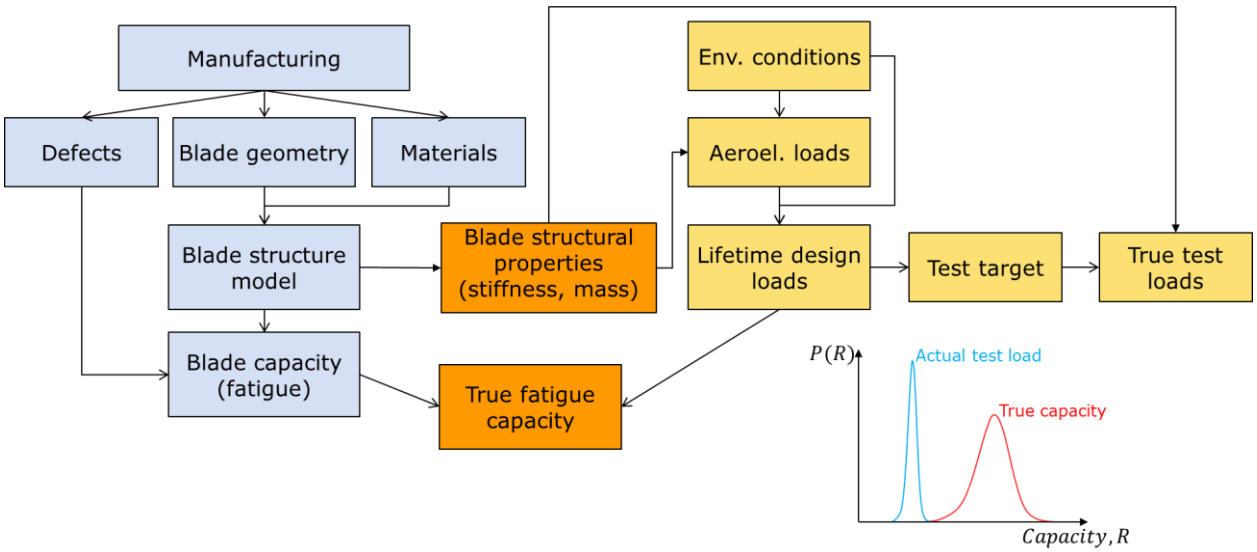

Figure 5.8.1 Uncertainty propagation chain in wind turbine blade design and testing

The computation of the likelihood of achieving sufficient test coverage is based on the reliability analysis concept. The reliability problem is defined mathematically in terms of the so-called limit state equation, which indicates the status of the structure as function of the actual values of the loads and material strength. For the purpose of test verification, the limit state equation is defined so that it indicates whether the test load L_{test} has actually exceeded the design load L_{design}, where both L_{test} and L_{design} are random variables dependent on the load, material, and model uncertainties. The probability of obtaining a successful test can then be computed by evaluating the limit state equation over the entire uncertainty distribution, determining the probability that $L_{test} \geq L_{design}$. Running such an analysis while assuming different test load factors, we obtain a curve showing what is the probability of a successful test as function of the test load factor (Figure 5.8.2). This gives possibility to determine the appropriate test load factor value that under the assumed conditions will give the desired confidence that the blade test is successful and has achieved a sufficient coverage.

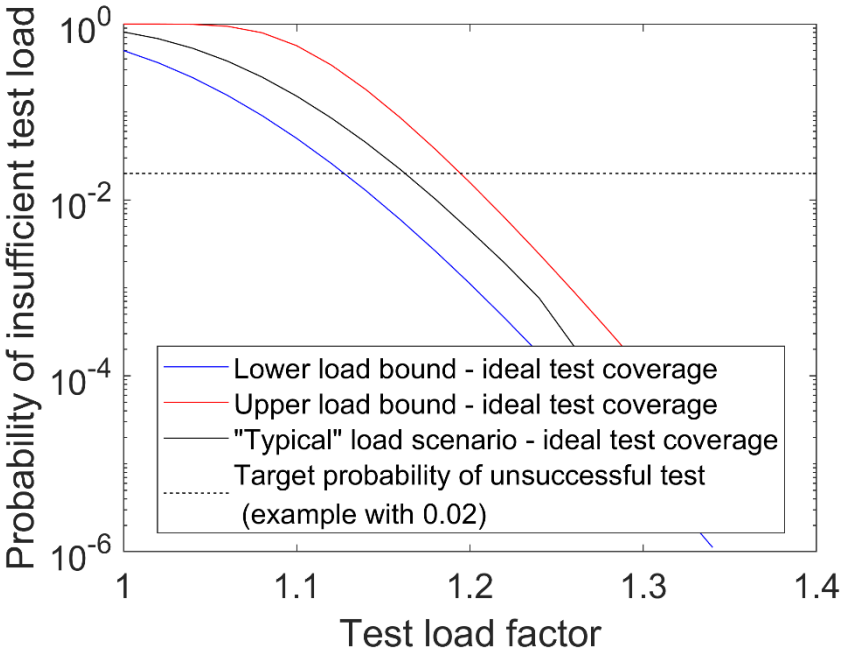

Figure 5.8.2 Test load factors examples as function of target probability for successful test.

The project has also delivered input to the IEC 61400-23 standard on blade testing which is currently under revision. DTU Wind Energy, SGRE, BLAEST and Ørsted are active in the standard maintenance team and seek to influence the standard to make sure that tools and methods developed in BLATIGUE will be adapted into the new version of the standard.

The project team has delivered text to the standard, so the multi-axis fatigue test method developed in BLATIGUE hopefully will be included in the new standard. This fulfils CM7. The preliminary text proposes that partial safety factors are reduced when multi-axis fatigue tests are used for certification tests. This is in line with the philosophy of the just adopted blade design standard IEC 61400-5. Reducing partial safety factors will not only make it possible to design lighter and cheaper blades, but also push the trend towards the use of such more advanced tests.

5.9 Dissemination

Galinos, C. (2018). Aeroelastic Analysis of B75 blade - Blatigue Project. DTU Wind Energy. DTU Wind Energy I No. 0616

Galinos, C. (2017). Aeroelastic Analysis of Olsen Wings 14.3m Blade - Blatigue Project. DTU Wind Energy. DTU Wind Energy E Vol. 635

Galinos, C., & Larsen, T. J. (2018). Aeroelastic Analysis of B49 blade - Blatigue Project. DTU Wind Energy I Vol. 638

Castro, O., Belloni, F., Stolpe, M., Yeniceli, S. C., Berring, P., & Branner, K. (2021). Optimized method for multi-axial fatigue testing of wind turbine blades. Composite Structures, 257, [113358]. https://doi.org/10.1016/j.compstruct.2020.113358

Castro, O., Berring, P., Branner, K., Hvejsel, C. F., Yeniceli, S. C., & Belloni, F. (2021). Bending-moment-based approach to match damage-equivalent strains in fatigue testing. Engineering Structures, 226, [111325]. https://doi.org/10.1016/j.engstruct.2020.111325

Castro, O., & Branner, K. (2021). Effect of tunneling cracks on structural property degradation of wind turbine blades. Composite Structures, 268, [113914]. https://doi.org/10.1016/j.compstruct.2021.113914

Castro, O., & Branner, K. (2021). Corrigendum to “Effect of tunneling cracks on structural property degradation of wind turbine blades” [Compos. Struct. 268 (2021) 113914]. Composite Structures, 273, [114293]. https://doi.org/10.1016/j.compstruct.2021.114293

Chen, X., Semenov, S., McGugan, M., Madsen, S. H., Yeniceli, S. C., Berring, P., & Branner, K. (2021). Fatigue testing of a 14.3 m composite blade embedded with artificial defects – damage growth and structural health monitoring. Composites Part A: Applied Science and Manufacturing, 140, [106189]. https://doi.org/10.1016/j.compositesa.2020.106189

Castro, O., & Branner, K. (2020). Preliminary multi-axial strain analysis in wind turbine blades under fatigue test loads. I O P Conference Series: Materials Science and Engineering, 942(1), [012044]. https://doi.org/10.1088/1757-899X/942/1/012044

Castro, O., & Branner, K. (2019). Effect of matrix cracks on stiffness degradation of laminated composite beams. In Proceedings of the 22nd International Conference on Composite Materials (ICCM22)

Lorenzo, E., Manzato, S., Peeters, B., Ruffini, V., Berring, P., Haselbach, P. U., Branner, K., & Luczak, M. (2019). Modal Analysis of Wind Turbine Blades with Different Test Setup Configurations. In M. L. Mains, & B. J. Dilworth (Eds.), Topics in Modal Analysis & Testing (Vol. 8, pp. 143-152). Springer. Conference Proceedings of the Society for Experimental Mechanics Series https://doi.org/10.1007/978-3-030-12684-1_14

Lorenzo, E., Manzato, S., Luczak, M., Peeters, B., & Branner, K. (2019). Strain-based operational modal analysis for wind turbine blades. In Proceedings of the 8th International Operational Modal Analysis Conference IOMAC. International Operational Modal Analysis Conference (IOMAC)

Chen, X., Trevisi, F., Berring, P., Yeniceli, S. C., Semenov, S., Madsen, S. H., & Branner, K. (2018). BLATIGUE Project Report-Standard Static Tests of a 14.3 m Olsen Wing Blade.

Ingeniøren March 3, 2017: ”Ny testcenter: Vindmøllevinger skal testes i flere retninger samtidig”

TV2 News July 9, 2019: Story about the BLATIGUE project in connection with a story about the positive evaluation of EUDP

DTU Wind & R&D. BLATIGUE-WP2-Design data for 15 m blade test excitation-Rev02, rev. 02, 2017-07-03

R&D. Design Description – Small Exciter, rev. 02, 2017-10-30

R&D. Market and competition analysis, 2019-06-25

R&D. Factory Acceptance Test Protocol, rev. 02, 2018-07-08

R&D. Site Acceptance Test Protocol, rev. 03, 2018-07-12

DTU Wind, BLAEST, SGRE & R&D. Design Data for 75m Blade Test Excitation, rev. 04, 2019-04-24

R&D. Design Description, 3190 BLATIGUE BCDA75, Rev 02, 2020.05.12

R&D. SAT protocol, BLATIGUE – Backlash Constrained Dual Axis Exciter, rev. 00, 2021-04-25

Test innovation needs for large blades
Period: 1 Oct 2019

Kim Branner (Invited speaker)
Wind Turbine Structures and Component Design
Department of Wind Energy

Description
Session on Blades – the future challenges
Degree of recognition: International

Related event

Wind Energy Denmark 2019
01/10/2019 → 01/10/2019
Herning, Denmark
Activity: Talks and presentations › Conference presentations

Full scale test of very large blades
Period: 28 Aug 2019

Kim Branner (Invited speaker)
Wind Turbine Structures and Component Design
Department of Wind Energy

Vindenergisystemer (S-588) møde: Dansk Standard udvalg
28/08/2019 → 28/08/2019
Denmark
Activity: Talks and presentations › Conference presentations

Testing capabilities and recent results from DTU Large Scale Facility
Period: 20 Jun 2019

Kim Branner (Invited speaker)
Wind Turbine Structures and Component Design
Department of Wind Energy

Wind Energy Science Conference 2019: Wind Energy Science Conference 2019
17/06/2019 → 20/06/2019
Cork, Ireland
Activity: Talks and presentations › Conference presentations

Recent results towards more realistic testing of wind turbine blades – BLATIGUE project
Period: 25 Feb 2019

Kim Branner (Speaker)
Martin Bonde Madsen (Speaker)
Wind Turbine Structures and Component Design
Department of Wind Energy
Degree of recognition: International

IEA Wind TEM # 94: Large Component Testing for Ultra- long Wind Turbine Blades
25/02/2019 → 26/02/2019
Boulder, Colorado, United States
Activity: Talks and presentations › Conference presentations

Subarticle & subcomponent testing
Period: 25 Feb 2019

Kim Branner (Speaker)
Wind Turbine Structures and Component Design
Department of Wind Energy
Degree of recognition: International

IEA Wind TEM # 94: Large Component Testing for Ultra- long Wind Turbine Blades
25/02/2019 → 26/02/2019
Boulder, Colorado, United States
Activity: Talks and presentations › Conference presentations

6. Utilisation of project results

In BLATIGUE the two main technologies developed are:

- An efficient multi-axis fatigue exciter for large blades
- Multi-axis fatigue test method for large blades

R&D already has the exciter on the market, but it will be further developed in the newly EUDP funded BLATIGUE-2 project. Part of the work in BLATIGUE-2 is to combine the test method and exciter into one integrated solution.

BLATIGUE also developed and demonstrated two other technologies that support the two main technologies above. These two support technologies are:

- Computer simulation tool for multi-axis fatigue testing of large blades
- 3D digital measuring system for fatigue testing of large blades

Both of these technologies will be further developed in BLATIGUE-2. The computer simulation tool will be integrated with the exciter and will therefore be commercialized by R&D. The 3D digital measuring system for fatigue testing will be further developed in BLATIGUE-2 and become measurement hardware and consultant services and will be commercialized by Zebicon.

6.1 Market and competition analysis for multi-axis exciters

The offshore share of the wind market is increasing while total wind market is stable as seen in the figure below. It is expected that the increasing offshore wind share and competition will drive test investments for large blades.

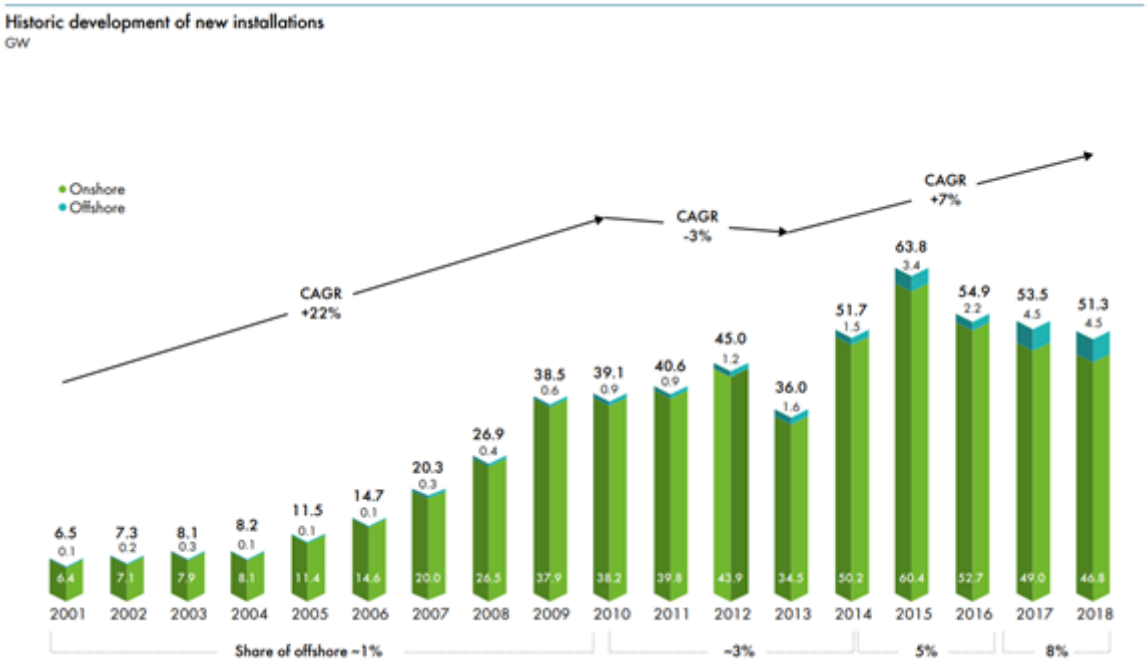

In order to meet the test requirements of the longer turbine blades, both public and private blade test facilities are increasing in both number and capabilities as shown in the following figures. As seen in the figures the blade test facilities are growing in size and numbers, with 7-10 test centers planned with blade lengths around 100m and a 107m blade test facility ready for test 2019.

Public blade test facilities

2015/16

Public Facility	Max Blade Length (m)	Root Bending Moment Capacity (M N m)	Static testing horizontal (H) or vertical (V)	Number of Blade Test Stands	Component Test Capabilities	Material / Coupon Testing
China General Certification (CGC) (China)	100			2		
Narec (UK)	100		H	3		
Fraunhofer-IWES (Germany)	90		V	3	Yes	Yes
Wind Technology Testing Center (USA)	90	84	V / H	3		
Blaest (Denmark)	85		V	5		
CENER (Spain)	75	100	H	2		
WMC (Netherlands)	63 (75m planned)		V / H	3	Yes	Yes
KIMS (Korea)	70	50		2		Yes
University of Maine (USA)	70		H	1	Yes	Yes
Wind Energy Technology Center (SGS) (China)	70		V	3		
National Wind Technology Center (USA)	50	16	V	3		
DTU-Risø Campus (Denmark)	29	9	V	1	Yes	Yes
DTU-Risø Campus (Denmark) (end of 2016)	45	20	V	3	Yes	Yes
IMA (Germany)	40			1		
CRES (Greece)	25					
Clarkson University (USA)	12		V	2	Yes	
CWET (India)						

Source: Test Center Capabilities, Fact Sheet, IEA Wind Task 35, May 2016.

Existing (2019)	Planned (2019)
Max Blade Length (m)	Max Blade Length (m)
	Fraunhofer-IWES: 115m
	BLAEST: 100m (option up to 120m)
	WMC (China): ??
	CGC: ??
	NWEST: ??
	SGS: ??
	State grid: ??

Information from public sources; i.e. press releases, industry news media, etc.

Private blade test facilities

2015/16	
Private Facility	Max Blade Length (m)
Sinovel (China)	100
Vestas (UK)	100
ZL (China)	100
Enercon (Germany)	80
LM (Denmark)	80
Siemens (Denmark)	75
Tecsis (Brazil)	70
Gujarat Suzlon (India)	65
Euros (Poland)	60
Vientek (Mexico)	60
HT Wind (China)	50
Modular Wind Energy (USA)	50
Tianwei Boading (China)	50
TPI (USA)	30
Goldwind (China)	

Existing (2019)	Planned (2019)
Max Blade Length (m)	Max Blade Length (m)
China Composites Group Corporation (=ZL): 120m	SGRE: ??m
CSIC: 100m	+ several confidential
Korea Institute of Materials Science (KIMS): 90m	
Envision: 80-100m	
Goldwind: 80-100m	
New Time Material (CRRC): 80m	
TPI: 60-70m	
Nordex: 70m?	

Source: Test Center Capabilities, Fact Sheet, IEA Wind Task 35, May 2016.

Patents

There are existing patents that concern dual-axis testing. A patent by IABG *(Vibration exciter for the stress testing of a rotor blade, system, test bench, and arrangement comprising such a vibration exciter, and operating method, IABG, PCT/EP2017/073998, WO 2018/055075 A1 Date of publication: 29.03.2018)* relies on a direct drive motor and a pushrod for blade excitation. A second patent by ORE Catapult (*Fatigue Testing, ORE Catapult, EP 3 237 873 B1, WO 2016/102968, Date of publication 23.01.2019*) concerns the test methodology and the use of test blocks and an optimization algorithm for optimizing test results.

Competitors

Test facilities with dual-axis test capabilities also exist at both Fraunhofer, IABG and ORE Catapult, each of them relying on different excitation principles.

Further description of increased turnover, exports, employment and additional private investments at the project partners is estimated in the project completion form (Afslutningsskema).

7. Project conclusion and perspective

In BLATIGUE we set off to mainly develop two technologies, namely advanced multi-axis fatigue testing method and multi-axis fatigue exciters - both for very large blades. This has happened. BLATIGUE has developed a fatigue test method and simulation tool that not only is effective, as the test goal can be reached virtually anywhere on the blade at the same time (that is not possible with current standard certification tests), but we have also shown that in some cases we can perform the tests 50% faster than current standard certification tests. In BLATIGUE, an innovative electric exciter has also been developed that is capable of performing the developed fatigue test method. This exciter is already on the market, as stated on the R&D website and sales material. So we have actually come further in terms of market introduction than we described in the BLATIGUE application. The BLATIGUE project has also made the project partners the international technology leaders within this area.

But we have also become wiser, and the BLATIGUE project has revealed some technological challenges that need to be addressed in order to achieve the full potential of the developed technologies. These are:

- Multi-axis fatigue testing methods are complicated and time-consuming to plan and configure, and R&D experience shows that it is very difficult to sell the exciter alone and without a test simulation and design tool.
- To obtain the full potential for using the multi-axis fatigue testing method it is needed to be able to adapt the method to specific industry needs. This can be done by having more tools like 1D masses, springs and dampers available.
- In addition to a mechanical exciter system, a complete solution supporting planning, execution and evaluation of the test is needed to perform multi-axis fatigue testing in a commercial setting.
- The industry needs to shorten the test time for future long blades more than is possible with the BLATIGUE technologies.

The next steps is to continue the work in the newly EUDP funded project BLATIGUE-2 which will start shortly after finalizing this project. The purpose of BLATIGUE-2 is to solve the challenges listed above, but also to take a much more holistic view on blade testing and certification with the aim of making the whole process significantly faster and much more efficient, while increasing the value of this process through digitalization, virtual sensing and improved measurement and inspection methods.